INSTITUTO SUPERIOR TÉCNICO
Universidade Técnica de Lisboa

Aero-Acoustic Optimization of Airfoils for Wind Turbines

Jaime Fernando Gomes Coimbra

Dissertação para a obtenção de Grau de Mestre em

Engenharia Mecânica

Júri

Presidente:	Professor Luís Rego da Cunha de Eça
Orientador:	Doutor André Calado Marta
Vogal:	Professor José Leonel Monteiro Fernandes

Maio 2012

To my parents and sister.

Acknowledgments

I would like to start by leaving my thanks to all those involved in my education and upcoming, which thankfully are too many to name in such a small text. I was fortunate enough to have known so many different and interesting individuals.

I would like to express my gratitude first to all of my teachers and professors that followed me in my academic journey for their patience, knowledge and wisdom. A special thanks to my thesis coordinator Dr. André Marta for his teachings, guidance and patience on this final stage of my degree and from whom I have learned so much during this work.

I also leave here a word of recognition to all those whom I never met personally and yet helped me in various ways to accomplish my work. Dr. Ruben E. Perez (from the Royal Military College of Canada) for his precious help in solving various technical pyOpt issues. Dr. Peter J. Eecen (from ECN Wind Energy), Prof. Ruud van Rooij and Prof. W.A. Timmer (from the Delft University of Technology) on their help and advisory on providing and using the RFOIL software. Patrick J. Moriarty (Senior Engineer at the National Wind Technology Center) for providing precious documents, without which my work could not have been completed. Also to Prof. Giorgos Leloudas (Technical University of Denmark) for his help in introducing me to the subject here developed.

Finally, but not least, a very special ”Thank you” to my family, my friends from many years and my colleagues from IST, for their support and help in going through this demanding and extenuating period of my life. You all gave precious contributes that helped me achieve my dream of becoming an engineer. Without you my world would be much less interesting to live in and I thank you for being part of it.

Resumo

O tema de design de perfis, no contexto das turbinas eólicas, é abordado com o objectivo de optimizar a geometria e avaliar o melhor compromisso entre performance aerodinâmica e aero-acústica. O trabalho desenvolvido recorre a um módulo de análise aerodinâmica, que consiste em duas subsecções, uma responsável pelo design e parameterização de perfis e outra dedicada à análise do escoamento. Um módulo aero-acústico, baseado nos modelos de Brooks, Pope e Marcolini e no esquema de análise de ruído do escoamento turbulento de aproximação de Moriarty, Guidati e Migliore, foi desenvolvido. A construção de geometrias de perfis baseia-se na descrição matemática das curvas de Bézier e o software Rfoil é usado para a modelação de camada limite. O programa desenvolvido integra ambos os módulos desenvolvidos num ambiente interactivo único. O módulo de Python, pyOpt foi o seleccionado como o ambiente de desenvolvimento interactivo no qual se efectuaram as várias optimizações. Um algoritmo genético foi seleccionado para operar sobre múltiplos minímos locais e problemas multi-objectivo. Várias famílias de perfis, comuns à tecnologia de turbinas eólicas, foram analisadas dos pontos de vista aerodinâmico e aero-acústico com as ferramentas desenvolvidas e usados como referência geral para comparação. Resultados de várias geometrias de perfis optimizados, que tanto minimizam ruído ou favorecem performance aerodinâmica, foram obtidos e classes de perfis aero-acusticamente optimizados foram identificados nas frentes de Pareto obtidas. Os resultados mostram que um aumento significativo na performance aerodinâmica pode ser conseguida à custa de um reduzido aumento no ruído.

Palavras-chave: geometria de perfis, turbinas eólicas, aero-acústica, optimização multi-objectivo, optimização multi-disciplinar

Abstract

The subject of airfoil design, in the context of wind turbines, is approached with the objective of optimizing the geometry for the best aerodynamic and aero-acoustic trade-off. The work developed is made up of four stages: the aerodynamic analysis module, which consists of two parts, one responsible for airfoil design and parameterization and another dedicated to flow analysis; an aero-acoustic module, based in the semi-empirical model from Brooks, Pope and Marcolini and the turbulent inflow prediction scheme from Moriarty, Guidati and Migliore; the integration of both modules in one single computational tool; and the development of a multi-objective optimization framework. The mathematical description of the airfoil geometry build tool is based on Bézier curves and, the wind turbine dedicated computational tool Rfoil has been used for boundary-layer modeling and inclusion of rotational effects. The code developed integrated both developed modules in a single interactive shell in Python. The Python module pyOpt was selected as the interactive development environment in which the optimization took place. A genetic algorithm was selected to handle multiple local minima and multi-objective problems. Several airfoil families, commonly used in the wind turbine technology, were analyzed from the aerodynamic and aero-acoustic perspectives with the developed tools, and used as reference for general comparison. Optimized airfoil geometries, that either minimize noise emission or favour aerodynamic performance were obtained and classes of aero-acoustically optimized airfoils were identified in the resulting Pareto fronts. Results show that very good aerodynamic performance can be achieved with negligible increase in noise levels.

Keywords: airfoil design, wind turbines, aero-acoustics, multi-objective optimization, multidisciplinary optimization

Contents

Acknowledgments v
Resumo vii
Abstract ix
List of Tables xiii
List of Figures xv

1 Introduction **1**
1.1 Wind power technology 1
1.2 Description of problem 3
1.3 Objectives 5
1.4 Approach and method 6

2 Fundamentals of acoustics **7**
2.1 Sound and noise fundamentals 7
2.1.1 Physical phenomena of sound waves 7
2.1.2 Main physical characteristics and properties of sound 8
2.1.3 Sound pressure and power levels 8
2.1.4 Sound spectrum, octave filters and weighting scales 9
2.2 Wind turbine acoustics 10
2.2.1 Sound and noise of WT 10
2.2.2 General description of sound and noise sources of WT 11
2.2.3 Wind turbine noise standards and regulations 12

3 Aerodynamics **13**
3.1 Aerodynamics and wind turbines 13
3.2 Airfoil shape 17
3.2.1 Airfoil geometry 17
3.2.2 Airfoil parameterization 19
3.3 Airfoil analysis 24
3.3.1 Semi-empirical method 25
3.3.2 RFOIL software 27

4 Aero-acoustic model of airfoils **29**
4.1 Selection of the airfoil noise prediction model . . . 29
4.2 Airfoil noise mechanisms . . . 31
4.2.1 Airfoil self-noise . . . 31
4.2.2 Turbulence Inflow . . . 37
4.2.3 Relevant parameters in sound propagation . . . 42

5 Optimization framework **45**
5.1 Numerical optimization methods . . . 46
5.1.1 Overview . . . 46
5.1.2 Applied optimization to WT technology . . . 47
5.2 Optimization strategy and procedure . . . 48
5.2.1 Objective functions, variables and constraints . . . 50
5.2.2 Optimization script and tools used . . . 52
5.2.3 Optimization problems and issues . . . 55

6 Optimization results and discussion **57**
6.1 Introduction . . . 57
6.2 Code verification and validation . . . 57
6.2.1 Comparison to the work of BP&M . . . 58
6.2.2 Turbulent inflow prediction scheme . . . 59
6.3 Reference airfoils . . . 60
6.4 Effect of the radial position . . . 61
6.5 Effect of the flow speed . . . 65
6.6 Variation of the source-observer distance . . . 68
6.7 Multi-objective optimization and Pareto front analysis . . . 69

7 Conclusions **77**
7.1 Achievements . . . 77
7.2 Future work . . . 78
7.3 Final remarks . . . 80

A AAcoustic: User's Manual **81**
A.1 Code structure and usage . . . 81
A.2 Contents, functions and tools used in the code . . . 82

B Example script files **85**
B.1 Python script example of a MOO . . . 85

Bibliography **99**

List of Tables

3.1 Flow conditions and rotor parameters of a HAWT for the Glauert's optimum distribution . . 16
3.2 Mathemathical methods typically used in airfoil design 20

4.1 Typical values used for ground roughness [Gato, 2010]. 39

5.1 Summary on WT specifications considered in this work 49
5.2 Airfoil parameters considered for optimization purposes (based on specifications from [Vestas, 2011b]) and [A/S, 2009] 50
5.3 Summary of the optimization tests performed 55

6.1 Test parameters used for reference airfoil 58
6.2 Comparison of BL parameters (BPM expressions vs. Rfoil) 59
6.3 Aerodynamic and aero-acoustic properties of several reference airfoils 60
6.4 Constant parameters used for obtaining OptFoils 3, 7, 15, 19, 27 and 31 62
6.5 Optimization results, to assess the effect of radial position on aerodynamic performance . 62
6.6 Optimization results, to assess the effect of radial position on noise levels 64
6.7 Constant parameters used for obtaining OptFoils 25, 29, 27 and 31 65
6.8 Optimization results, to assess the effect of flow speed on aerodynamic performance . . . 65
6.9 Optimization results, to assess the effect of flow speed on noise levels 66
6.10 Direct comparison between OptFoils 25 and 29 and OptFoils 27 and 31 66
6.11 Constant parameters for airfoils 31 and 32 68
6.12 Optimization results, to assess the effect of source-observer distance on noise levels . . . 68
6.13 Fixed parameters for the selected MOO 70
6.14 Optimization results for OptFoils 38 to 42 71

List of Figures

1.1 Historical references of windmills [Manwella et al., 2009]. 1
1.2 Present technological levels of WT, in terms of capacity 2
1.3 World leaders in wind energy 3
1.4 Wind farms in Portugal 4

2.1 Acoustic thermometers [Fonseca, 2007]. 9
2.2 Sound weight scale 10
2.3 Background and mechanical noise sources of a WT 12

3.1 Example of a modern HAWT 14
3.2 Actuator disc applied to a HAWT 15
3.3 Detailed view of the blade cross-section and respective coordinate systems 17
3.4 Blade cross-section examples 18
3.5 Example of the NACA 2415 airfoil geometry, set with different point distributions 19
3.6 Example of the effects of Hicks & Henne functions on the surface of a NACA 0012 21
3.7 Connected Bezier 22
3.8 Bezier modification 23
3.9 Bezier reference geometry 24
3.10 Rfoil improvements 27
3.11 Rfoil measurements in a 2.35m blade 28

4.1 TBL-TE noise mechanism 32
4.2 BL separation noise mechanism 33
4.3 LBL-VS noise mechanism 34
4.4 TE bluntness related noise mechanism 35
4.5 Blade tip noise mechanism 37
4.6 Turbulence inflow noise 38
4.7 Acoustic map of a real HAWT 40
4.8 Directivity of sound parameters 42

5.1 Parameters considered in the optimization procedure 50
5.2 Example of search space for each CP 51

5.3 Diagram of code *AACOUSTIC* 53
5.4 Optimization flow diagram 54
5.5 Illustration of optimizer performance 55

6.1 Code validation: SPL computation results I 58
6.2 Code validation: SPL computation results II 59
6.3 Geometries of the selected reference airfoils 61
6.4 Optimized geometries, to assess the effect of radial position on aerodynamic performance 62
6.5 Optimized geometries, to assess the effect of radial position on noise levels 64
6.6 Optimized geometries, to assess the effect of flow speed on aerodynamic performance . 66
6.7 Optimized geometries, to assess the effect of flow speed on noise levels 67
6.8 Optimized geometries, to assess the effect of source-observer distance on noise levels . 69
6.9 Pareto front for the MOO with $U = 20[m.s^{-1}]$, $r_e = 250.0[m]$ and $r/R = 0.90$ 70
6.10 Selected optimized geometries taken from the Pareto front 71
6.11 OptFoils that minimize SPL values 72
6.12 C_p distribution of the geometries that minimize SPL 72
6.13 $1/3$ octave spectra of the geometries that minimize SPL 73
6.14 OptFoils which maximize aerodynamic performance 73
6.15 C_p distribution of OptFoils which maximize aerodynamic performance 74
6.16 $1/3$ octave spectra results of the geometries that maximize the C_l/C_d ratio 75

Chapter 1

Introduction

1.1 Wind power technology

Wind energy collection technologies have seen major developments and outbreaks in the last 30 years, but it has been a common technological solution since ancient times. The first documented wind power collection technology is attributed to Hero (fig. 1.1 a)), in Alexandria in the 1^{st} century A.D. , passing by the Seistan windmills of Al Masudi in ancient Persia around 644 A.D., and first appearing in northern Europe much later, around the 10^{th} or 11^{th} century [Vowles, 1930], [B. Woodcroft, 1851].

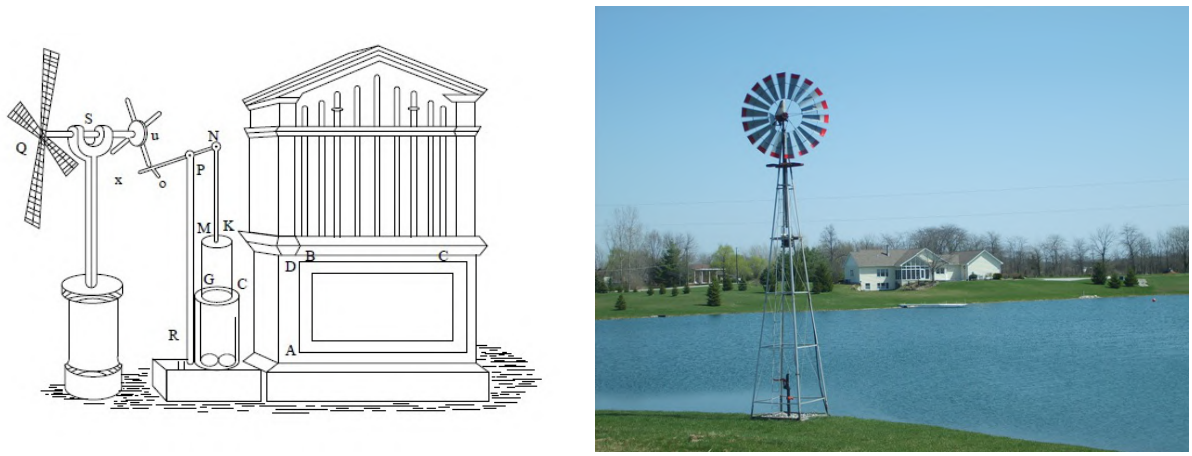

(a) Hero's windmill

(b) Traditional American windmill

Figure 1.1: Historical references of windmills [Manwella et al., 2009].

The introduction of scientific testing and evaluation of windmills, began in the 18^{th} century, with the englishman John Smeaton [Manwella et al., 2009], who formulated three basic rules that are still applied even today:

- The speed of the blade tips is ideally proportional to the speed of wind.
- The maximum torque is proportional to the speed of wind squared.
- The maximum power is proportional to the speed of wind cubed.

These guidelines were the forerunner for making windmills common technologies in the 18^{th} century in Europe, and to convert wind energy into mechanical power. They soon spread to the rest of the world, being one of the most famous examples the traditional American windmill (fig. 1.1).

In the 1970's, works like those from Carson [1962] or Meadows et al. [1972] presented some of the first phylosophies focused on environment and sustainability and made many people aware of the environmental consequences of industrial development with no limits, too dependent on fossil fuels, which sparkled a growing environmental awareness amongst the several spheres of society. Governments and enterprises in general, immediately sought alternate energy sources that could be less hazardous to the planet. The application of wind energy collecting technologies for electrical power production started in the USA, Denmark and Germany, first with great promise (motivated by government aids and incentives) but those initiatives quickly faded due to low energy output (primitive technologies) or economical liability.

However, modern research and development in Europe and America allowed the wind power industry to finally establish itself in the world economy. The 21^{st} century has seen some of the major European suppliers establish manufacturing plants in emerging economical countries, such as China, India, but also in the United States, which had stagnated this industry in the 1990's. In more recent times, the size of the largest commercial WTs have reach power outputs like 6MW, with machine capacity rising to as much as 10MW in several projects under design nowadays [Ferreira, 2011]. This is a very good indicator for assessing the commitment of governments and countries in general to make good use of this technology.

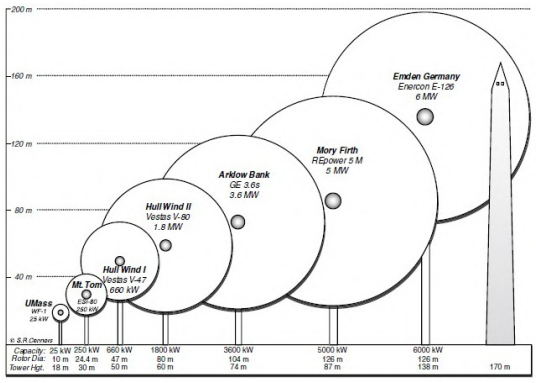

(a) Typical Wind Turbine Sizes [Gato, 2010].

(b) Biggest Wind Turbine in the World (Enercon E-126, Germany) [Ferreira, 2011].

Figure 1.2: Present technological levels of WT, in terms of capacity

According to the World Wind Energy Association [WWEA, 2011], the current worldwide wind capacity reaches 196 630MW, out of which 37 642MW were added in 2010, with a continuous growth at an increased rate of 29% in 2008 but with a slight slowing down in 2009. All wind turbines installed by the end of 2010 worldwide are generating 430TWh per year (more than the total electricity demand of the United Kingdom), making up for more than 2.5% of the global electricity consumption. As seen in fig. 1.3, China continues its role as the most dynamic wind market since the year 2008, claiming number one position from the USA in 2010 and, presenting a value of 18 928MW of wind energy installed. North

America and Asia are catching up with the Europe in terms of new installations, where the emerging eastern European countries stand out. Germany (27 215MW) is still Europe's leader in wind energy, followed by Spain (20 676MW) and despite dropping two positions since 2009, Portugal still stands in a very respectable 11^{th} position, as seen in fig. 1.3.

Position 2010	Country / Region	Total capacity end 2010 [MW]	Added capacity 2010 [MW]	Growth rate 2010 [%]	Position 2009	Total capacity end 2009 [MW]	Total Capacity end 2008 [MW]	Total Capacity end 2007 [MW]	Total Capacity end 2006 [MW]
1	China	44.733,0	18.928,0	73,3	2	25.810,0	12.210,0	5.912,0	2.599,0
2	USA	40.180,0	5.600,0	15,9	1	35.159,0	25.237,0	16.823,0	11.575,0
3	Germany	27.215,0	1.551,0	6,0	3	25.777,0	23.897,0	22.247,4	20.622,0
4	Spain	20.676,0	1.527,2	8,0	4	19.149,0	16.689,0	15.145,1	11.630,0
5	India	13.065,8	1.258,8	10,7	5	11.807,0	9.587,0	7.850,0	6.270,0
6	Italy	5.797,0	950,0	19,6	6	4.850,0	3.736,0	2.726,1	2.123,4
7	France	5.660,0	1.086,0	23,7	7	4.574,0	3.404,0	2.455,0	1.567,0
8	United Kingdom	5.203,8	1.111,8	27,2	8	4.092,0	3.195,0	2.389,0	1.962,9
9	Canada	4.008,0	690,0	20,8	11	3.319,0	2.369,0	1.846,0	1.460,0
10	Denmark	3.734,0	309,0	8,9	10	3.465,0	3.163,0	3.125,0	3.136,0
11	Portugal	3.702,0	345,0	10,3	9	3.357,0	2.862,0	2.130,0	1.716,0
12	Japan	2.304,0	211,0	10,1	13	2.083,0	1.880,0	1.528,0	1.309,0
13	The Netherlands	2.237,0	15,0	0,7	12	2.223,0	2.235,0	1.747,0	1.559,0
14	Sweden	2.052,0	603,8	41,7	15	1.448,2	1.066,9	831,0	571,2
15	Australia	1.880,0	3,0	0,2	14	1.877,0	1.494,0	817,3	817,3

Figure 1.3: Top 15 countries leading wind energy power [WWEA, 2011].

These figures are the proof that governments and countries worldwide are making huge efforts to reduce their dependence on oil and carbon based fuels to provide for the growing electricity demand, and simultaneously demonstrates that wind power technologies are here to stay, either in large wind farms or with massive WT in small numbers. The current technological stage of wind generators has reached a significantly advanced level and now requires continuous improvements and upgrades for its general public acceptance, in order to achieve a perfect balance with its environments.

1.2 Description of problem

As it has been pointed out in the previous section, countries worldwide are making major investments in the wind energy business, but the continuous proliferation of this technology however is not without its flaws.

The technology employed in WTs, is obviously related to the "wind density" present in the location where the WT is placed [Gato, 2010]. Therefore the sitting of wind farms or isolated large wind generators, will often be related with the presence of valleys, small ground elevations or other similar ground characteristics, that favour wind flow and rapid streams of atmospheric air, which are usually and, most likely, near small populated rural and open areas, though in some cases wind farms are built next to large populated areas, thus presenting one major downside of this technology: the direct impact in the community in which it is inserted. This impact has three main topics, according to Manwella et al. [2009], which are:

1. territorial, not always the selected and ideal terrain to place a wind turbine/farm is free to do so;
2. visual, a traditional wind farm completely alters the natural landscape;

3. noise impact, which is the main inconvenient associated to WTs for its direct impact on general public and natural wildlife.

The first two topics are mainly political or economical in nature, so it follows then that from all three it is the last one which, from the engineering point of view, can be better controlled and subject of further improvement.

The phenomenon of noise impact from WT has been reported in detail in several relevant works, proving the existence of the problem and relevance of the matter specifiically on how it may affect health, wildlife and other important parameters in general [S.Stephens et al., 1982], [Colby et al., 2009], [Drewitt and Langston, 2006].

These impact on rural communities are becoming more common with each site built which, following the trends presented in the previous section, are likely to occur in increasing number, in coming years. Proof of that is the Portuguese example, as seen in figure 1.4a), where it is noticeable the bigger density of wind farm sites in the more interior and rural areas, away from the biggest cities in the country. Note as well the specific case of the biggest wind farm[1] in Portugal (with 240MW installed capacity), as figure 1.4b) illustrates how close to the nearby village of Melgaço it is [Sá and Rosa, 2008].

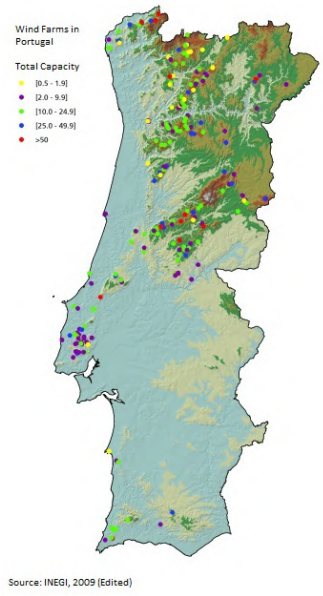

(a) Wind farm distribution in Portugal [INEGI, 2009]

(b) Biggest wind farm in Portugal at Melgaço, Viana do Castelo, near the northern frontier with Spain [Sá and Rosa, 2008]

Figure 1.4: Wind farms in Portugal

We can acknowledge then, that wind farms become a serious and real problem at these locations for they will certainly irradiate a significant amount of sound and noise while working, where even at minimal wind speeds they may be the biggest noise source in the vicinity of a small rural town, when in comparison to the usual rural noise sources. This situation has been a case study for a very long time, beginning in the late 1980's with works like [Hubbard and Shepherd, 1990] or [Grosveld, 1985,]. Several recent case studies and surveys, like [S.Stephens et al., 1982], have been conducted with the

[1] According to the website "Portal da Energia", this is still the 13^{th} biggest Wind Farm in the world

population living near wind farms to assess precisely that. The effects of WT noise in general wildlife and domestic animals is also relevant, as it ultimately affects humans. For further details refer to reports like [Drewitt and Langston, 2006] or [NWCC, 2010], for example.

In greater relevance, the subject of how public health is affected by WTs and/or wind farms is relatively new and has not been of major concern to engineers and companies until very recently. Published studies about the effects of noise originated in wind farms and turbines have identified several potential effects on health, of which many are officially recognized as hazardous to people by the World Health Organization [Davidsen and Andersen, 2009]. The most important effects are hearing loss, annoyance, sleep disturbance, mental health, effects on performance and cognition, vibro-acoustic disease, wind turbine syndrome and even respiratory effects. Further details about the medical aspects of these effects are reported in recent works such as [Colby et al., 2009] or [Leventhall, 2003].

Many surveys and studies have been conducted by independent entities to assess near the populations, the effects of living near WTs and, in general reports show that there is never a complete agreement of all habitants from a certain population in regard to WTs. Factors like direct benefits from living near the WTs or compensations to help face the problems encountered do not seem enough to minimize this impact [van den Berg et al., 2008].

With all this, one can see that, from the engineering point of view, decreasing noise radiation from WT should be taken into account, which is in fact a possibility. The challenge is in doing so, without compromising the main advantages and best qualities of the wind energy technologies.

1.3 Objectives

A simple definition of sound (or noise) is that it originates in the movement of air, induced by any source of movement, that will then propagate in the form of sound waves through air. We can immediately recognize that all the elements required for high noise radiation are present in the normal functions of a wind turbine, and two sources become instantly relevant: aerodynamic and mechanical sources [Manwella et al., 2009], [Hubbard and Shepherd, 1990]. However, as will be discussed in detail in the next chapter, aerodynamics gains much more relevance on this matter since the mechanical sounds from gears, moving parts or any other mechanical elements involved in a wind turbine, are much more easily concealed when compared to the aerodynamic sources.

In order to declare the main objective of the present thesis, one must first identify the best approach to the study of aerodynamic noise source, in order to avoid formulating a too extensive problem and to not lose objectivity. Without going into technical details just yet, we can say that noise resulting from aerodynamic parameters will result from both the interaction of the entire blade(s) with air/wind and the conditions of the local wind characteristics, as well as other conditions such as rotor configuration and hub height. As these aspects are all accounted for in the design stages of the WT, we note that the specifics about the subject of aerodynamic noise can be studied more easily when accounting solely for its most important and elementary parameter that produces that noise, which is the airfoil(s) shape(s) present in the blades. This is true because the true origin of aerodynamic noise from a WT is originated in

the interaction of the airfoil geometries that define all blade sections, with the flow around them [Wagner et al., 1996]. Moreover, the physical parameters that allow a WT to capture the energy of the wind and measure its potential (power) are, ultimately directly related to the airfoil shape [Manwella et al., 2009]. Thus, since both noise and power output are inherently connected by the same single component of a WT, analyzing the geometric shape of the airfoils is the simplest and most efficient way to improve the acoustic radiation of a WT, while maintaining as much as possible the typical power output of the turbine.

We can now state the main objective of this work as finding the best airfoil geometry that delivers optimum aerodynamic efficiency (high lift and low drag) as well as low noise aero-acoustic radiation. We shall declare from this point on that the only aerodynamic analysis here performed will be in regard to the airfoils that make the cross-sections of the blades, and not to the entire blade geometry (meaning that full blade geometry analysis is out of the scope of this work).

1.4 Approach and method

What we described above as the main objective of the work (find the best airfoil geometry that delivers the best compromise between aerodynamic efficiency and low noise radiation) is also a typical description of any optimization problem, where we analyze and study a situation/problem and its main issues and struggle to find the best configuration in which we get the most of the best aspects and the least of the worst. The specific problem of wind turbine noise is then related to various disciplines and scientific subjects. Areas of knowledge and interest in this work are, obviously acoustics, aerodynamics and fluid mechanics, aero-acoustics, numerical computation and mathematics and most importantly optimization procedures and algorithms, all have a key role in this work. The line-up of this work will start by developing numerical models for building and processing airfoil geometries, secondly perform aerodynamic analysis of those airfoil geometries (in order to account for flow behavior), the modeling and implementation of noise prediction schemes for the airfoil and optimizing that result, by relating geometric properties, aerodynamic coefficients and noise levels. Some of the stages of this work are characterized for introducing new aspects such as new strategies for using established theories or the development of new specific computer codes. Of course ultimately, the main new elements this work is expected to introduce are the optimized airfoil geometries, since the focus of this optimization is to help the engineer in the design stages of the airfoils and blades, by giving a realistic evaluation and prediction of the noise radiated from the airfoil he/she is building.

This thesis first presents the acoustic fundamentals to understand the problem at hand and introduces some important assumptions concerning noise, relevant to the work (chapter 2). Some basic aerodynamic topics necessary to the problem and a description of the method and tools used for processing airfoil geometries and flow analysis are presented next (chapter 3). It follows the definition of the aero-acoustic analysis and modeling (chapter 4). The optimization framework, along with all related relevant information regarding code algorithms, is then described (chapter 5). Finally, the main code verification and validation, followed by the most important optimization results are presented (chapter 6), and the thesis is concluded with a description of the main achievements and conclusions (chapter 7).

Chapter 2

Fundamentals of acoustics

In this chapter, the fundamentals of acoustics are presented. The objective of this introductory chapter is to highlight the main topics of acoustics and noise to the reader who is less comfortable with the subject and/or remember some of the main parameters of the theory to the more enlightened reader, as well as point out some relevant assumptions required for the work here presented. It begins with a general description of the physics of sound and the main properties that characterize sound and noise. The importance of frequency, sound pressure and power levels is presented as well as other particularities. Then, a short and general description is given of the relation between WT technology and the theory of acoustics. The basic sound radiation theory of all main sound and noise sources associated with WTs will be presented. Although acoustics is presented here in a very summarized form, it still bears a high relevance to our objective in this thesis, and the more curious reader should report to more detailed references [Júlio M. Silva, 2008], [Lau, 2011], [Fonseca, 2007], [Hubbard and Shepherd, 1990] or [Manwella et al., 2009].

2.1 Sound and noise fundamentals

2.1.1 Physical phenomena of sound waves

Imagine a tuning fork set vibrating. In its movement it will compress air in one side and cause an expansion in the opposite side. Its constant vibrating movement will trigger successive compressions and expansions of layers of air, which in turn will acquire the behaviour of propagating waves, perceived as sound. Both fluids and solids have inertia and elasticity and, therefore, can transmit sound waves. The speed of sound through air is defined as

$$c_0 = \sqrt{\frac{\gamma p}{\rho}} \tag{2.1}$$

where γ is the specific heat ratio of air, *p* is the atmospheric pressure [N/m^2 or Pa] and ρ is the density [kg/m^3]. In standard ambient conditions of pressure and temperature, the speed of sound is 340 m/s, a value set as reference for the rest of the work.

2.1.2 Main physical characteristics and properties of sound

One of the most important properties of sound is frequency (f), which is defined as the inverse of the number of pressure variations of the emitting source per second, known as period (T), $f = 1/T$, measured in Hertz [Hz]. The speed of sound in a substance does not depend on frequency, only on physical properties of that substance. In general, most sources of sound do not have a single frequency, like the example of the tuning fork given earlier that has a clean (pure) sound, but are rather the composition of several sounds with various frequencies simultaneously. An healthy human ear is sensitive enough to recognize frequencies as low as 20Hz and up to 20,000Hz. Infra-sounds are those with frequencies below the lower limit of 20Hz and ultra-sounds lie over the upper limit of 20,000Hz. Both are inaudible to humans.

The other very important property of sound waves is wave length (λ), which is the distance travelled by sound during one period of the vibration. Just like any uniform movement in space is defined by the product of speed and distance, so is the wave length defined by the product of the speed of sound in a substance and the period of vibration:

$$\lambda = c_0 T = \frac{c_0}{f} \tag{2.2}$$

Wave length has a very interesting relation to the behaviour of reflecting sound waves, for it proposes a limitation to the law of sound reflection: any reflecting surface must have dimensions of the same order of the wave length of the incident sound wave. Should the surface be smaller than that wave length, a different phenomena occurs called diffraction.

2.1.3 Sound pressure and power levels

The presence of a sound source leads the layers of air to suffer displacements and pressure variations that can be defined by sinusoidal expressions. As an example of a harmonic plane wave propagation in the x-direction, consider:

$$\xi = \xi_0 \sin\left[k\left(x - \upsilon\right)t\right] \tag{2.3}$$

The new variable presented, *k*, is the wave number and represents the number of wavelengths that exist in a distance of 2π. It is defined as $k = 2\pi/\lambda$. This means that if one wants to measure those displacements and variations, he cannot resort to the mean values of these sinusoidal expressions, for those will be null. Hence for measuring purposes, a root mean square is much more convenient. This requires a logarithmic scale, appropriate for the broad frequency spectrum that the human ear can perceive. Because that spectrum is very wide concerning frequency, it will be even bigger concerning power levels, and a logarithmic scale ”compresses” that wide range of values into a more adequate scale. The unit that defines this scaling is the *bel* and is used in decimals, or rather in *decibels* (dB), otherwise the *bel* would compress the sound pressure scale too much. The *decibel* is set as the logarithmic relation of a certain pressure and a reference pressure. The pressure reference value, p_{ref} , has been

set as the human earing threshold in response to a sound emitted with a 1000Hz frequency. It is defined as $p_{ref} = 2{\times}10^{-5}$ Pa. For any value of sound pressure, *p*, the Sound Pressure Level (SPL) is defined by

$$SPL[dB] = 10\log\left(\frac{p^2}{p_{ref}^2}\right) = 20\log\frac{p}{p_{ref}} \tag{2.4}$$

When the pressure p, equals p_{ref}, the result is zero, which means the SPL is 0 dB. For an increment of 200 μPa, the SPL is increased by 20 dB, up to a limit of 140 dB, representing the human threshold of pain. This relation between pressure and the *decibel* is a very realistic one, and many authors resort to what is usually called an acoustic thermometer, to exemplify that relation, with every day noise sources, as illustrated in 2.1.

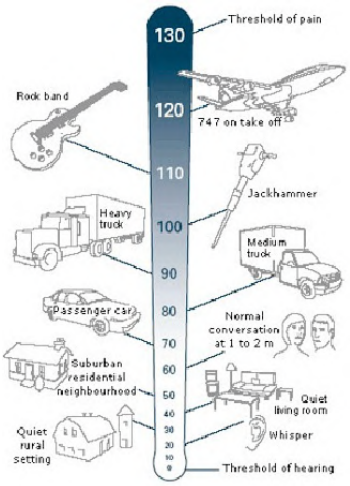

(a) Traditional acoustic thermometer

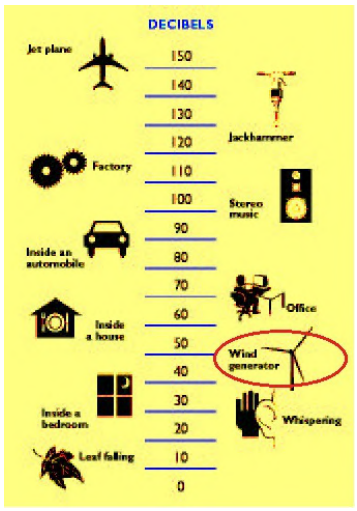

(b) Detail of wind turbine noise, in an acoustic thermometer

Figure 2.1: Acoustic thermometers [Fonseca, 2007].

When the frequency spectrum of a source is available, the Total Sound Pressure Level (SPL_{total}) may be determined as the logarithmic sum of the SPL values in the considered frequency range,

$$SPL_{total} = 10\log\sum_{i=1}^{N} 10^{\frac{SPL_i}{10}} \tag{2.5}$$

where SPL_i is the SPL value of the i^{th} frequency in the spectrum. This is equivalent to a situation where multiple sources are radiating noise, each in its own frequency.

2.1.4 Sound spectrum, octave filters and weighting scales

Any given sound source will typically be composed of an infinite number of components, each with a different frequency. It is then obviously impossible to measure a continuous spectrum, but a discrete one is much more suitable. The accuracy of this discrete process is dependent on the filters used in the data acquisition method. Filtering individual frequencies (on a 1Hz basis) is totally inefficient, whereas isolated frequency bands is much better. If a series of filters is used at the same time, with the

highest frequency of one filter coinciding with the lowest frequency of the next filter, the coverage of all the audible sound spectrum is possible (octave spectrum). The most commonly used of this filters is the octave filter, but a more accurate measure can be achieved if using a 1/3 octave filter, much more suitable for the task at hand concerning SPL values from WT.

Finally, there is another important aspect in sound and acoustics engineering not yet mentioned. There are four, generally used acoustic measurement scales (A, B, C and D - apart from the purely linear scale, with no corrections whatsoever - see fig. 2.2). Of all four the most commonly used is the A weighted scale, because it resembles the most to the human perception of sound [Júlio M. Silva, 2008], and is usually used in important acoustic measuring like industrial noise regulation or analysis of building acoustics and will also be used here.

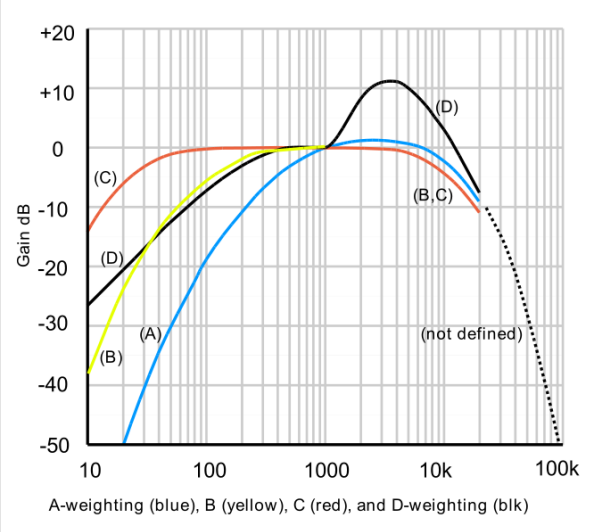

Figure 2.2: Typical sound weight scales [Sociedad Espanola de Acústica, 2005]

2.2 Wind turbine acoustics

2.2.1 Sound and noise of WT

There are four types of noise that can be generated by wind turbine operation: tonal, broadband, low-frequency, and impulsive.

Tonal: Tonal noise is defined as noise at discrete frequencies. It is caused by wind turbine components such as meshing gears, interaction of the flow with the blade surface (nonlinear boundary layer instabilities), the discontinuities resulting from the flow when leaving the blade (vortex shedding from a blunt trailing edge), or unstable flows over holes or slits.

Broadband: This is noise characterized by a continuous distribution of sound pressure with frequencies greater than 100 Hz. It is often caused by the interaction of wind turbine blades with atmospheric turbulence, and is also generally described as a characteristic ”swishing” or ”whooshing” sound.

Low-frequency: Low-frequency noise is comprised by all audible noise in the range of 20 to 200 Hz. It is usually associated with the rotation of the blades or rotation of lifting surfaces and the passage of

blades through tower velocity deficit or wakes. The connection to rotation suggests that frequency is related to blade passing frequency which is most relevant in downwind configurations of wind turbines. Because only upwind configurations are here considered and because of the the frequency range in which these noises are considered, they immediately become nearly irrelevant.

Impulsive: Consist in short acoustic impulses or thumping sounds that vary in amplitude with time. Early works like [Grosveld, 1985,] and [Grosveld and K. P. Shepherd and, 1985] performed some of the very first sound measurements in real scale generators. One of the immediate main conclusions at the time was the configuration of the rotor, being an upstream (or upwind) rotor less noisy and a downstream one noisier due to the interaction of the tower wake with the blades, being that noise impulsive in character.

2.2.2 General description of sound and noise sources of WT

Some manufacturers make their own noise assessment of their machines, like the Vestas manufacturer for example, who states that its machines will produce overall noise values ranging from 98 to 107 dB(A) [Vestas, 2011a]. Nowadays the accepted noise sound sources from a WT are four: mechanical, aerodynamic, background and turbulent inflow noise (though this last one is inherently related to the aerodynamics of a WT and it will here be described as a sub-category of the aerodynamic noise sources because of its high relevance). A summary of each of these noise sources follows. A more detailed review is included in the texts of [Wagner et al., 1996] and [Manwella et al., 2009].

Background Noise Sources: These can be various in nature: wildlife activity such as birds and farm animals, human activity within the premises of a WT, such as farm harvesting, factory labouring, traffic, etc, wind interaction with multiple objects such as facilities, trees and vegetation, terrain, or other local lithographic characteristics. If the background noise levels are higher than the ones radiated from a WT, the receiver will not notice the WT. Of course, it also works the other way around. Figure 2.3 demonstrates how relevant background noise is, at different wind speeds, when compared to WT noise. The importance of background noise is to assess the so called Receiver Response and a more interested reader should refer to the studies and surveys of [Cummings, 2010], [S.Stephens et al., 1982], [Colby et al., 2009] and/or [van den Berg et al., 2008] for more detailed information on the subject.

Mechanical Noise Sources: Mechanical noise originates from the relative motion of mechanical components and the dynamic response that results. Mechanical noise is transmitted along the structure of the turbine and is radiated from its surfaces. The main sources of such noise can been seen in fig. 2.3b). The figure shows the type of transmission path and example sound power levels for the individual components of a typical WT. Since the emitted noise is associated with the rotation of mechanical and electrical equipment, it tends to be tonal (of a common frequency) in character, although it may have a broadband component. Though relevant in an acoustic measurement, mechanical noise in modern wind turbines is mostly tonal and nearly negligible.

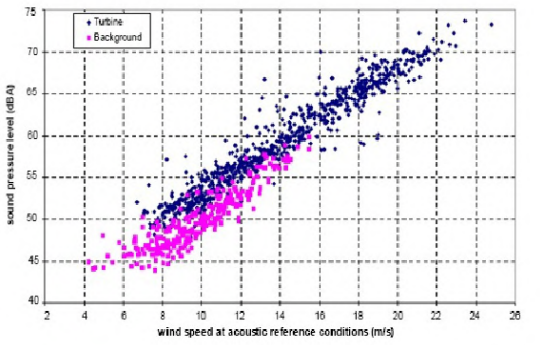

(a) Comparison between WT noise and typical background noise near wind farms [Vargas et al., 2009].

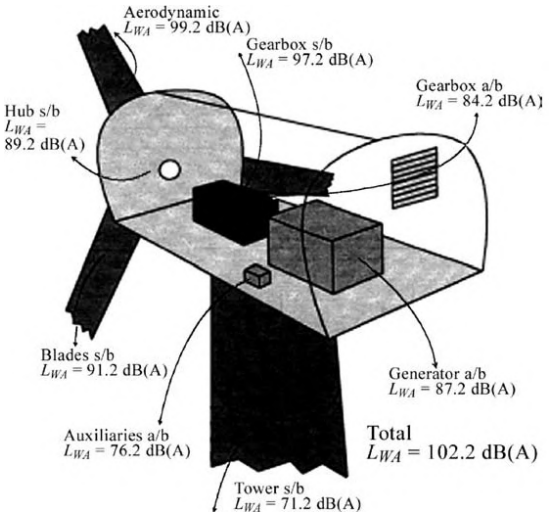

(b) Example of mechanical noise sources in a typical 115m, 2MW WT [Wagner et al., 1996].

Figure 2.3: Background and mechanical noise sources of a WT

Aerodynamic Noise Sources: Aerodynamic noise originates from the flow of air around the blades and a large number of complex flow phenomena generate this type of noise. It generally increases with tip speed or tip speed ratio. It is broadband in character and is the main source of wind turbine noise. When the wind is turbulent, the blades can emit low-frequency noise as they are buffeted by changing winds. The various aerodynamic noise mechanisms are divided into three groups: (1) low-frequency noise, (2) inflow turbulence noise, and (3) airfoil self-noise. The last two parameters are the most relevant to this work as both are directly related to the airfoil geometry and will be presented in detail in chapter 4.

2.2.3 Wind turbine noise standards and regulations

In the scope of this work, it will be interesting to understand how most countries face the subject of noise from WTs from the judicial point of view. No general common laws exist, as each country approaches the problem in its own way, but it is relevant to say that noise restrictions exist, with examples of proposed laws in Denmark, Portugal and the United Kingdom, setting general noise thresholds at 40 to 45 dB(A) in total emitted SPL. Most laws enforce entities to make regulated noise assessments with specific preset parameters and following international standards, such as the EN 45000. In more recent years, concern on this matter has increased for low-frequency noise [Leventhall, 2003], [Vargas, 2008].

Chapter 3

Aerodynamics

This chapter begins by presenting the basics of aerodynamics, required for correctly integrating the airfoil theory into the subject of WTs. The following text will also present to the reader the methods and techniques used in the final code developed, as well as point out the most relevant algorithms created. It is assumed from here on that the reader has a minimum amount of experience with the subjects of fluid mechanics and aerodynamics, leaving here some interesting references on these subjects if that is not the case (see [de Brederode, 1997], [Eça, 2010], [Houghton and Carpenter, 2003] or [Bloomer, 2000]).

The chapter continues by presenting the airfoil geometry methods used here, followed by the discretization techniques used in the code developed. The later section is of major importance as the methods and resources used in the airfoil design and parameterization stages are presented and how are these used in the scope of the work. The external tools (external as in not developed in this work and collected from other authors) required for other aerodynamic analysis, are then presented, compared and selected in order to be used here.

3.1 Aerodynamics and wind turbines

Following the introduction to the subject of wind power collecting technologies, in section 1.1, let us proceed to a more detailed view on the fundamentals and theories that make modern **Horizontal Axis Wind Turbines** (**HAWT**) work.

General description of the technology: The structure itself is rather simple and fairly common nowadays (see fig. 3.1). The *rotor* is made of three blades (rarely more or less are used, unless for specific WT), fixed to a *hub*. The hub is responsible for the blade control and for connecting the rotor mechanism to the rotor shaft (and consequently to the electrical generator). The *nacelle* is the container that holds all mechanical organs of the machine (gearbox, rotor brake, bearings, etc) as well as the generator and control systems.The *bedplate*, which connects the nacelle to the tower, is responsible for a very important movement of the WT, the *yaw* system, allowing the HAWT to face the direction of the wind flow, almost as a sunflower follows the sun. Finally, the *tower* is the structure that holds the machine in place

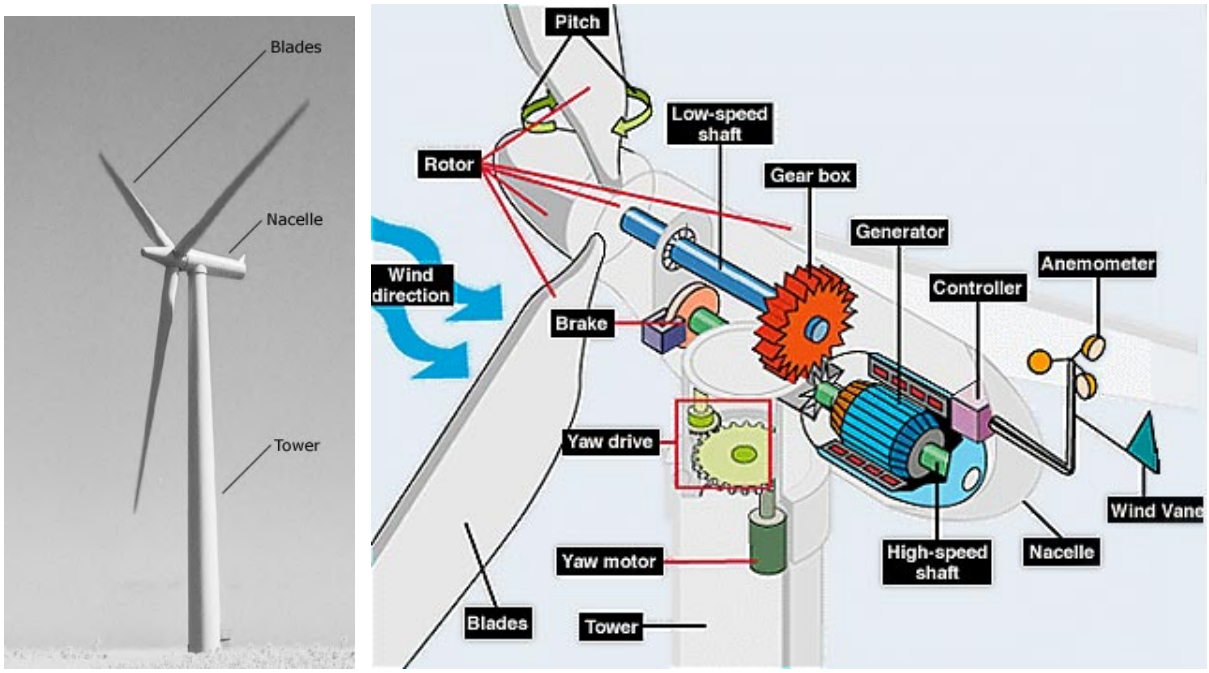

(a) Modern HAWT (b) Modern HAWT (detailed view of the nacelle)

Figure 3.1: Example of a modern HAWT [Aksu, 2011].

and that connects the HAWT to the electrical grid ([Manwella et al., 2009], [Gato, 2010], [van Bussel, 2011]).

Integrating this work in a real life application: In the specific context of this work, there are some basic assumptions relevant to emphasize and that will hold for the remainder of this thesis. When performing the final optimization procedure, some generic aspects about the WT and the wind are required to be set as constants. The best approach to estimate these values is to think of a real WT and place it in a real scenario. Beginning with the most relevant parameters regarding the wind, the freestream is assumed at all times parallel to the axis of rotation of the WT. It is also important to establish some generic parameters regarding the WT itself, that may be directly related with the airfoils here being optimized. A WT in the power range of 2 to 3 MW is considered, which provides an estimate about its size and rotor diameter. Typical values for tower height of these machines are 70 to 80m tall, rotor diameter is 80 to 90m (maximum blade span of 45m). About the location or the site, it is interesting to account for actual known cases[1], like suburban environments or rural locations. This kind of information will be continuously updated throughout this thesis, each time it is relevant to specify it in the context of the chapter it is inserted.

Aerodynamics of a modern HAWT: The main principles that make a WT work are the same as the ones used in any other axial turbomachine. A common strategy used to study these machines can be accomplished when combining the linear momentum theory over the blades with the axissymetric induced flow of an actuator disc. The disc is set over the rotor and comprised in a control volume from

[1] Following the author's own experience, the wind farm near the location of Malveira, in the suburbs of Lisbon has been used as reference model to approach this problem

a downstream to an upstream boundary (or stream-tube boundary, see fig. 3.2). This method is derived from the ship industry, and is usually attributed to Rankine and Froude [Gato, 2010], and follows the assumptions that the fluid flow is homogeneous, incompressible and in steady state; no frictional drag accounted; an infinite number of blades are present; uniform thrust over the disc or rotor area; and the static pressure far upstream and far downstream of the rotor is equal to the undisturbed ambient static pressure.

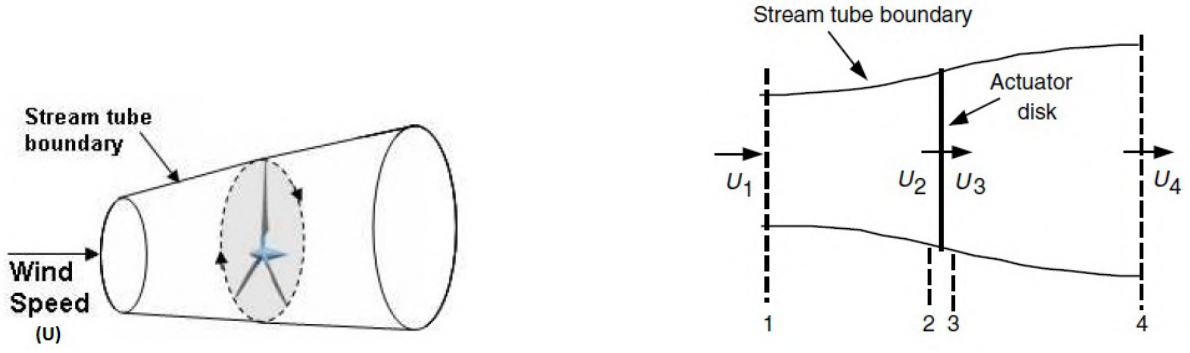

(a) Streamtube control volume over a HAWT (velocity of undisturbed flow is *U*)

(b) Actuator disc applied to a HAWT (specific velocities at locations 1, 2, 3 and 4 are as shown)

Figure 3.2: Actuator disc applied to a HAWT [Manwella et al., 2009].

In addition to this, the model may take one more important assumption in regard to the wake, which separates the theory in two [Gato, 2010], [van Bussel, 2011]. First, the simplest method, known as the actuator disc with non-rotating wake (Rankine-Froude) assumes no rotation in the wake and secondly, the more realistic Glauert's optimum distribution. Basically the difference is that in the first approach the flow is considered linear and only variations in the axial direction are considered being the radial component of the flow reduced to zero. The second method accepts a 2D flow and presents rotation of the wake, which is associated to an increasing pressure in the radial direction, downstream of the disc. This means that the radial and tangential components of the velocity at the location indexed as 3 (following the schematics from figure 3.2) are dependent on the radial position (r), and the rotation of the wake introduces a few parameters that are relevant to point out:

$$a(r) = \frac{U - U_{2a}(r)}{U} \tag{3.1}$$

$$a^{'}(r) = \frac{-U_{2t}(r)}{2\Omega r} \tag{3.2}$$

$$x = \frac{\Omega r}{U} \tag{3.3}$$

The first parameter a is called the axial induction factor ($a < 1$) and relates with the decrease of U when approaching the blade due to the rotation effect. The second parameter a' is the induction factor of rotation and x is a dimensionless variable called simply as velocity ratio, which relates the rotational speed Ω ($rad.s^{-1}$) with the freestream velocity U and is quite useful to set a specific cross-section radial

position of the blade, as it accounts for r as well. In fact, this last parameter is called tip velocity ratio (λ) when it accounts for the tip of the blade (having $r = R$), which for most modern WT takes the value of 7 [Gato, 2010]. For the case of a HAWT in the power range of 2 to 3 MW, the blade span ranges from 35 to 40m in length [Enercon, 2010], [Vestas, 2011a].

x	a	a'	x	a	a'
0.25	0.280	1.364	4.00	0.332	0.0137
0.50	0.298	0.543	4.50	0.332	0.0108
0.75	0.310	0.294	5.00	0.332	0.00880
1.00	0.317	0.183	5.50	0.332	0.00728
1.25	0.322	0.124	6.00	0.333	0.00612
1.50	0.324	0.0894	7.00	0.333	0.00451
1.75	0.326	0.0672	8.00	0.333	0.00346
2.00	0.328	0.0524	9.00	0.333	0.00273
2.50	0.330	0.0342	10.00	0.333	0.00222
3.00	0.331	0.0240	11.00	0.333	0.00183
3.50	0.331	0.0177	12.00	0.333	0.00154

Table 3.1: Flow conditions and rotor parameters of a HAWT for the Glauert's optimum distribution [Gato, 2010].

Blade Element Momentum: The actuator disc theory alone does not deliver detailed information about the flow over the blades nor does it relate the analysis performed over the HAWT with the blade geometry. The Blade Element Momentum theory (or **BEM** [Gato, 2010], [van Bussel, 2011]) is a very important add-on to this model as it allows the study of the flow around the blade, while crossing it by its cross-section (airfoil geometry) at a distance r, from the axis of rotation (fig. 3.3). The BEM theory performs an analysis over the blade cross-section by setting the local flow conditions immediately before and after the airfoil, while accounting for the rotational effects of the blade (by including the rotational factors described above) [van Bussel, 2011], which is of great relevance to the task at hand in this work. This is very important not only for better and more accurate results, but also to take full advantage of the selected tools for performing these flow analysis, as it will be detailed later in section 3.3. It is worth noting that for the remainder of this work, the relative velocity of the flow over the airfoil will be computed in regard to the coordinate system presented in fig. 3.3, and the effective angle of attack on the airfoil will be selected according to this system. This means that a very important parameter cannot be forgotten when analyzing the full scale WT and its blades, which is the *twist* angle (θ_r). In fact, angle θ_r should be the section pitch angle (θ_p), which is the sum of the blade cross-section twist angle and the blade pitch angle [Manwella et al., 2009]. As a result of all this, the relative velocity of the airfoil (*W*), accounting for full effect of rotational effects using table 3.1, can be computed using all above equations and strictly following the coordinate system presented in fig. 3.3 as

$$\left.\begin{aligned} \tan\phi = \frac{U(1-a)}{\Omega r(1+a')} = \frac{(1-a)}{x(1+a')} \\ \sin\phi = \frac{U(1-a)}{W} \end{aligned}\right\} \quad \Longrightarrow W = \frac{U(1-a)}{\sin\left[\arctan\left(\frac{1-a}{x(1+a')}\right)\right]} \tag{3.4}$$

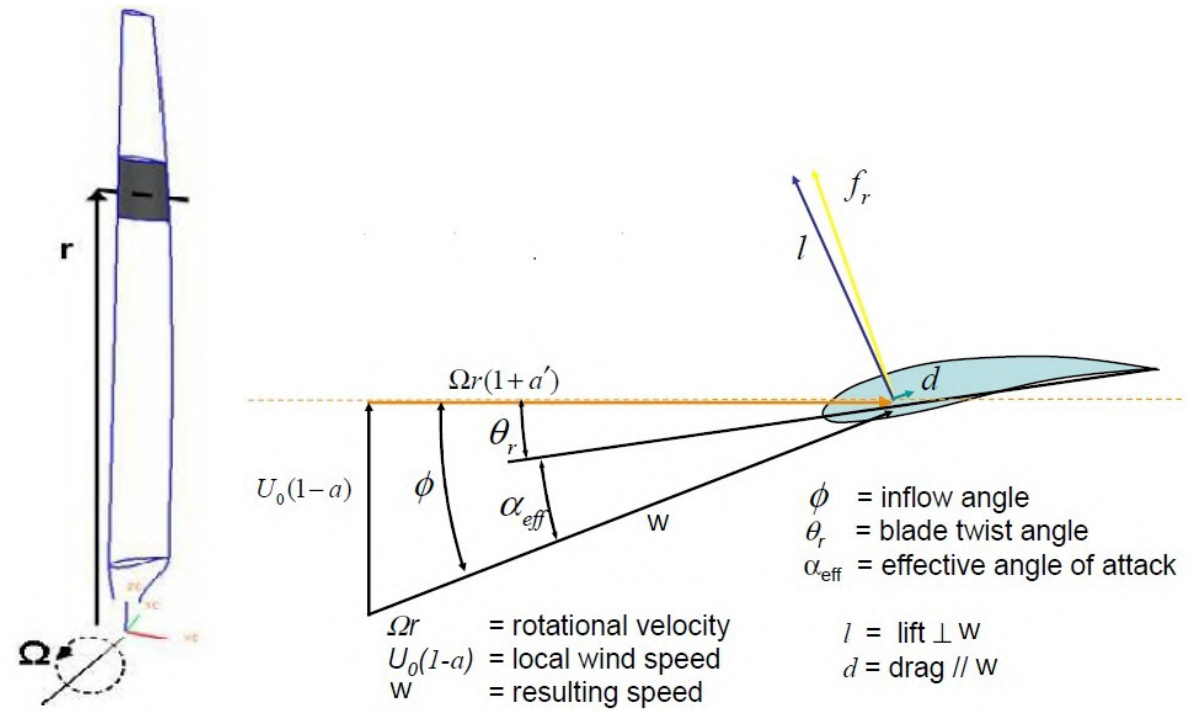

(a) Example of blade cross-section, at position r

(b) Detail of coordinate system used in the HAWT case

Figure 3.3: Detailed view of the blade cross-section and respective coordinate systems [van Bussel, 2011], edited.

Airfoils for use in WT: Many works have been developed on the subject of airfoils for use in WT (for example [Timmer and van Rooij, 2003], [Migliore and Oerlemans, 2004] or [Fuglsang et al., 1999], present the experimental results on wind tunnel tests on some of the most suitable airfoils for use in modern WT), because each application has its own requirements and specifications and wind turbines are not different. One of the most important issues in WT design is precisely the blade design, which must take into account several important characteristics such as structural integrity or aerodynamic performance, thus requiring that more than one airfoil geometry is present in its structure (fig 3.4). This means that the search for several airfoil geometries is required and so the objective of this work will also proceed in that direction, of developing more than one airfoil for a single blade.

3.2 Airfoil shape

3.2.1 Airfoil geometry

This section introduces the starting point of this work. In order to optimize an airfoil, being a purely aerodynamic or an aero-acoustic optimization, one must first set a base airfoil geometry as reference. Airfoil geometry can become a rather broad subject as airfoils may be used for many applications and many efforts to establish general standards for this subject have been attempted over the years. Historically, conventional airfoils began with the works of the brothers Wilbur and Orville Wright in the first mechanized airplane, in 1903. Others followed, like the French aviators Farman and Antoinette or the German

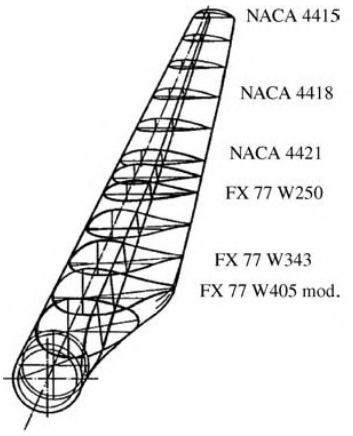

Figure 3.4: Example of the several airfoil geometries used in an old WT blade [Manwella et al., 2009].

Gottingen Institute for Aerodynamic Investigation [Mason, 1995]. In the USA, the predecessor institution of todays National Aeronautics and Space Administration (NASA), the National Advisory Committee for Aeronautics (NACA), established in 1930 a series of guidelines for the geometric definition of an airfoil by a series of 4 digits, in which:

- The first number indicates the camber;
- And the second corresponds to the coordinate where the maximum camber occurs, in decimals
- The last two digits set the relative thickness of the airfoil, t ($100 \times t$ gives the last two digits in the NACA 4-digit denomination);

The airfoil is set in a dimensionless axis where both the x and y coordinates are normalized by the chord, as well as the thickness. The result is a geometry limited in the x-axis, between 0 and 1, and where the x and y coordinates are expressed in percentage of the chord. This is possible because the x-axis is aligned with the chord [Mason, 1995], [de Brederode, 1997].

The NACA 4 digit series proves to be a good starting point for producing reference airfoil geometries. Of major importance in the design of an airfoil surface is the option to set a larger number of points that set the surface at specific locations, by not necessarily setting a uniform distribution for the points over the surface (see fig. 3.5a)). Take the example shown in fig. 3.5c)), where the more detail is given to the TE section, where the flow leaves the airfoil. In most design processes, that section of the surface is usually left open (first and last points do not need to be on top of each other –see [de Brederode, 1997]) which results in a geometric discontinuity. This discontinuity can be used to measure the TE bluntness which in the scope of airfoil self noise prediction, this bluntness value requires great accuracy because it is critical for a proper and correct aero-acoustics prediction scheme, as we will acknowledge in the next chapter. In this work, a computational algorithm has been used for describing the airfoil surface, that gives the user the option to choose which part of the surface to have a higher concentration of points, as well as the number of points to be used in each section, leaving the remaining geometry described with a simple uniform distribution. The options available are a uniform point distribution, a distribution focused on the leading edge (fig. 3.5b)), another focused on the trailing edge (fig. 3.5c)) and finally a

hybrid version that allows for higher concentration of points on both the leading and trailing edges (fig. 3.5d)).

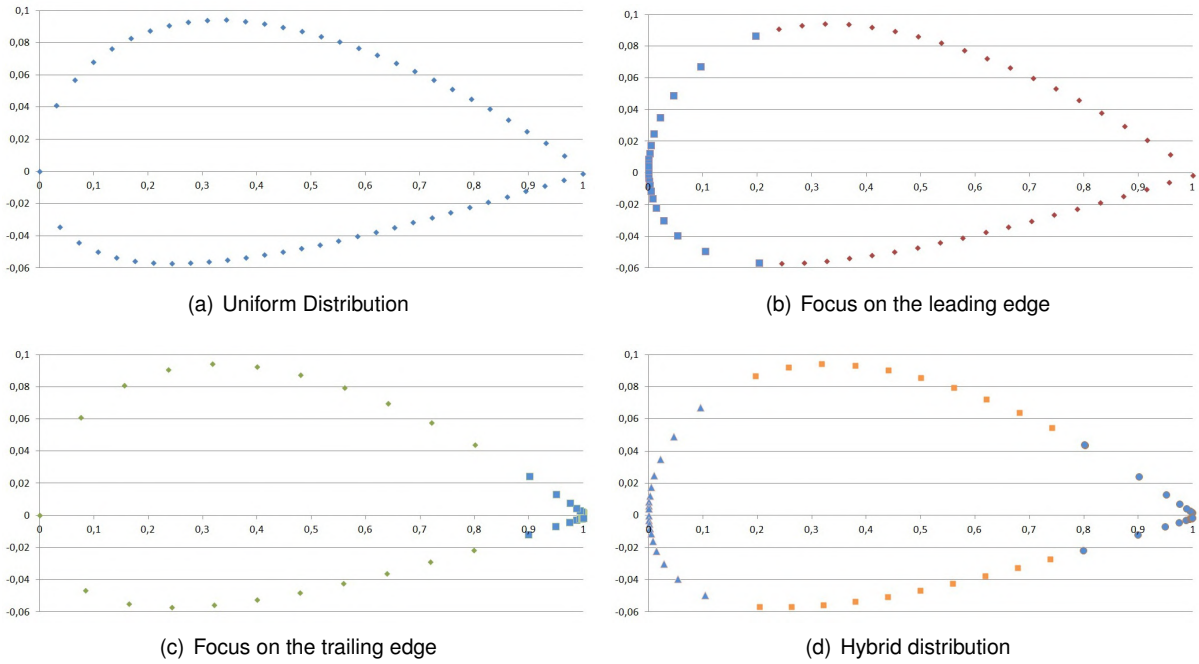

(a) Uniform Distribution

(b) Focus on the leading edge

(c) Focus on the trailing edge

(d) Hybrid distribution

Figure 3.5: Example of the NACA 2415 airfoil geometry, set with different point distributions

A NACA 5 digit series also exists and follows an approximate theory to the 4 digit series [Jacobs and Pinkerton, 1935]. The 5 digit series airfoils are also used in this work, though limited to the numbers 2xx12, where xx may be 10, 20, 30, 40, 50, 21, 31, 41 and 51. Because of its simplicity and because it has become common practice over the years to use NACA airfoils in many sectors of the aeronautical industry (including the wind turbine field), this method for defining an airfoil geometry was one of the chosen to set a primary reference airfoil geometry. In addition to that purpose, this method was also used to obtain several reference NACA airfoils to make direct comparisons to the optimized airfoil geometries obtained here.

3.2.2 Airfoil parameterization

The airfoil geometry is directly related to its aerodynamic operating characteristics, C_l and C_d. Having a reference geometry, we can now worry about how to alter the surface shape to improve the relation of C_l and C_d coefficients.The surface disturbances introduced in the original airfoil reference may range from local small increments to global shape alterations of the surface. Many parameterization studies of airfoil geometry can be found in the references section, being some of the most important [Drela, 1998], [Song and Keane, 2004] and [Samareh, 1999]. These references are a good starting point to get to know the most important parameterization methods most suitable for airfoil design and also present some good cross comparison to acknowledge which may be better.

The work of [Grasso, 2008] is focused on this subject alone and presents a very complete and interesting comparison between the many methods available and presently used (table 5.3). As we

Table 3.2: Comparison of various mathemathical methods typically used in airfoil design [Grasso, 2008].

Parameterization	**Advantages**	**Disadvantages**
Hicks & Henne functions	Few parameters	Harmonic expression
		Not easy user usage
6^{th} degree Legendre function	Polynomial expressions	6^{th} degree expression
		Not easy inflection controllability
3^{rd} degree spline curves	Polynomial expressions	Necessity of segmentation to accurate description
3^{rd} degree Bezier curves	Polynomial expressions	Necessity of segmentation to accurate description
	Direct connection between parameters and geometry	
	Easy inflection points controllability	
	Easy user usage	
	Approximant formulation	

can see from this work, the selection of the parameterization method depends highly on the level of disturbance we want to make on the surface and if one is willing to work with more or less variables. The designer must bear in mind two important criteria. The first criterion takes into account the capability of the formulation to describe and control of the airfoil shape. Because of the use, in this context, of regularity and derivative properties, control of inflection points are particularly important to evaluate the potentialities of a formulation. The second criterion takes into account the quantity of parameters necessary to describe the curve and the geometrical meaning of these parameters. The connection between mathematical formulation and geometrical interpretation is very important to help the designer to set up the design variables and to predict, for example, which zone of the airfoil will be modified; in this way also local modifications are possible. The Hicks & Henne bumps technique and the Bezier curves formulations are the most popular techniques and are briefly described next.

Hicks & Henne bumps: The Hicks & Henne [Hicks and Henne, 1978] bumps, have been used for many years in airfoil parameterization for its simplicity and ease in implementing as a computer algorithm. The basic idea is to use a mathematical function (of either sinusoidal or exponential nature) by a specified number of points, between 0 and 1 in the x range, and then add the resulting y coordinates to the y coordinates of the original surface

$$y_{modshape} = y_{original} + \sum_{i=1}^{N} a_i f_i(x) \tag{3.5}$$

The number of parameters the user needs to input is rather small which contributes to its simplicity. These parameters are the number of functions, or bumps, to introduce (*N*), the nature of the function to use,

$$Exponential \rightarrow f(x) = a.\frac{\sqrt{x}(1-x)}{e^{bx}} \tag{3.6}$$

$$Sinusoidal \rightarrow f(x) = a.\sin(\pi x^b)^3 \tag{3.7}$$

and its respective variables of amplitude and phase (a, for amplitude and b, for phase in the case of a sinusoidal and length in the case of an exponential). The main resulting advantage it offers is the ability for producing either big or small increments/decrements on the surface, as well as many of these bumps as desired. It also offers the option for local and specific variations of the surface, as the authors of the work [Hicks and Henne, 1978] state, especially for small variations near the leading edge when using exponential functions. The biggest disadvantage of the method is that both the sinusoidal nature of the functions, and the knowledge of the exact values of the controlling parameters within the functions to obtain these bumps, or in other words the control of the inflection points, is rather difficult. Figures 3.6a) and 3.6b) illustrate very effectively those disadvantages.

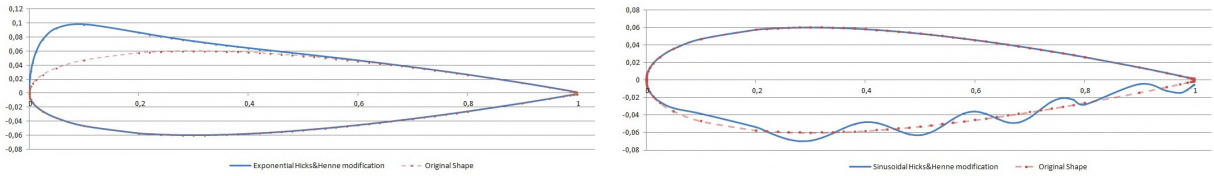

(a) Exponential function

(b) Sinusoidal function

Figure 3.6: Example of the effects of Hicks & Henne functions on the surface of a NACA 0012

Bezier curves: A Bezier curve is somewhat more complex than the previous method but offers major advantages when used in an optimization process like the one presented here (many authors have successfully used this method in similar works [Wenming et al., 2008], [Derksen and Rogalsky, 2010], [Prasanth and Lal, 2010]). The potential of the Bezier curves offers solutions to problems in several fields such as computer graphics ([Tang and Désidéri, 2002]) because of the easy control of the inflection points it allows. Furthermore, it bears a rather small number of variables making it a user friendly method. In the specific airfoil design application, it presents major advantages when searching for an unknown specific geometry because it does not bear the inconveniences of sinusoidal expressions or high order polynomials. For these reasons and others explained in detail next, this will be the parameterization method used in this work.

Let us begin by the basics and present the mathematical general description of a Bezier curve (binomial form):

$$\begin{aligned}\mathbf{B}(t) &= \sum_{i=0}^{n} \binom{n}{i} (1-t)^{n-i} t^i \mathbf{P}_i \\ &= (1-t)^n \mathbf{P}_0 + \binom{n}{1} (1-t)^{n-1} t \mathbf{P}_1 + \cdots \\ &\cdots + \binom{n}{n-1} (1-t) t^{n-1} \mathbf{P}_{n-1} + t^n \mathbf{P}_n, \quad t \in [0,1],\end{aligned} \tag{3.8}$$

Of major interest in the scope of this work, are the 2^{nd} and 3^{rd} order Bezier curves:

$$\mathbf{B}(t) = (1-t)[(1-t)\mathbf{P}_0 + t\mathbf{P}_1] + t[(1-t)\mathbf{P}_1 + t\mathbf{P}_2] \ , t \in [0,1] \tag{3.9a}$$

$$\mathbf{B}(t) = (1-t)^3\mathbf{P}_0 + 3(1-t)^2 t\mathbf{P}_1 + 3(1-t)t^2\mathbf{P}_2 + t^3\mathbf{P}_3 \ , \ t \in [0,1] \tag{3.9b}$$

Bezier curves have several properties that are relevant to point out [Scarbrough, 1992]:

1. The basis functions are real;
2. The degree of the polynomial defining the curve segment is one less than the number of defining polygon points;
3. The curve generally follows the shape of the defining polygon;
4. The first and last points on the curve are coincident with the first and last points of the defining polygon;
5. The tangent vectors at the ends of the curve have the same directions as the first and last polygon spans, respectively;
6. The curve is contained within the convex hull of the defining polygon, i.e., within the longest polygon obtainable with the defining polygon vertices;
7. The curve exhibits the variation diminishing property: the curve does not oscillate about any straight line more often than the polygon itself;
8. The curve is invariant under an affine (linear) transformation.

Additionally, several Bezier curves may be connected, given that the user respects the connectivity conditions (fig. 3.7): the final point of a first Bezier curve will coincide with the first point of a second Bezier curve, if the tangent over the common point includes the previous and next points of either Bezier curves [Grasso, 2008].

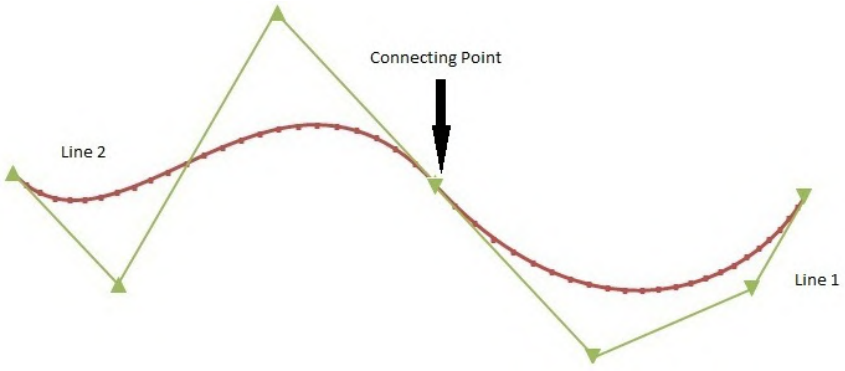

Figure 3.7: Example of two Bezier lines connected

The shape of the Bezier curve is controlled by the position of the **control points** (**CP**). This is a major advantage since instead of working with a set of x and y coordinates to define the curve, like in the Hicks & Henne bumps, we have a set of just three or four points, according to the curve order, which will be the controlling variables in the final optimization. However the user must always part the airfoil geometry

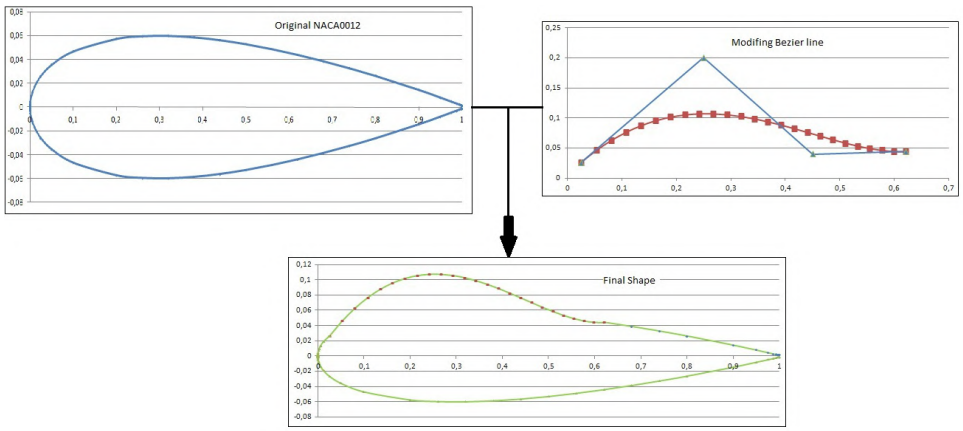

Figure 3.8: Example of the modification of the NACA 0012 geometry with a single 3^{rd} order Bezier line

into several sectors defined by as many Bezier curves, because one single Bezier curve is insufficient to set an entire airfoil geometry. Hence the partition of the geometry into several sectors presents the major downside of this method because one must know from the start the coordinates of the control points of all curves that build the final surface as close to the desired airfoil shape as possible. Hence, two approaches were taken in this work regarding Bezier curves:

1. The first approach begins with a reference shape set from a NACA 4 digit surface. A Bezier curve is then used in the same way as before in the Hicks & Henne method, only instead of creating a line from a specific mathematical function and adding the resulting coordinates, we will be creating a Bezier curve, setting the first and last control points over the original geometry and then choosing the coordinates of the inner control points, thus creating a new shape and replacing that shape with the original sector surface, as illustrated in fig. 3.8. The option of adding as much Bezier curves as we may need is available at this point, to allow the user to superposition several Bezier curves on top of each other.

2. The objective of the second approach is to create an entire airfoil reference geometry set solely by a number of Bezier lines, rather than by the usual NACA 4 digit description,to more easily control the disturbance imposed on the airfoil surface. The strategy taken uses a set of four Bezier curves (four sectors, 16 control points where 6 are coincident) connected to each other. The application of Bezier curves to airfoil design is usually associated to an optimization process of its own, with the objective of searching the coordinates of all control points that comply with the Bezier connectivity conditions and accurately set a reference geometry that defines a smooth aerodynamic shape. This optimization process serves only to identify the coordinates of the control points that set a reference geometry, but will not need to be performed here as several references already deliver the coordinates of some airfoils that can be used as start point. The work of [Grasso, 2008] presents the approximate control point coordinates of a generic airfoil shape (see fig. 2). When in possession of the coordinates of all control points, the disturbance of the geometry may begin by simply moving the control points (only one or all at the same time), thus reshaping the airfoil surface either globally or locally. The only control points that cannot be moved are the ones setting both

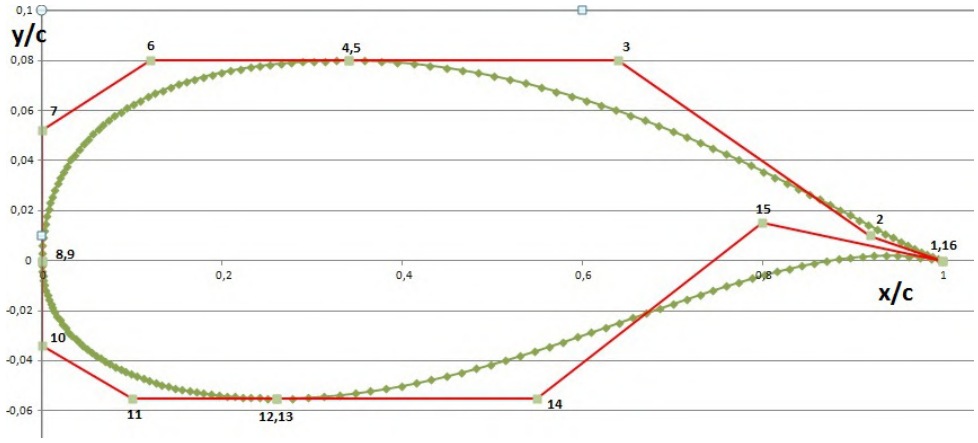

Figure 3.9: Airfoil surface built with reference control points shown

edges of the airfoil. The use of the Bezier curves in describing the airfoil geometry present us with the connectivity issues (as described above) but, in addition to this, special attention is required to the amount of mobility that is allowed to the CP in the coordinate system used. In other words, it is important that the optimization to be performed here follows the trend in which the airfoil geometry is at all times an aerodynamic body, not allowing the Bezier curves to deliver shapes that resemble the least with an airfoil, while maintaining enough room for developing an optimized airfoil. This issue of the relative positions of each CP to each other, is of major importance to this work, as it presents a source of required geometric constraints to be used in the optimization procedure, and will be discussed in detail in section 5.2.1.

3.3 Airfoil analysis

Having designed and obtained an airfoil geometry, as described in section 3.2, it is now of major importance to analyze the corresponding aerodynamic properties and study its performance and behaviour as best as possible, when under working conditions. This stage of the work requires the usage of external tools and, for that, a careful evaluation and selection of available computational tools is performed. The noise from WT is somehow related to the physical phenomena that occur over the airfoil surface, in particular the boundary layers (BL) that develop and especially with the turbulence levels. All BL parameters δ, δ^* and θ are of major relevance to know these aspects of the flow. We also know that noise from WTs is directly related with the characteristics of the interaction developed between the flow and the airfoil surface. In most cases of a working airfoil, the flow presents itself more disturbed and turbulent when accounted for over the trailing edge coordinate (situation where events like separation or transition are more likely to have occurred already, upstream of this point) then we may assume that the boundary layer parameters should be computed in this coordinate (over the trailing edge), where the effects of turbulence and its adversity are more likely to influence noise levels.

3.3.1 Semi-empirical method

Many simple procedures are available for computing the BL parameters (like the method of Thwaites [Eça, 2010]) that can give a rather good estimate of these values. These methods deliver quite good estimates of the boundary layer values, but are highly analytical in nature and a careful analysis, like the one necessary here, always ends up resorting to computational tools, for its processing speed and capacity. A survey for finding the most suitable method is then required.

In the scope of aero-acoustics, the semi-empirical work of Brooks et al. [1989] (**BP&M**), is a major reference in the airfoil self noise research, and will be called upon continuously. Before advancing to the aero-acoustic testing, which is based in measurements of a NACA 0012 airfoil, the authors formulated the following expressions for a flow analysis with $\alpha = 0^o$, and present a simple method for computing the boundary layer parameters over the trailing edge, normalized by the chord and dependent only on the *Re* number as well as the angle of attack (α) or rather using as reference the zero angle of attack (subscript 0) for the situation where these symmetric airfoils generate zero lift. Furthermore, the same experiment accounted for situations where tripped boundary layers may be present or not:

Case of heavily tripped boundary layer

$$\frac{\delta_0}{c} = 10^{[1.892 - 0.9045 \log Re + 0.0596 (\log Re)^2]} \tag{3.10a}$$

$$\frac{\delta_0^*}{c} = \begin{cases} 0.0601 Re^{-0.114} & ,Re \leq 0.3 \times 10^6 \\ 10^{[3.411 - 1.5397 \log Re + 0.1059 (\log Re)^2]} & ,Re > 0.3 \times 10^6 \end{cases} \tag{3.10b}$$

$$\frac{\theta_0}{c} = \begin{cases} 0.0723 Re^{-0.1765} & ,Re \leq 0.3 \times 10^6 \\ 10^{[0.5578 - 0.7079 \log Re + 0.0404 (\log Re)^2]} & ,Re > 0.3 \times 10^6 \end{cases} \tag{3.10c}$$

Case of untripped boundary layer

$$\frac{\delta_0}{c} = 10^{[1.6569 - 0.9045 \log Re + 0.0596 (\log Re)^2]} \tag{3.11a}$$

$$\frac{\delta_0^*}{c} = 10^{[3.0187 - 1.5397 \log Re + 0.1059 (\log Re)^2]} \tag{3.11b}$$

$$\frac{\theta_0}{c} = 10^{[0.2021 - 0.7079 \log Re + 0.0404 (\log Re)^2]} \tag{3.11c}$$

The work of Brooks et al. [1989] continues with some more important equations, for this specific flow analysis of airfoils. Taking into account the test apparatus of the experiment, the authors describe the need to set a corrected angle of attack, due to the effects of the wind tunnel walls, α_*, representing the angle in free air required to give the same lift as α would give in the tunnel. The correction is originally for small camber effects only, but many authors still use this as reference for highly modified airfoil shapes (e.g. [Moriarty and Migliore, 2003], [Leloudas et al., 2007] or [Zhu et al., 2005]) like the ones we will be using here. From these values of corrected angles of attack, the boundary layer values for both sides of

the airfoil (suction - subscript *s* - and pressure side - subscript *p*) were given:

Pressure side boundary layer values (valid for tripped and untripped flow)

$$\frac{\delta_p}{\delta_0} = 10^{[-0.04175\alpha_* + 0.00106\alpha_*^2]} \tag{3.12a}$$

$$\frac{\delta_p^*}{\delta_0^*} = 10^{[-0.0432\alpha_* + 0.00113\alpha_*^2]} \tag{3.12b}$$

$$\frac{\theta_p}{\theta_0} = 10^{[-0.04508\alpha_* + 0.000873\alpha_*^2]} \tag{3.12c}$$

Suction side boundary layer values - tripped flow

$$\frac{\delta_s}{\delta_0} = \begin{cases} 10^{0.0311\alpha_*} & ,0^o \leq \alpha_* \leq 5^o \\ 0.3468(10^{0.1231\alpha_*}) & ,5^o < \alpha_* \leq 12.5^o \\ 5.718(10^{0.0258\alpha_*}) & ,12.5^o < \alpha_* \leq 25^o \end{cases} \tag{3.13a}$$

$$\frac{\delta_s^*}{\delta_0^*} = \begin{cases} 10^{0.0679\alpha_*} & ,0^o \leq \alpha_* \leq 5^o \\ 0.381(10^{0.1516\alpha_*}) & ,5^o < \alpha_* \leq 12.5^o \\ 14.296(10^{0.0258\alpha_*}) & ,12.5^o < \alpha_* \leq 25^o \end{cases} \tag{3.13b}$$

$$\frac{\theta_s}{\theta_0} = \begin{cases} 10^{0.0559\alpha_*} & ,0^o \leq \alpha_* \leq 5^o \\ 0.6984(10^{0.0869\alpha_*}) & ,5^o < \alpha_* \leq 12.5^o \\ 4.0846(10^{0.0258\alpha_*}) & ,12.5^o < \alpha_* \leq 25^o \end{cases} \tag{3.13c}$$

Suction side boundary layer values - untripped flow

$$\frac{\delta_s}{\delta_0} = \begin{cases} 10^{0.03114\alpha_*} & ,0^o \leq \alpha_* \leq 7.5^o \\ 0.0303(10^{0.2336\alpha_*}) & ,7.5^o < \alpha_* \leq 12.5^o \\ 12(10^{0.0258\alpha_*}) & ,12.5^o < \alpha_* \leq 25^o \end{cases} \tag{3.14a}$$

$$\frac{\delta_s^*}{\delta_0^*} = \begin{cases} 10^{0.0679\alpha_*} & ,0^o \leq \alpha_* \leq 7.5^o \\ 0.0162(10^{0.3066\alpha_*}) & ,7.5^o < \alpha_* \leq 12.5^o \\ 52.42(10^{0.0258\alpha_*}) & ,12.5^o < \alpha_* \leq 25^o \end{cases} \tag{3.14b}$$

$$\frac{\theta_s}{\theta_0} = \begin{cases} 10^{0.0559\alpha_*} & 0^o \leq \alpha_* \leq 7.5^o \\ 0.0633(10^{0.2336\alpha_*}) & ,7.5^o < \alpha_* \leq 12.5^o \\ 14.977(10^{0.0258\alpha_*}) & ,12.5^o < \alpha_* \leq 25^o \end{cases} \tag{3.14c}$$

Subroutines were built in the final code to perform these calculations, but they do not present the main source for boundary layer parameters computation. The reason is simple: as the authors based their experiments on a group of NACA 0012 airfoils, in which only the chord value varied, the only inputs required for this expressions are the angle of attack, the velocity of the undisturbed flow and the

chord. They do not account for other airfoil geometries or geometry alterations, which means that these expressions should only be used when performing acoustic measurements of the NACA 0012 airfoil and not used on highly deformed airfoils. This means that reliability of future aero-acoustic prediction should take this fact into account, and the expressions are only to be used for verification of the computer code developed and to confirm a correct interpretation of the work. It is worth noting that the experiments used hot-wire probe measurements in the boundary layer/near-wake region of the sharp trailing edge of the airfoils, making it a rather realistic set of values, as one can state in the results of the same work.

3.3.2 RFOIL software

Though it delivers reasonable results, the BP&M method is not suitable for the highly deformed airfoils that will certainly be used here and if one wants a more accurate value of the boundary layer parameters as well as a more suitable method that accounts for geometry, then more extensive calculations are required that account for specific characteristics like rotational effects over the airfoil (as described in section 3.1), the particularities inherent to the trailing edge geometric discontinuity (open or closed trailing edge) or even more relevant to this work, methods that do not present any obstacles when accounting for the highly modified shape of the airfoil as accurately as possible, for a better aero-acoustic prediction scheme. All that means resorting to well established and reliable computational software and for that reason, the main optimization process shall account for the results from external software used and not the previous expressions obtained from the BP&M model, although a secondary optimization may be performed for comparison (validation of the NACA 0012 example, only). Of course these softwares also rely on old semi-empirical studies and calculation techniques, but they are certainly more reliable for this purpose than the previous method, which applicability is limited to the NACA 0012 airfoil.

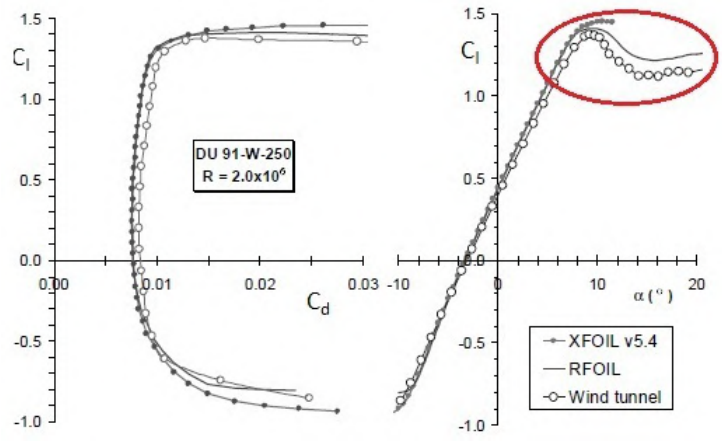

Figure 3.10: Example of Rfoil improvements in comparison to Xfoil and experimental data, for the DU 91-W2-250 airfoil [Timmer and van Rooij, 2003].

The chosen software for use in this work has been the *RFOIL software* [B. O. G. Montgomerie, 1997]. RFOIL is a modified version of the XFOIL software from Drela and Youngren [2001]. It has been developed by researchers at the National Aerospace Laboratory (NLR) and the DELFT University [B. O. G. Montgomerie, 1997], funded by the ECN project in the Netherlands, for improvements in wind turbine

research. The main improvements presented by RFOIL (in comparison to its predecessor) are mainly related to the 3D effects that occur in stall conditions. Specifically, in the description of the 3D flow past a wind turbine rotor blade and quasi 2D boundary layer equations, that retain centrifugal and Coriolis terms with higher order terms. Radial pressure gradients were added to the previous XFOIL version used as base. The corresponding integral representation was implemented in an improved version (more accurate near stall computations, as shown in detail in fig. 3.10). More relevant to this work, the RFOIL software *calculates rotating sectional aerodynamic coefficients using two input parameters* [B. O. G. Montgomerie, 1997] (in other words accounts for the rotational effects in cross sections of the blade), as well as the local solidity. The main conclusions and results taken from the application of the software by its creators, showed the typical ”rotating” triangular pressure distribution and the associated high lift coefficients to be better predicted than before. The same researchers used aerodynamic data from experimental wind turbines and cross-referenced to RFOIL values, revealing that 2/3 of the local solidity gives the better agreement (see fig. 3.11).

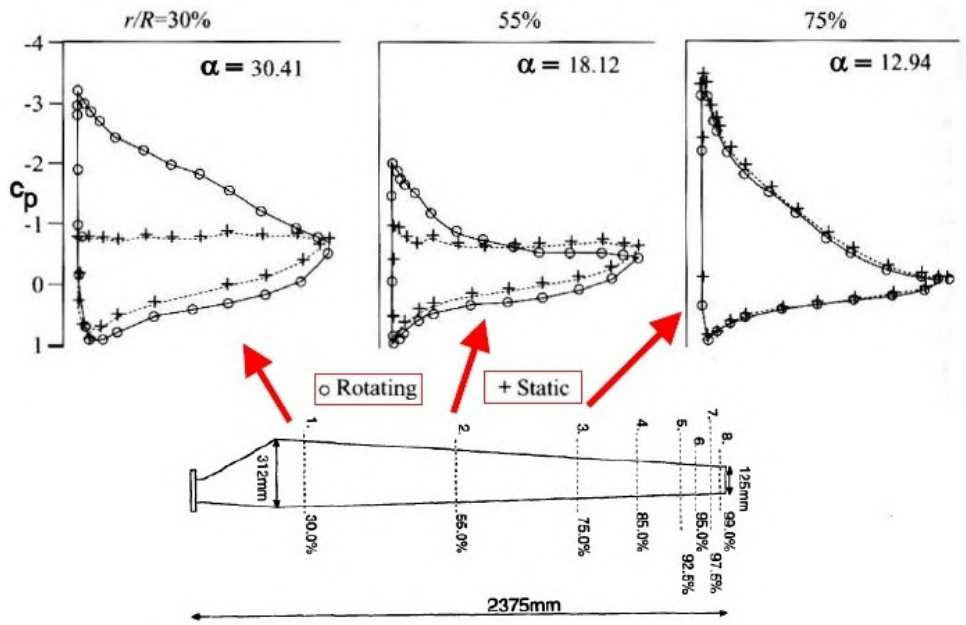

Figure 3.11: Example of Rfoil analysis (static pressure for rotating and static measurements) of 3 cross section elements in a 2.35m blade (EWEC, 1991) [van Bussel, 2011].

The results taken from RFOIL, which include δ, δ^*, θ, all from both sides of the airfoil (pressure and suction sides), as well as all relevant aerodynamic coefficients (C_f, C_p, C_l and C_d) regarding the airfoil analysis, may then be used or processed. RFOIL is therefore a sufficiently strong and complete numerical tool to compute realistic values of the boundary layer values and widely referenced for this purpose (see for example [Hjort, 2005], [Oerlemans and Schepers, 2009] or [Timmer and van Rooij, 2003]). For all these reasons this is the software chosen for use in this work as the main BL parameter calculation tool.

Chapter 4

Aero-acoustic model of airfoils

In this chapter the issue of aerodynamic noise generation from WT and the specifics of airfoil related sound and noise will be presented. The main physical processes and mechanisms that generate noise will be identified and evaluated, and the aero-acoustic noise prediction scheme used in this work is selected and presented. The fundamental theories of aero-acoustics used in this work, can be found in references such as Lau [2011] or Goldstein [1976] for better understanding of the subjects approached here. An overview of the basics of the Lighthill acoustic analogy, the Kirchhoff's integral equations and the Curle's solution may be necessary as all are quite relevant for this chapter, and the reader less familiar with these topics is invited to learn its most fundamental concepts.

4.1 Selection of the airfoil noise prediction model

As stated in the beginning of this work, WT noise is a rather recent concern for engineers and although research has been conducted for quite some time on the subject, the application of that knowledge is currently in its early stages and quite limited. Some of the most recent works (e.g. [Tickell et al., 2004] or [Gliebe et al., 2000]) that focus on the subject, present thourough comparisons of several available computer codes applied to WT noise prediction (like the SILANT software [Boorsma, 2011]) and an immediate conclusion is that most commercial softwares currently available for this application are either insufficient and quite unreliable in the level of detail they deliver, or extremely expensive potentially demoting their usage. On the other hand, research into aerodynamic noise from airfoils has also been conducted for quite some time, as the works of Brooks and Schlinker [1983] or Ffowcs-Williams [1970] demonstrate. Originally these studies were conducted for helicopter technologies, but immediately showed great interest when applied to WTs. The reason is simple: both technologies create similar operating conditions for the airfoils involved. The main differences are obviously the flow velocities involved (bigger in the helicopter rotor, acquiring the characteristics of compressible fluids) and the direction of the flow (in WTs the energy is collected from the flow rather than transferred to).

Already referenced before, the work of Brooks et al. [1989], developed at NASA, was one of the first to successfully make use of previous helicopter researches and later used by others in applications

for WTs [Lowson, 1993a] establishing itself as one of the most relevant works on the subject. The prediction scheme presented in this work (usually called the Brooks, Pope & Marcolini model - BP&M) is based on the aero-acoustic measurements of the NACA 0012 airfoil, using several microphones, with very accurate experimental results, due to the use of an acoustically controlled wind tunnel as a testing environment, allowing the authors to develop a semi-empirical prediction scheme with simple and direct mathematical expressions for computing noise sound pressure levels, dependent only on boundary layer parameters and flow characteristics. However, this presents the biggest limitations of the work: 1) the empirical nature of the expressions (computations resort to several iterative procedures); and 2) the formulations obtained to compute the BL parameters are not suitable for generalization to other airfoils (especially cambered ones), as these may not present as accurate sound pressure values as they do for the reference airfoil NACA 0012 used in the experiment.

A different approach was taken in what is today called by some authors the TNO model, originally presented by Parchen [1998]. This method models very accurately (in some aspects it is better than the BP&M model) the boundary layer behaviour on an airfoil and its effects on the far field noise. It relies on a boundary layer prediction routine (at the time of this text, it was only tested with XFOIL) to obtain the boundary layer parameters, which will be used to model the surface pressure fluctuations on the airfoil and the resultant far-field noise. Though the model uses less empiricism than the BP&M model, it still bears a certain level of empiricism in the boundary layer modeling, such as the integral length scale.

These are the two main methods used for the subject nowadays. When comparing the two models, one would immediately say that the most accurate one should be used when predicting noise from an airfoil. However, the choice of the prediction scheme must also account for other factors such as suitability to easy code development and less computer processing usage and memory. This would exclude immediately the TNO model as it is numerically more complex and its better results are more likely to occur when the model is coupled to a Computational Fluid Dynamics code, according to Franck Bertagnolio [2008]. That means more processing power needed and a more delayed optimization process and ultimately the method delivers results only as good as the BP&M work or slightly better. Furthermore, it is a rather recent model and not tested as extensively as the BP&M model.

Both methods present advantages and disadvantages, but the direct comparison between them has resulted in the choice of the BP&M model for this work. Despite its age and empiricism, the BP&M model is still extensively used nowadays, even in important projects funded by governments and commercial entities [Fuglsang and Madsen, 1996], [Moriarty and Migliore, 2003], [Hjort, 2005], for predicting the main five airfoil self-noise mechanisms (discussed in detail in the next subsection). Also the age of the BP&M model has allowed for several improvements and experimental validations over the years in the scope of WT aero-acoustics (see [Moriarty et al., 2005], [Moriarty and Migliore, 2003] and [Fuglsang and Madsen, 1996] for example), showing today a level of scientific and computational maturity that is quite suitable for the optimization process here performed. Of major interest to the applicability of this model in this work will be its response to the inclusion of the rotational effects. In other words, these effects will most likely develop conditions that will favour higher values of important parameters like the relative velocity on the airfoil or the effective angle of attack. This however is not expected to seriously

compromise the model nor its usefulness for a realistic estimate of the SPL values.

Thus, the chosen method used here will attempt to take the best of the two presented methods, being slightly different from that of the TNO model, where the main difference is the BL computation tool (which is here the Rfoil software) but still based on the BP&M model for computing the SPL values. This is a similar strategy used in commercial projects like the already referenced SILANT software.

4.2 Airfoil noise mechanisms

As it has been highlighted already in this work, the main source of noise from WTs comes from its aerodynamic characteristics, specifically the several blade cross sections used. This subject is usually called **airfoil self-noise** but it is not the only phenomena that generates aerodynamic noise. The several noise mechanisms are computed together resorting to equation 2.5, and presented in regard to the respective 1/3 octave band centered frequencies. The nature of the flow and interaction of the same with the airfoil is also responsible for noise, as it will be detailed in the following subsections.

4.2.1 Airfoil self-noise

As its name indicates, airfoil self-noise is generated in the passage of the flow over the airfoil geometry that defines the blade cross section. The BP&M model identified five aerodynamic mechanisms responsible for broadband and tonal noise. These noise mechanisms are characterized by several auxiliary expressions, that serve both as level adjustments and correctional factors, being some defined by specific *Strouhal* numbers and others characterized by spectral shape functions. These parameters are all very important for the correct computation of the SPL values, and it is their computation that make up the main source of empiricism of the study presented in that work, as they are based on several interpolation processes. Though very important, its presence here would create a too extensive text and run of course from the scope of the work, so the definition of those parameters will not be presented here, only the most fundamental expressions. This remark is made to invite the more interested reader to look for details on this, in the original model [Brooks et al., 1989] for better understanding. Two parameters will repeatedly appear in the following expressions ($\bar{D}_h$ and $\bar{D}_l$), being these the directivity function values. These will be discussed in detail in subsection 4.2.3.

Turbulent Boundary Layer - Trailing Edge (TBL-TE) Noise: The interaction of boundary layer turbulence with airfoil trailing edge produces broadband frequency noise. The original model proved disappointing in accounting for TBL-TE noise because for accurate prediction of this noise sufficient information about the turbulent boundary layer convecting over the trailing edge is required. That issue is slightly improved when using a more complete boundary layer computation method (like the RFOIL tool) and suitable for other airfoil geometries, instead of the original expressions from BP&M which use the experimental results from the reference airfoil NACA 0012 (see sec. 3.3).

The noise mechanism is presented with the computation of the pressure side (subscript - p) and

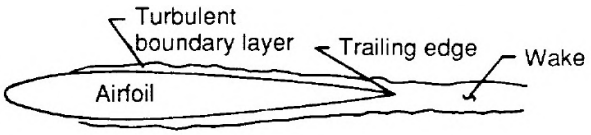

Figure 4.1: Representation of the TBL-TE noise mechanism [Brooks et al., 1989]

suction side (subscript - s) SPL values independently, because they have similar yet slightly different computation methods

$$SPL_p = 10\log\left(\frac{\delta_p^* Ma^5 d\bar{D}_h}{r_e^2}\right) + A\left(\frac{St_p}{St_1}\right) + (K_1 - 3) + \Delta K_1 \tag{4.1a}$$

$$SPL_s = 10\log\left(\frac{\delta_s^* Ma^5 d\bar{D}_h}{r_e^2}\right) + A\left(\frac{St_s}{St_1}\right) + (K_1 - 3) \tag{4.1b}$$

The term *d* accounts for the airfoil semi-span and r_e stands for the source-observer distance. The function *A* is the spectral shape function of the ratio between the Strouhal number (St_i, where i = p or s) and the empirical peak Strouhal number (St_1). The required Strouhal definitions are given by

$$St_p = \frac{f\delta_p^*}{U} \tag{4.2a}$$

$$St_s = \frac{f\delta_s^*}{U} \tag{4.2b}$$

$$St_1 = 0.02Ma^{-0.6} \tag{4.2c}$$

The K_1 parameter is an amplitude function dependent only on Reynolds number and ΔK_1 is a level adjustment for the pressure-side contribution for nonzero angles of attack. Its contribution is set by the angle of attack and the Reynolds number based on δ_p^* characteristic length:

$$K_1 = \begin{cases} -4.31\log Re + 156.3 & ,Re < 2.47\times 10^5 \\ -9.0\log Re + 181.6 & ,2.47\times 10^5 \leq Re \leq 8.0\times 10^5 \\ 128.5 & ,8.0\times 10^5 < Re \end{cases} \tag{4.3a}$$

$$\Delta K_1 = \begin{cases} \alpha_*[1.43\log Re_{\delta_p^*} - 5.29] & ,Re_{\delta_p^*} \leq 5000 \\ 0 & ,5000 < Re_{\delta_p^*} \end{cases} \tag{4.3b}$$

Separation-Stall (SEP) Noise: Noise originates from the interaction of the highly disturbed flow with the surface when boundary layer separation occurs. It is usually broadband in nature and becomes increasingly relevant as the separation takes place closer to the leading edge (large scale separation). In other words it is due to most likely occur in near stall conditions. The noise mechanism is usually associated and computed together with the TBL-TE noise mechanism because both share similar scaling laws. To differentiate stalled flow from normal flow conditions, the authors proposed an angle of attack ($(\alpha_*)_0$) from which the flow is stalled. This means that for angles of attack up to $(\alpha_*)_0$, TBL-TE noise is

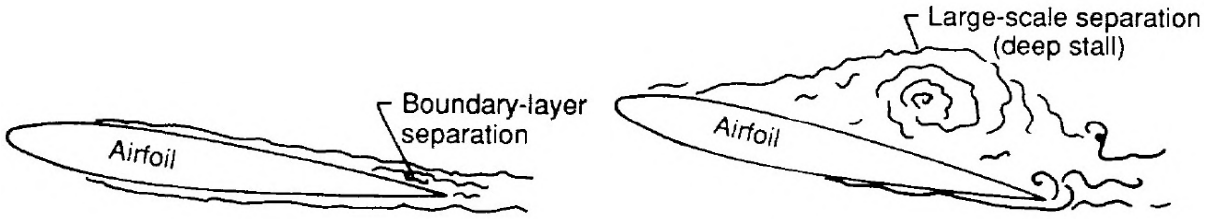

(a) Boundary-layer separation (b) Large-scale separation

Figure 4.2: Representation of the BL separation noise mechanism [Brooks et al., 1989])

computed as before and separation noise is given by

$$SPL_{SEP} = 10\log\left(\frac{\delta_s^* Ma^5 d\bar{D}_h}{r_e^2}\right) + B\left(\frac{St_s}{St_2}\right) + K_2 \tag{4.4}$$

where B is the spectral shape function for separation noise with

$$St_2 = St_1 \times \begin{cases} 1 & ,\alpha_* < 1.33^o \\ 10^{0.0054(\alpha_* - 1.33)^2} & ,1.33^o \leq \alpha_* \leq 12.5^o \\ 4.72 & ,12.5^o < \alpha_* \end{cases} \tag{4.5}$$

K_2 is an amplitude function dependent on *Ma* and given by

$$K_2 = K_1 + \begin{cases} -1000 & ,\alpha_* < \gamma_0 - \gamma \\ \sqrt{\beta^2 - (\beta/\gamma)^2(\alpha_* - \gamma_0)^2} + \beta_0 & ,\gamma_0 - \gamma \leq \alpha_* \leq \gamma_0 + \gamma \\ -12 & ,\gamma_0 + \gamma < \alpha_* \end{cases} \tag{4.6}$$

where

$$\gamma = 27.094Ma + 3.31 \quad \gamma_0 = 23.43Ma + 4.651 \tag{4.7a}$$

$$\beta = 72.65Ma + 10.74 \quad \beta_0 = -34.19Ma - 13.82 \tag{4.7b}$$

The angle of attack for which the switch to stalled flow occurs is said to be either equal to the peak of the K_2 function (defined previously by γ_0) or whenever α_* exceeds 12.5^o, whichever occurs first.

This correction of the angle of attack has a direct effect on the previously presented TBL-TE mechanism. Should the angle of attack exceed that of $(\alpha_*)_0$, the TBL-TE computation reaches a maximum and will not contribute for the total SPL value computation, and the respective SPL values is set as

$$SPL_p = -\infty \tag{4.8a}$$

$$SPL_s = -\infty \tag{4.8b}$$

and the separation noise is then computed by

$$SPL_{SEP} = 10\log\left(\frac{\delta_s^* Ma^5 d\bar{D}_l}{r_e^2}\right) + A'\left(\frac{St_s}{St_2}\right) + K_2 \tag{4.9}$$

Note that the same spectral function A used before for computing TBL-TE noise (now called A') is used here, only now a Reynolds number three times bigger than before ($3 \times Re$) will be used. Also the directivity function is now set for low frequency range.

Laminar Boundary Layer - Vortex Shedding (LBL-VS) Noise: Originates in the non-linear boundary layer instabilities interacting with the airfoil surface, radiating mainly tonal noise (usually associated to a typical Von Kármán's instability phenomena in low *Re* regimes). Again for the 1/3 octave filter LBL-VS noise is given by

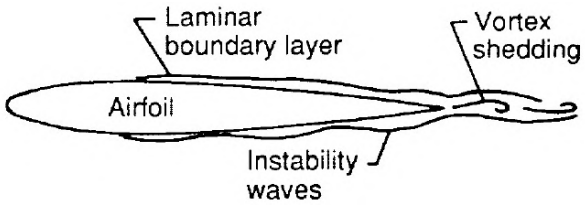

Figure 4.3: Representation of the laminar BL instabilities that create the vortex shedding noise mechanism [Brooks et al., 1989]

$$SPL_{LBL-VS} = 10\log\left(\frac{\delta_p Ma^5 d\bar{D}_h}{r_e^2}\right) + G_1\left(\frac{St'}{St'_{peak}}\right) + G_2\left(\frac{Re}{(Re)_0}\right) + G_3(\alpha_*) \tag{4.10}$$

The Strouhal definitions are set by

$$St' = \frac{f\delta_p}{U} \tag{4.11a}$$

$$St'_{peak} = St' \times 10^{-0.04\alpha_*} \tag{4.11b}$$

$$St'_1 = \begin{cases} 0.18 & ,Re \leq 1.3 \times 10^5 \\ 0.001756Re^{0.3931} & ,1.3 \times 10^5 < Re \leq 4.0 \times 10^5 \\ 0.28 & ,4.0 \times 10^5 < Re \end{cases} \tag{4.11c}$$

The model also makes use of the spectral shape functions $G_1(e)$ (where $e = St'/St'_{peak}$), the peaked level shape function $G_2(d)$ (with $d = Re/(Re)_0$) and amplitude function $G_3(\alpha_*)$ to adjust the final value

for this noise mechanism SPL values:

$$G_1(e) = \begin{cases} 39.8 \log e - 11.12 & ,e \leq 0.5974 \\ 98.409 \log e + 2.0 & ,0.5974 < e \leq 0.8545 \\ -5.076 + \sqrt{2.484 - 506.25(\log e)^2} & ,0.8545 < e \leq 1.17 \\ -98.409 \log e + 2.0 & ,1.17 < e \leq 1.674 \\ -39.8 \log e - 11.12 & ,1.674 < e \end{cases} \tag{4.12a}$$

$$G_2(d) = \begin{cases} 77.852 \log d + 15.328 & ,d \leq 0.3237 \\ 65.188 \log d + 9.125 & ,0.3237 < d \leq 0.5689 \\ -114.052(\log d)^2 & ,0.5689 < d \leq 1.7579 \\ -65.188 \log d + 9.125 & ,1.7579 < d \leq 3.0889 \\ -77.852 \log d + 15.328 & ,3.0889 < d \end{cases} \tag{4.12b}$$

The Reynolds number for use in the peak scaled function G_2,$(Re)_0$ is given as function of the angle of attack,

$$(Re)_0 = \begin{cases} 10^{(0.215\alpha_* + 4.978)} & ,\alpha_* \leq 3.0 \\ 10^{(0.120\alpha_* + 5.263)} & ,3.0 < \alpha_* \end{cases} \tag{4.13}$$

Finally the angle-dependent level for the shape curve is

$$G_3(\alpha_*) = 171.04 - 3.03\alpha_* \tag{4.14}$$

Trailing Edge Bluntness - Vortex Shedding (BLUNT) Noise: The presence of the geometric discontinuity due to the bluntness of the trailing edge of the airfoil has always been a major concern in airfoil theory. As the flow leaves the trailing edge, the flow separates from the surface, due to the geometric discontinuity present, which contributes to the destabilization of the wake and consequently to the occurrence of the vortex shedding phenomena [de Brederode, 1997]. As its name indicates, this mechanism is more likely to create periodic instabilities, again like the von Kármán wake.

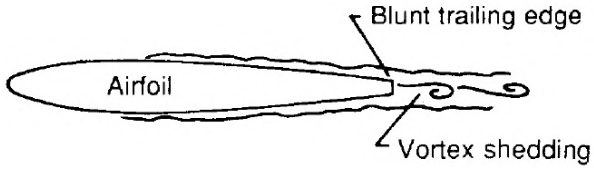

Figure 4.4: Representation of the TE bluntness related noise mechanism [Brooks et al., 1989]

This noise mechanism is tonal in nature and directly related to the geometry of the trailing edge. As before, the NACA 0012 airfoil serves as basis for the experimental measurements of the original model, where the authors used several extensions to the trailing edge of that airfoil (ranging from sharp edges

to blunt edge plates) to acknowledge the effects of the geometry in the SPL values. Of major relevance to point out from these experiments is the effect of the TE wedge angle. The authors concluded that sharper TE would have a smaller spectral density in frequency. The trailing edge bluntness noise spectrum for the 1/3 octave filter used is given by

$$SPL_{BLUNT} = 10\log\left(\frac{hMa^{5.5}d\bar{D}_h}{r_e^2}\right) + G_4\left(\frac{h}{\delta^*_{avg}}, \Psi\right) + G_5\left(\frac{h}{\delta^*_{avg}}, \Psi, \frac{St'''}{St'''_{peak}}\right) \tag{4.15}$$

The Strouhal definitions are given by

$$St''' = \frac{fh}{U} \tag{4.16a}$$

$$St'''_{peak} = \begin{cases} \frac{0.212-0.0045\Psi}{1+0.235(h/\delta^*_{avg})^{-1}-0.0132(h/\delta^*_{avg})^{-2}} & ,0.2 \leq h/\delta^*_{avg} \\ 0.1(h/\delta^*_{avg}) + 0.095 - 0.00243\Psi & ,h/\delta^*_{avg} < 0.2 \end{cases} \tag{4.16b}$$

The h/δ^*_{avg} term is the ratio of trailing edge thickness *h*, to the average boundary-layer displacement thickness δ^*_{avg}, where

$$\delta^*_{avg} = \frac{\delta^*_p + \delta^*_s}{2} \tag{4.17}$$

The noise mechanism resorts to the spectral functions G_4 and G_5 where the term Ψ is the solid wedge angle, in degrees, between the sloping surfaces upstream of the trailing edge. For a flat plate $\Psi = 0^o$, whereas a NACA 0012 airfoil has $\Psi = 14^o$. The determination of this parameter for other geometries is made resorting to calculation procedures involving an interpolation between the spectra for $\Psi = 0^o$ and 14^o (the flat-plate and NACA 0012 references). A routine has been developed to compute this wedge angle using the coordinates of the points that make up the TE. The code developed will also automatically discard the results in 1/3 octave spectra for SPL_{BLUNT} whenever Ψ is off limit.

Function G_4 delivers the peak level spectrum:

$$G_4(h/\delta^*_{avg}, \Psi) = \begin{cases} 17.5\log\left(h/\delta^*_{avg}\right) + 157.5 - 1.114\Psi & ,h/\delta^*_{avg} \leq 5 \\ 169.7 - 1.114\Psi & ,5 < h/\delta^*_{avg} \end{cases} \tag{4.18}$$

The interpolation mentioned before is performed when computing the shape spectrum defined by the function G_5

$$G_5\left(\frac{h}{\delta^*_{avg}}, \Psi, \frac{St'''}{St'''_{peak}}\right) = (G_5)_{\Psi=0^o} + 0.0714[(G_5)_{\Psi=14^o} - (G_5)_{\Psi=0^o}] \tag{4.19}$$

Tip Vortex Formation (TIP) Noise: The main reason why any blade works is due to the pressure difference between the upper and lower sections. When considering the tip region of any blade this presents major problems. The blade tip has always presented aerodynamic problems to engineers, namely the formation of tip vortices. From the aero-acoustic point of view, the noise originated from this

phenomenon is associated with the turbulence in the locally separated flow region at the tip where the vortex is created. However, this noise mechanism introduces specific 3D effects and even if it is directly related with the shape of the airfoil, which is our subject under analysis here, it will run out of the scope of this work. The fact that this mechanism in not yet fully understood and its small contribution to SPL values exemplified in the tests from the original BP&M work, present valuable arguments to discard it from the final optimization procedure. This approach has been common practice when using this model by other authors (e.g. [Oerlemans and Schepers, 2009], [Lowson, 1993a] or [Moriarty et al., 2005]) and will be accepted here as well.

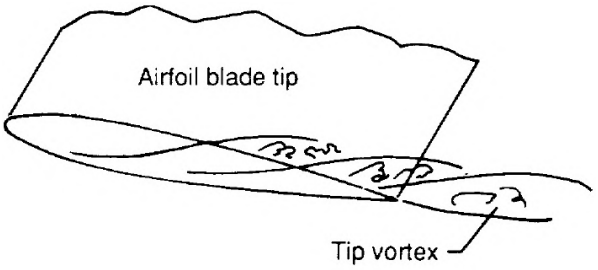

Figure 4.5: Representation of the blade tip related noise mechanism [Brooks et al., 1989]

The noise spectrum in a 1/3 octave presentation is predicted by

$$SPL_{TIP} = 10\log\left(\frac{Ma^2 Ma_{max}^3 l^2 \bar{D}_h}{r_e^2}\right) - 30.5(\log St'' + 0.3)^2 + 126 \tag{4.20}$$

The Strouhal definition is given by

$$St'' = \frac{fl}{U_{max}} \tag{4.21}$$

The flow over the blade tip consists of a vortex of strength Γ with a viscous core, whose spanwise extent at the trailing edge is *l*. This term is set by the authors, for a rounded tip,

$$l/c \approx 0.008\alpha_{tip} \tag{4.22}$$

where α_{tip} is the angle of attack of the tip region to the incoming flow.

4.2.2 Turbulence Inflow

Noise due to **turbulence inflow** exists because of the interaction of the blades with the atmospheric turbulence and despite not being a recent subject, it is still today a controversial topic due to its complexity and difficulty in predicting it. Although this noise source is intrinsically aerodynamic, it has more to do with the atmospheric boundary layer and upstream flow conditions than with the airfoil itself, but the total SPL radiated from the airfoil is ultimately related to the interaction between this turbulence and the geometry of the leading edge of the airfoil as we will acknowledge next.

From the physical point of view, as the upstream flow approaches a WT, the turbulence intensity will vary in height according to the established temperature gradients and the interaction with the ground

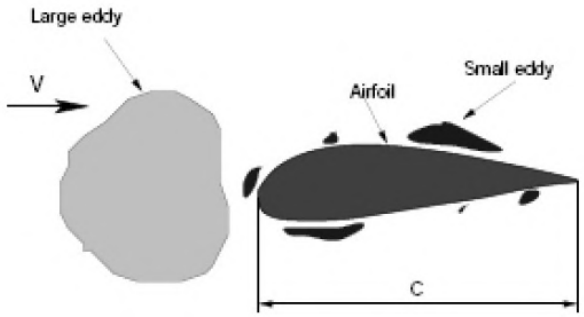

Figure 4.6: Representation of the turbulence inflow related noise mechanism [Zhu et al., 2005]

surface. The variation of turbulence will then introduce shear stresses which, in turn, induces rotation in air masses becoming turbulent vortices (or eddies). When these eddies reach the leading edge of the airfoil they will interact in different ways depending on their relative sizes. Low or high frequency noise will then occur if the eddy size is larger or smaller, respectively, than the chord length, meaning that the chord is a critical parameter here. For this reason, inflow is responsible mainly for broadband noise.

The theory and work developed by Amiet [1975] on "Acoustic radiation from an airfoil in a turbulent stream" serves as reference to almost every work associated to aero-acoustics of airfoils and turbulence inflow. It presents the formulation of an expression capable of predicting the SPL of a flat plate immersed in a turbulent stream. The work consists of analyzing the fluctuations in lift of an airfoil (using the flat plate case instead of the actual airfoil) due to the turbulent flow field, that ultimately result in the generation of sound. The method simplifies the problem by placing the observer directly over-head the airfoil (the time differences can be neglected this way). The original expression for computing the SPL values, in 1/3 octave filters, is

$$SPL_{1/3} = 10\log\left[\frac{Ld}{z^2}Ma^5\frac{\bar{u^2}}{U^2}\frac{K_x^3}{(1+K_x^3)^7/3}\right] + 181.3 \tag{4.23}$$

where *Ma* is the Mach number, *L* is the integral length scale, $\bar{u}$ is the intensity, *d* is the airfoil span and K_x is the particular value $k_x = -\omega/U = \pi f c/U$ for chordwise wavenumber. The biggest limitation of this work was the replacement of the airfoil geometry for a flat plate, not taking into account the geometry of an airfoil. It is also claimed by the author the possibility for under-prediction in low flow velocity and higher frequencies. This last parameter was later improved by Lowson [1993b] who proposed a different formulae, based on this one, providing a smooth transition between low and high frequency computations

$$SPL_{Inflow} = SPL^H_{Inflow} + 10\log\left(\frac{LFC}{1+LFC}\right) \tag{4.24a}$$

$$SPL^H_{Inflow} = 10\log\left(\frac{\rho^2 c_0^2 Ld}{r_e^2}Ma^3U^2\bar{u^2}\frac{K_x^3}{(1+K_x^3)^{7/3}}\bar{D}_h\right) + 58.4 \tag{4.24b}$$

Being LFC, the low frequency coefficient, defined as

$$LFC = 10S^2MaK^2\beta^{-2} \tag{4.25}$$

with

$$S^2 = \left[\frac{2\pi K}{\beta^2} + \left(1 + 2.4\frac{K}{\beta^2}\right)^{-1}\right]^{-1} \tag{4.26a}$$

$$\beta^2 = 1 - Ma^2 \tag{4.26b}$$

The expressions are based on the work of Amiet, hence not so different. As stated above the turbulence length scale (L) and intensity (I) are very important but also very complex subjects. The values of these parameters used in this work follow the general guidelines proposed by the IEC (International Electrotechnical Comission) standards. These IEC standards are extensively used for that purpose in many recent works (see [Zhu et al., 2005] or [Moriarty and Migliore, 2003]), regarding inflow turbulence noise, and deliver good and realistic values for the task at hands. The parameters are a function of ground roughness (z_0) and height above ground (z), which become necessary inputs in the code developed to compute the inflow turbulence noise, following the expressions

$$I = \gamma\frac{\log(30/z_0)}{\log(z/z_0)} \tag{4.27a}$$

with γ here being an auxiliary parameter set as

$$\gamma = 0.24 + 0.096\log z_0 + 0.016(\log z_0)^2 \tag{4.27b}$$

$$L = 25z^{0.35}z_0^{-0.063}, \text{ [m]} \tag{4.27c}$$

Surface	$z_0[m]$
Cities with high buildings; forests with high trees	0.7
Suburbian environment; fields with moderatly tall trees	0.3
Small settlements; fields with trees and fences	0.1
Open fields, few houses and trees	0.03
Plane fields with small vegetation	0.01
Deserts and offshore sites	0.001

Table 4.1: Typical values used for ground roughness [Gato, 2010].

There is a relevant issue worth noting here, regarding the values taken by z (heigth above ground). The works of Oerlemans and Schepers [2009] show experimental data on noise assessment and present interesting results, for full scale WT. In the form of an acoustic map, the report shows that the downward movement of the blade, radiates the most noise levels as seen in fig. 4.7. Furthermore, the same report states that the most noise values are found to be mostly at the tip region. This is only brought up in this section, to help the reader visualizing where the airfoil should be placed, relevant to

Figure 4.7: Representation of the acoustic map over a real HAWT [NLR, 2010]

the ground. For optimization purposes it will be here stated that the optimized airfoil will be considered to be at an approximate height above the ground equal to the hub height, as if it were performing the same downward movement.

The works of Amiet and Lowson are not yet enough for correctly predicting the SPL values of this noise mechanism (as they alone do not account for airfoil geometry) and the original model of BP&M does not account for this noise mechanism at all, as it focused solely on the airfoil structure and turbulent inflow noise is usually predicted when accounting for the entire blade. But researchers have continuously worked for better noise prediction schemes, some by improving the model of BP&M on various aspects, others by including the ability to predict this noise mechanism and even to account for the airfoil geometry. Works like the ones presented by Zhu et al. [2005], [Vargas, 2008] or [Zhu, 2004], which analyze the full blade, usually resort to well established numerical methods, like the Blade Element Method, for predicting this noise mechanism. For the case study in question of the section airfoil of the blade, the works of Moriarty et al. [2004] and Moriarty [2004b] present a very complete (and computationally demanding) method that relies on the numeric simulation of the interaction of the flow with the geometry of the airfoil using the acoustic analogy theory and boundary-element methods. In this method, the turbulence in the incoming flow is represented by harmonic gusts of vorticity that are assumed to passively convect along the streamlines of the steady mean flow around the airfoil. The boundary-element method allows the computation of mean flow and the interaction of sound waves with the solid airfoil surface. This method is very suitable for the task at hands because it delivers great confidence in predicting SPL values from different airfoil geometries, rather than just the flat plate configuration like the original work of Amiet delivers. However the own authors of the work admit it is incompatible with an efficient and swift optimization process, when performing the design of an airfoil, because of its numeric nature and extensive detail for simulating the flow (the number of streamlines and the distance between them are required for the computation and are a clear example of the level of detail inherent to the model), making it a very slow process, even with today's processing technologies. The more recent work, by the same authors

[Moriarty et al., 2005], presented a simplified version of the original method (Guidati simplified model or simplified boundary-element model). The simplification towards the original work was accomplished by reducing the full boundary-element method to a simple linear relation of geometric dimensions of an airfoil and assuming the vorticity to be concentrated into thin vortex sheets that coincide with the streamlines, without significant loss in accuracy (the accuracy of the method was validated against results from the original method [Moriarty et al., 2004]). The method, instead of absolute SPL values for a certain geometry, delivers differences in SPL values compared to that of a flat plate. In other words, when coupled with the prediction scheme from Amiet, for a flat plate, this simplified method is able to give the SPL value for different airfoil geometries. What the results show is that in the range of Mach between 0.1 and 0.2, the plot of ΔSPL vs. the *St* number can be approximated to a linear relation, in which the only variable is the slope of that line. Furthermore, researchers acknowledged that the most significant effect on that relation comes from variations on airfoil thickness whereas camber or different angles of attack do not influence so much the calculation of these inflow turbulence SPL values. This correlation is valid because it is generally known that airfoils with ”blunt” leading edges produce less inflow turbulence noise than those with a ”sharp” leading edge. The relation is therefore directly related to the geometry. Using the optimum quadratic relation between the slope (SL) and the ”Inflow Turbulence noise Indicator” (IT), the authors formulated the following expression

$$SL = 1.123IT + 5.317IT^2 \tag{4.28}$$

where $IT = D_{rel,1\%} + D_{rel,10\%}$ and $D_{rel,\%}$ refers to the airfoil relative thickness at 1% and 10% chord from the leading edge, respectively. Note that the flat plate case is the specific condition where IT = 0. The direct computation of the ΔSPL values is finally possible through

$$\Delta SPL = -[1.123(D_{rel,1\%} + D_{rel,10\%}) + 5.317(D_{rel,1\%} + D_{rel,10\%})^2] \left(\frac{2\pi fc}{U} + 5\right) \tag{4.29}$$

The specific SPL values for the airfoil in question is easily obtained from

$$SPL_{airfoil} = \Delta SPL + SPL_{flatplate} \tag{4.30}$$

The model does present some limitations. The authors state that the accuracy of the model is very good for *Strouhal* values up to 75, in comparison to the original work. As a result of this *Strouhal* limitation the authors also state that for the typical *Mach* number of 0.2 this *Strouhal* number corresponds to $f = 4kHz$ for a 0.2m chord airfoil and 800Hz for a 1m chord airfoil. These values are declared to be a range of validity of the model where the results from the original work developed [Moriarty and Migliore, 2003] are met with a maximum difference of 2dB, meaning that the code developed takes this suggestion under consideration and will not account for the influence of this noise mechanism when *Strouhal* is above 75, being the computed values for the flat plate the ones used for the remaining *Strouhal* numbers (or frequencies). Despite this, the method presents itself as a valuable addition to the selected prediction scheme, suitable for the optimization process here being performed, and its detailed

description by the authors allows for easy identification of any misleading results that may occur.

4.2.3 Relevant parameters in sound propagation

Sound, as any physical phenomena, is subject to the influence of several factors, and all have its relevance to any engineering process that relates directly (or indirectly) to it. The sound radiated from any source is not the same sound perceived by an observer at a certain distance and sound propagation obeys certain laws of Physics, which will impose distortions either by amplifying or reducing its pressure levels. For this reason, it is important to bear in mind some of the main phenomena that have a potential effect on SPL computations performed here.

Directivity: At the beginning of this section two parameters were introduced, $\bar{D_h}$ and $\bar{D_l}$, which are present in all SPL formulations considered. These very important parameters account for the directivity of sound, a phenomenon of sound reduction which depends on the position of an observer relative to a noise source. This means that sound has a directional component by having a strong noise amplitude in one direction and in other directions noise is reduced to a certain extent. This concept is exemplified in fig. 4.8, representing a static observer and a flat plate in motion, where the plate is the noise source to be considered.

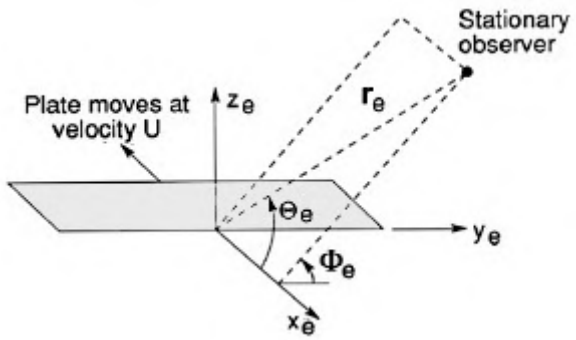

Figure 4.8: Example of sound directivity from a flat plate with an observer at a fixed position [Brooks et al., 1989]

Of major relevance to this subject is the local coordinate system presented, with Θ_e and Φ_e being the directivity angles, at which the observer's position is relative to the x axis, while r_e accounts for the distance between the trailing edge (source) and the observer position. The sound directivity functions for high frequency is given by

$$\bar{D_h} = \frac{2\sin^2(\Theta_e/2)\sin^2(\Phi_e)}{(1+M\cos\Theta_e)[1+(M-M_c)\cos\Theta_e]^2} \tag{4.31}$$

This equation can be applied to all SPL computations in which the flat plate (or noise source) is at an angle of attack α with the flow. This is true as the discussed noise mechanisms before are all mainly high frequency in character. However, because it was derived with the plate assumed to be semi-infinite, $\bar{D_h}$ becomes inaccurate at shallow upstream angles ($\Theta_e \longrightarrow 180^o$). This creates the single exception

to the method, for stalled-airfoil noise. At high angles of attack, the large-scale eddies present in the suction side of the airfoil, give way to low-frequency noise that is better predicted by

$$\bar{D_l} = \frac{\sin^2\Theta_e \sin^2\Phi_e}{(1 + M\cos\Theta_e)^4} \tag{4.32}$$

The overbar in the parameters is a characteristic that they are "*normalized by the TE noise radiated in the* $\Theta_e = 90^o$ *and* $\Phi_e = 90^0$ *direction*" (quoting Brooks et al. [1989]). If we look at equation 4.31, the immediate effect of this normalization is the fact that an observer positioned along the Z_e axis will experience the highest noise levels because $\bar{D_h} = 1$. On the other hand, if the observer is positioned along the plane XY_e, the directivity will become zero and in most of the noise equations we will have a term like $log(0)$ which will obviously return an invalid result. Another relevant aspect of these directivity functions is the fact that they use a Doppler correction in amplitude. The correction is made by application of the Doppler factor, $(1 - Mcos\Theta_e)^{-1}$, that appears as a denominator in the expressions. However, the Doppler effect correction will only become fully achieved if the center frequencies are shifted due to the moving source. Nevertheless, these frequency shifts will result in little difference in the frequency values and are not very relevant.

Specific routines were included in the main code developed for accounting for these directivity parameters, but its use will be reduced to the simplest method and its effect in the final optimization will be such that directivity issues should be minimal, so that the highest SPL values result from the analysis. For that, the observer will be fixed in a position immediatelly behind the airfoil and above the same, which results in $\Theta_e = \Phi_e = 90^o$, as suggested in the works of Brooks et al. [1989].

Absorption effects: The air thermodynamic properties are directly related to how sound propagates. The energy contained within the sound waves are absorbed to a certain extent due to the presence of air molecules and thermal conductivity. Most of the experimental works developed on the subject of WT noise always account for this effect and show that it is more relevant for higher frequencies. The work of Zhu [2004], following directive ISO 3891, provides an expression to account for this effect as a SPL loss ([in dB]

$$L_\alpha = -\alpha \times r \tag{4.33a}$$

$$\alpha = (0.02 + 0.36f + 0.036f^2) \times 10^{-2}, \text{ [dB/m] and f in [kHz]} \tag{4.33b}$$

where r [in m] is the distance travelled by the sound wave and α is an attenuation factor [dB/m]. This is of major importance when accounting for a full sized WT, especially if one is taking into account the location of the WT or regional effects that may have a major effect on local temperature gradients. For the case staudy of the airfoil cross section of the blades however, it can be negleted.

Other effects: Several more relevant effects are present in the WT noise subject, though from the point of view of this work, its impact on computed SPL values from airfoils alone may not prove to be so

important. Topics like distance from the noise source to the observer are accounted for in the directivity expressions, but others like refraction caused by wind and temperature gradients, the fact that a WT is approximated to a point as a noise source and even terrain effects (like reflection and refraction or morphology near the WT) all have an important role when accounting for the noise irradiated from a real WT. However in the case study of the airfoils, these aspects are somewhat irrelevant and may be here neglected.

Chapter 5

Optimization framework

To introduce the subject of optimization, consider the following simple and general description: every optimization procedure begins with the setting of a cost function (the *objective function*), which depends on a set of *design variables* (or *decision variables*) and restrictions (*constraints*). Generally speaking, the problem then develops in the direction of optimizing the value of the objective function (either minimize or maximize its value), by adjusting the values that the variables take while satisfying the restrictions. Mathematically, this can be described as follows

$$\begin{aligned} \text{minimize} \quad & f(x) \\ \text{by varying} \quad & x \in \mathbb{R}^n \\ \text{subject to} \quad & g_j(x) \leq 0, \qquad j = 1, 2, \ldots, M \\ & h_k(x) = 0, \qquad k = 1, 2, \ldots, L \\ & x_i^L \leq x_i \leq x_i^U, \quad i = 1, 2, \ldots, N \end{aligned} \tag{5.1}$$

where the objective function is f(x), for a set of design variables contained in x_i (*N* variables). The inequality and equality constraints are set, respectively, by vectors g_j (*M* inequality constraints) and h_k (*L* equality constraints). The last equation presents the bounds that set the search space and are generally called as *side constraints*. The constraints and bounds define the feasible search region. Obviously the subject of applied numerical optimization is much more complex and a more detailed background is recommended to the reader less comfortable with it ([Pedregal, 2004], [Bonnans et al., 2006], [Fletcher, 2000], [Diweakar, 2008]).

The chapter will begin with an overview of two of the main optimization algorithms available and a brief discussion on some relevant works by other authors that applied optimization tools on some of the topics here approached (mainly airfoil geometry and WT acoustics). This first section will focus on the selection of the optimization algorithm, most suitable for the task at hand. Following this, the main optimization procedure used is presented, detailing all relevant parameters of the present problem (objective function, variables, search space) as well as introducing the main optimization tools used.

5.1 Numerical optimization methods

5.1.1 Overview

Numerical optimization is extremely versatile and used in almost all fields of science, and engineering is no exception. Since engineering reaches a wide range of scientific applications, all quite different from each other, this means that each different problem is approached in a specific way, nearly resulting in one optimization procedure for each problem. Optimization algorithms range from Linear Programming, Non-Linear Programming, Integer Programming, Mixed Integer Linear Programming, Mixed Integer Non-Linear Programming, Discrete Optimization, Stochastic optimization and multi-Objective optimization [Diweakar, 2008]. Hence, it is quite difficult to state which approach or combinatorial method is more suitable to a specific problem, as all methods present advantages and disadvantages. A careful analysis on two of the most popular optimization methods is required in order to approach the present problem as efficiently as possible.

Gradient-based algorithms The most common and generally known category of optimization techniques is gradient-based. These algorithms use the gradient of the objective function to find an optimal solution by adjusting the values of each decision variable, as the problem runs each iteration towards a lower objective function value (minimum). The variable adjustment is proportional to the reduction in the objective function value. From a practical point of view, these methods are prone to converge on a local minima because they rely solely on the local values of the objective function in their search. They are best used on well-behaved systems, where there is one clear optimum. This means they will work well in high-dimensional spaces provided these spaces do not have local minima. Additional dimensions make it harder to guarantee that there is no local minima that could trap the search routine. As a result, as the dimensions (parameters) of the search space increase, the complexity of the optimization technique increases as well [Bonnans et al., 2006], [Pedregal, 2004].

Genetic Algorithms Genetic algorithms (**GA**) are heuristic search algorithms inspired by the mechanics of natural selection and biological evolution. Based on the idea of survival of the fittest, they combine the fittest string structures with structured yet randomized information exchange to form a search algorithm with some of the innovative flair of human search (they are usually associated to the growing field of computer artificial intelligence [Diweakar, 2008]. Unlike a simulated reasoning process, the search procedure of GA is modeled after the process of natural selection in which the abstract representation of a candidate solution, termed an *organism*, and organisms are grouped into sets of *populations*. Successive populations are called *generations*. The generic algorithm is described as follows:

1. Generate initial population, $G(0)$
2. While termination criteria are not satisfied, continue search for $t = t + 1$
3. Select $G(t)$

4. Recombine $G(t)$
5. Evaluate $G(t)$
6. Return to 2

In most applications, an organism consists of a single chromosome, which represents a solution string of length *n* in the form of a vector. Each entry in the vector is an allele, or a gene, representing a set of decision variable values. The setting of the **Initial Population** ($G(0)$) marks the beginning of the search. This can be chosen heuristically or randomly and the consequent generation $G(t+1)$ are chosen by a randomized selection procedure, composed of four operators:

- **Reproduction** - process in which individual strings are copied according to their objective function or fitness (*f*), meaning that solution strings that are fitter, and which have shown better performance, will have higher chance of contributing to the next generation;
- **Crossover** - this operator randomly exchanges parts of the genes of two parent solution strings of generation $G(t)$, to generate two child solution strings of generation $G(t+1)$;
- **Mutation** - serves to increase the variability of the population, by randomly selecting a gene or solution string, and then changes the value of this gene in its permissible range;
- **Immigration** - a rather new concept in GA theory, it is the process of adding new fitter individuals who will replace some existing (and less promising) members in the current genetic pool.

The stopping criteria of the search may be triggered by finding an acceptable approximated solution, either fixing the maximum number of generations to be evaluated or by some other specific criteria of the problem at hand. GA are quite reliable for global optimizations and multi-objective problems and that also makes up the main issue when resorting to GA: they only determine global Pareto optimal values [Pedregal, 2004], [Mitchell, 1999].

5.1.2 Applied optimization to WT technology

Much of the research material about applied optimization to WT design is taken directly from the aeronautics research. Researchers and scientists working in this area have focused mainly on blade and airfoil design [Grasso, 2010], [Lutz et al., 2005]. Several references focus on the application of numerical optimization to airfoil design through Bezier lines, as described in this work, but mainly for aerodynamic purposes and no noise assessment [Derksen and Rogalsky, 2010], [Wenming et al., 2008]. Others have researched on optimizing aero-acoustic noise from an existing WT [Hjort, 2005], [Oerlemans et al., 2009], but with no airfoil optimization. In conclusion, there are several works on the matter of how to optimize an airfoil, there are works and papers on computational methods for predicting aero-acoustic noise of an airfoil (see 3.3) and others work upon power output optimization of a real life WT. The few that relate these topics in the context of WT noise ([Lutz et al., 2007], [Lutz et al., 2005], [Oerlemans et al., 2009], [Franck Bertagnolio, 2008]), each follow different optimization strategies and do not present

one single approach for each common problem faced. In addition to this, consider the survey here taken on some works that focused on airfoil optimization ([Drela, 1998], [Padula and Li, 2002], [Gherman and Schulz, 2006]). As a consequence of this analysis, one can acknowledge that there is no mandatory rule on which optimization procedures are better for this specific objective, as each author may sometimes approach the same problem in a different way, resulting in the selection of a different optimization method.

Following this simple survey, it is clear the freedom of choice researchers have on this matter and from this we can acknowledge that the process of selecting a suitable optimization method is also rather dependent on external factors (such as computational expense). The selected method of optimization for use in this work will be a GA. The main reasons for this choice reside in the computational nature of the work here developed, to which this method is quite suitable, for its natural characteristic for finding global solutions instead of local minima (remember that the real objective is to set an airfoil geometry set with several CPs, meaning that an exact optimum solution for each CP is difficult, but a general geometry very close to the optimum is better) and for the experience related by some authors in their works, when applying these algorithms in some interesting aerodynamic optimization problems [Gardner and Selig, 2003], [Dunn, 1997], [Gardner and Selig, 2003], [Méndez and Greiner, 2003] as they can deliver reliable results. In addition, GA are very well suited to multi-objective problems, which is something also pursued in this work. A downside of these methods is that they typically require a large number of evaluations of the fitness functions, which translates into aero-acoustic analysis in our case.

5.2 Optimization strategy and procedure

The main strategy taken here to optimize the airfoil geometries consists on using a GA. This approach is used as suggested in [Marler and Arora, 1997], where special attention to the final results is taken as these algorithms only deliver global solutions and not local minima. The strategy will follow the traditional procedure of setting an objective function first, and defining its design variables and respective search space. Two optimization procedures result from this methodology as one will focus on optimizing its aerodynamic coefficients (maximize C_l/C_d). The other follows the inverse search (minimize SPL value radiated from the airfoil). Of major interest to this work is the possibility of a multi-objective optimization (MOO), meaning that in the context of WT and airfoil aero-acoustics, it is interesting to see how the airfoil geometry optimization evolves when the objective is to, simultaneously, maximize the aerodynamic coefficients ratio and minimize the total SPL value. So in the end we will be using two objective functions, in three different procedures, as described in subsection 5.2.1.

Before proceeding to the final mathematical definition of the optimizations here performed, we will first review the working conditions to which the airfoils to be optimized are subjected to. From the several previous chapters of this work, we can now summarize parameters like maximum SPL value, height above ground or ground roughness, blade radial positions of interest, wind velocity, and so on, required to make the optimization procedures as real as possible and that can be used as reference. The reference values regarding WT blade specifications are taken from real HAWT, as stated in product

specifications of internationally known manufacturers, like Vestas and Enercon [Vestas, 2011a], [Vestas, 2011b], [Enercon, 2010]:

- From section 2.2.3, we concluded that a generally accepted threshold for maximum SPL values radiated from a single WT, near a moderatelly populated areas is 45dB(A), which is useful to set a noise constraint, if required;

- From sections 3.1 and 4.2 many WT specifications were presented which can help integrate the airfoil under consideration in the WT. Some new relevant parameters are here added and summarized as well (table 5.1).

Parameter	**Range of values**
Power class [MW]	2 - 3
Hub Height (z [m])	70 - 80
Nominal revolutions (Ω [rpm])	15 - 17
Cut-in wind speed (U_{min} [ms^-1])	3 - 6
Rated wind speed (U_{max} [ms^-1])	14 - 20
Blade length (R [m])	40 ≈ 45
Effective angle of attack (α [deg]	0 - 25
Distance Source-Observer (r_e [m])	200 - 2000
WT Site/Location (z_0 [m])	0.3

Table 5.1: Summary on WT specifications considered in this work

With this information about the working conditions of the WT, and consequently the airfoil, we can now summarize and set the reference values that will be used for all parameters involved in the optimization operations. These values are responsible for the final results, which means careful consideration on each one was taken to guarantee as much as possible an accurate aerodynamic simulation and SPL prediction while attending for considerable generalization to the WT power class considered. First of all, the minimum and maximum wind velocities considered here are as shown in table 5.1, so for the specifics of optimization operations the values of 15 and 20 ms^{-1} will be used, as they represent typical values at which WT deliver better power output. The distance from source-to-observer is only required to account for a realistic assessment of WTs when near populated areas. For this procedure, the values of 250m and 1000m will suffice to understand how the airfoils being optimized, may be influenced by this parameter in particular and how noise emission may become irrelevant (or not) with increasing distance from the source. The height above ground, as explained in section 4.2.2, will be that of the hub ($z = 80m$) and for the ground roughness the respective value for suburban environments ($z_0 = 0.3$), as exemplified in fig. 5.1a). All remaining parameters directly related to blade specifications were considered while using as reference the blades used in commercial real WT (e.g. V90-3.0MW Vestas machine [Vestas, 2011a] and the Siemens SWT-2.3-93 [A/S, 2009]) and assuming a blade length of 44m and constant taper, for simplicity. This was required to estimate chord lengths and compute chord-to-radius (c/R) ratios (fig. 5.1b)). It is relevant to note as well that the velocity ratio values for each blade cross-section considered were estimated, assuming that the tip velocity ratio of the WT is 7, or in other words a constant rotational speed of 16rpm, which is a very common value for most multi-MW WT.

Parameter	Airfoil #1	Airfoil #2	Airfoil #3
Chord (c [m])	3.6	1.4	0.8
Airfoil span (L [m])	7.2	2.8	1.6
Maximum rel. thickness (t/c [%])	40	18	18
Radial position (r/R)	0.10	0.65	0.90
Velocity ratio (x)	0.70	4.55	6.30
Chord-to-Radius ratios (c/R)	0.08182	0.03182	0.01818

Table 5.2: Airfoil parameters considered for optimization purposes (based on specifications from [Vestas, 2011b]) and [A/S, 2009]

)

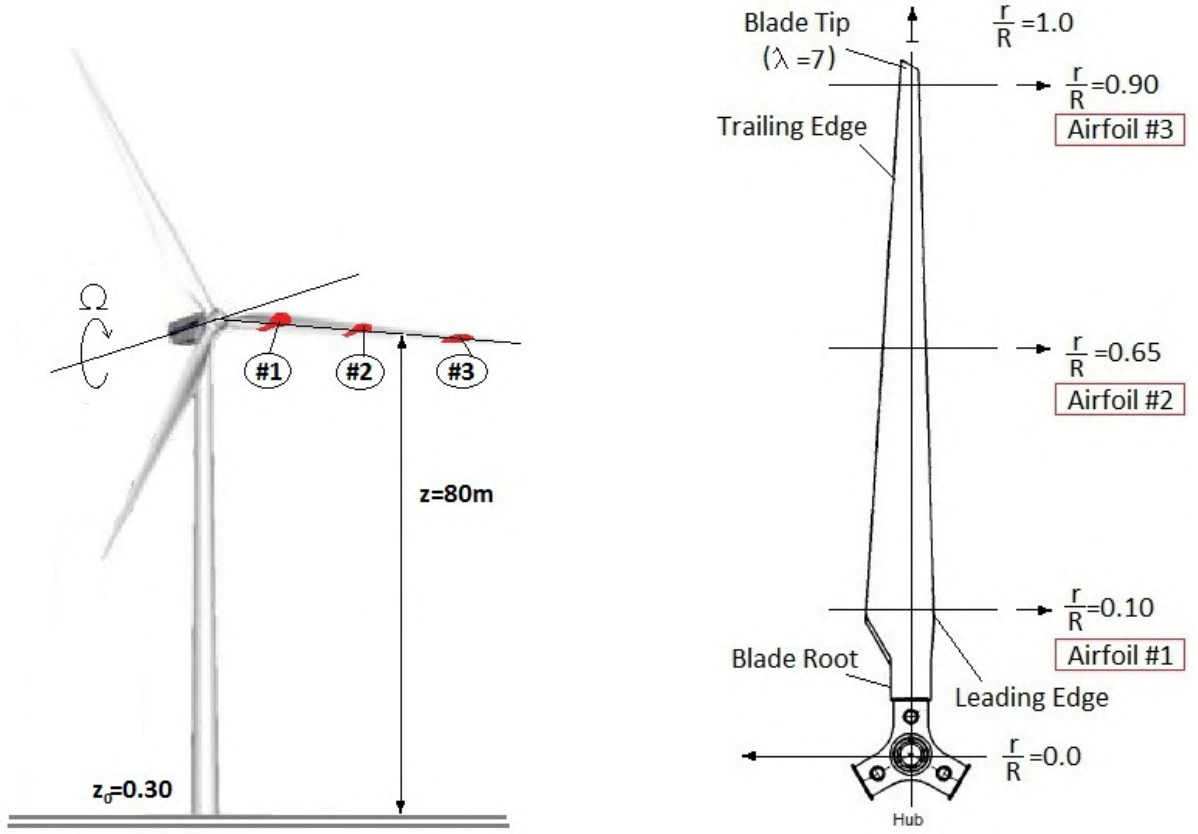

(a) Specifications for height above ground and ground roughness considered in the optimization

(b) Specifications considered for the several airfoil positions

Figure 5.1: Parameters considered in the optimization procedure

5.2.1 Objective functions, variables and constraints

The objective functions, design variables and constraints (as well as limits and search space) will now be detailed and specified. To begin with, the objective functions defined and used here were for one the ratio between the aerodynamic coefficients and secondly the total SPL value estimated from the airfoil. The design variables are the coefficients and parameters that can be used to alter the airfoil geometry (for the Bezier shaped airfoil, it is the CP coordinates). Also, the effective angle of attack of the airfoil is used as a design variable because it can be directly related with the resulting aerodynamic performance and amount of noise radiated and because it is assumed that the airfoil is integrated in a WT with pitch control. The constraints used will be mainly geometrical in nature or specific to some

issues encountered. In sec. 3.2.2, an issue was identified when using Bezier lines for this application. The problem is how the relative location of each CP to each other, is both maintained in order to always deliver an aerodynamic body and at the same time, to allow enough mobility and freedom of search to the CPs, in order to deliver a reliable result. This compromise between freedom of mobility and carefullness in the placing of each CP was based in the assumption that the final optimized airfoil has its CPs located relatively to each other, approximatelly in the same way as the reference base (initial) airfoil has its CPs. Consider fig. 5.2, where it is possible to see how this criteria affects mainly CPs 3, 11 and 15. For example, the position of CP_6 is directly related with the position of CP_3. Therefore as a result of this, a careful analysis of the effects of moving the points was performed and this served as well to find a feasible search space for each CP, or rather design variable. The constraints were then added to the optimization algorithm as differences between each consecutive CP. The search space considered

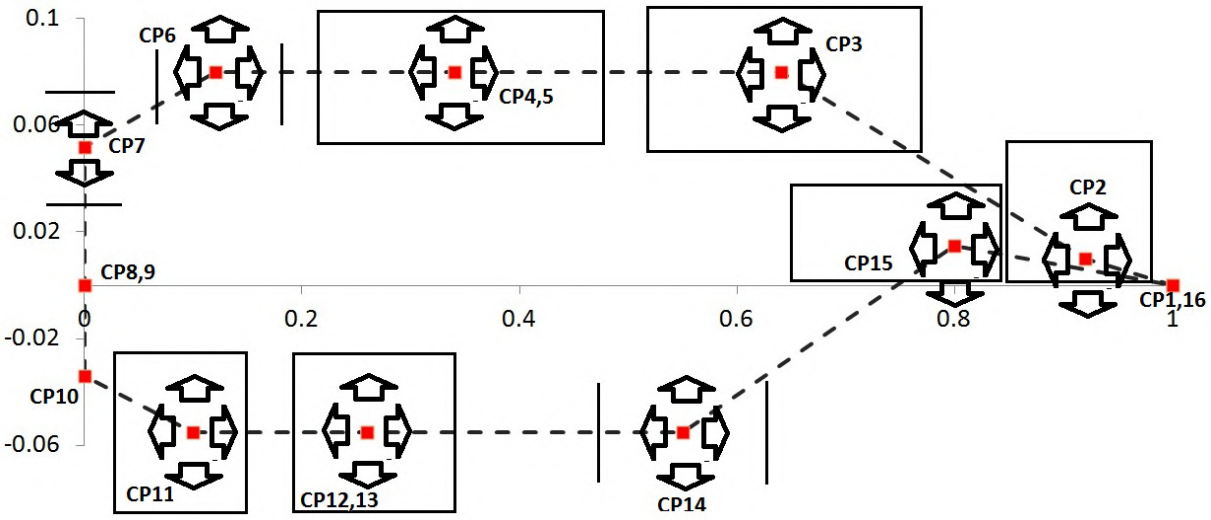

Figure 5.2: Example of a used set of starting positions of each CP (for generic reference airfoil) and a possible search space allowed of each CP

is of major relevance, especially when using GA, as it could be a major source of operational time cost. Basically, if the search space of a variable is left as wide as possible, when the GA populates that space it will be granted of too much space and may scatter the initial organisms too much. The crossover procedure would eventually narrow the search space with increasing fitness but it would take a big number of generations. And since using a higher value of individuals for the populations is not guarantied to attenuate this effect, a tuning procedure was also conducted here to narrow as much as possible the search space of each design variable. A qualitative assessment on some preliminary optimization tests was conducted, that allowed to see how the CPs would evolve in regard to their initial position. An obvious conclusion from this is that each optimization procedure allows for a specific refinement, but generally the modifications in the search space parameters were never too radical, meaning that in some cases one single CP could be allowed to move slightly more than before. Following this, the fixing of CPs 7 and 10 over the y axis became a necessity, for any subsequent optimizations and in the end all non-fixed CPs responsible for the design, were given slightly narrower search spaces, specific of each respective case.

Following the description of the involved parameters in the optimization, we can now present the mathematical definition of the optimizations here performed

$$
\begin{aligned}
\text{maximize} \quad & f_1(x) = \frac{C_l}{C_d} \\
\text{minimize} \quad & f_2(x) = SPL_{total} \\
\text{subject to} \quad & CP_{x,i} \geq CP_{x,i+1}, \quad i = 2,3,5 \\
& CP_{x,i} \leq CP_{x,i+1}, \quad i = 11,13,14 \\
& CP_{x,15} \leq CP_{x,2} \\
& CP_{y,i} \leq CP_{y,i+1}, \quad i = 2,3 \\
& CP_{y,7} \leq CP_{y,4} \\
& CP_{y,11} \geq CP_{y,12} \\
& CP_{y,15} \geq CP_{12} \\
& CP_{y,2} \geq CP_{y,15} \\
& t/c \leq j, \qquad j = 0.18, 0.40 \\
& CP_{x,i} = CP_{x,i+1}, \quad i = 4,12 \\
& CP_{y,i} = CP_{y,i+1}, \quad i = 4,12 \\
& C_l \geq 0.0001 \\
& C_d \leq 1.0000
\end{aligned}
\tag{5.2}
$$

where $f_1(x)$ is the objective function for the aerodynamic optimization that maximizes C_l/C_d and $f_2(x)$ is the objective function for the aero-acoustic optimization, which minimizes the total SPL value. The MOO will of course use both $f_1(x)$ and $f_2(x)$. All constraints account for the geometric restraints imposed on the CP coordinates of the Bezier lines. The side constraints are in regard to the lower and upper limits of the Bezier CP (as illustrated in fig. 5.2) and constraints were also imposed on the aerodynamic coefficients and relative thickness.

5.2.2 Optimization script and tools used

Aero-acoustic airfoil analysis: A brief description of the algorithm of the code developed in FORTRAN (F95), which was the compiler used to build the main computational tool created (program AAcoustic) to perform all airfoil geometry related operations, such as reference geometry build and modified airfoil parameterization, perform BL analysis and parameter computations and finally to compute and account for the aero-acoustic SPL values.

The code is made up of two main menus: ”Airfoil geometric analysis” and ”Aero-acoustic analysis”. The first menu, as the name states, is responsible for the operation of all routines assigned to geometry related tasks. The ”NACA” entry allows for the computation of the set of coordinates of any NACA 4 series airfoil and some NACA 5 digits series. The ”BEZR” entry enters the function in which operations

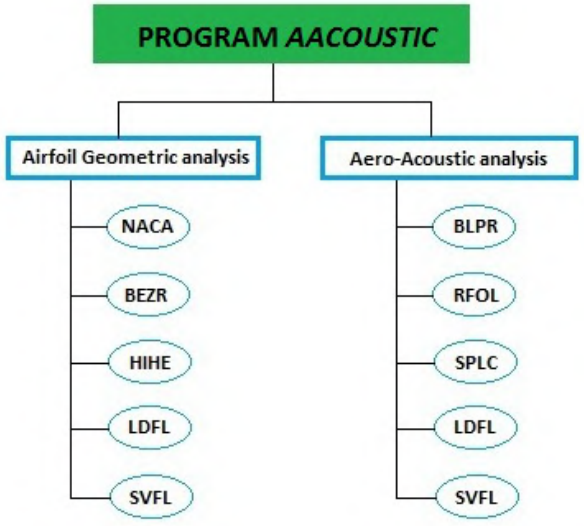

Figure 5.3: Flow diagram of the final code developed *AACOUSTIC*

with Bezier curves can be accomplished (introduce a Bezier curve on a pre-determined geometry or build an entire geometry from scratch). The ”HIHE” option enters the function responsible for computing Hicks & Henne functions and introduce them in a preset geometry. ”LDFL” and ”SVFL” options stand for the ability to load and save, respectively, a set of coordinates to a file. The second menu of the code, controls both the BL computation tools and the aero-acoustic prediction scheme. The first two are used to call the routines responsible for computing the BL parameters required, ”BLPR” will use the original BP&M expressions and ”RFOL” will use the Rfoil software. The entry ”SPLC” computes the aero-acoustic $1/3$ octave spectra values for the BL parameters computed, which in turn were obtained using a preset geometry. More details of the code can be seen in appendix B, the user's manual of the code.

Optimization algorithms: The optimization process consists on a computational tool that integrates the main code developed (AAcoustic), the Rfoil software and the optimizer interface in one single shell. The code developed in Python for this purpose is quite straightforward and simple, though it did prove to be somewhat of a challenge as one of the main objectives of this script was to call external programs, namely the main code developed in FORTRAN (AAcoustic) and to input commands on those same external tools. All that work was developed in the object-oriented Python language, as the scheme illustrated in fig. 5.4 demonstrates. The optimization process resorted to an external available computational tool called *pyOpt* [Ruben E. Perez, 2011] which consists of an object-oriented framework developed specifically for formulating and solving optimization problems. It is a Python module that uses a variety of integrated optimization algorithms which are accessible through a common interface. Its main features are the ability for true separation between the optimization problem formulation and its solution by different optimizers, an easy integration of all major optimization algorithms (gradient-based, gradient-free and population-based), can solve optimization problems where the function evaluations, from the model applications, run in parallel environments.

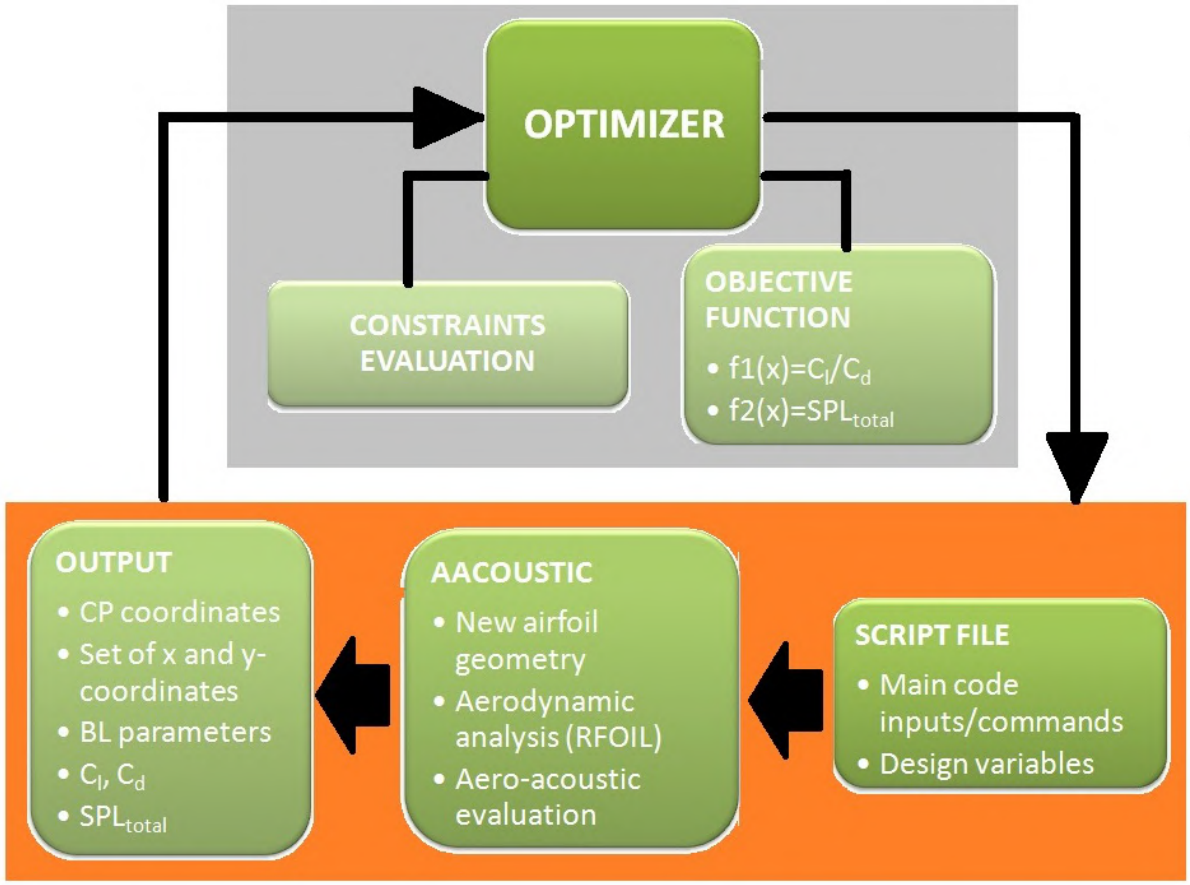

Figure 5.4: Optimization flow diagram

The robustness of the module, regarding specific applications in several engineering problems, has been put to the test in the works of [Perez et al., 2011]. The selected optimizer from pyOpt to be used here was the Non Sorting Genetic Algorithm II (*NSGAII*). It is a non-dominating sorting algorithm that solves non-convex and non-smooth single and multi-objective optimization problems. A global optimization is achieved as the algorithm enforces the constraints, through a tournament selection-based strategy. A *script* example of a MOO performed in this work, is presented in appendix B, in the original format of the Python language.

For a more efficient final optimization process, several test operations were performed for different values used for initial population and generations, for one reference airfoil. The objective was to assess the best compromise between initial population number[1] and maximum number of generations, and know the minimum call functions required before the objective function begins to stabilize in a global solution. Also, the combination of these two values (which is the same as considering the total call functions performed) is directly related to the total time of the operation. This evaluation is resumed in table 5.3 and illustrated in fig. 5.5) from which we can take the values for the initial population size (148) and maximum number of generations (135) that yield the best compromise.

[1] A relevant feature of this optimizer is that it uses always the same *seed* for generating the initial population

Test	Function calls	Initial population	Number of generations	Objective function value (C_l/C_d)	Time [s]	Relative gain [%]
1	10 000 20 000 30 000 40 000	100 100 100 100	100 200 300 400	204.6 205.5 205.5 -	3 510 6 516 9 743 -	- 0.42 0.00 -
2	10 000 20 000 30 000 40 000	148 148 148 148	68 135 203 270	203.9 205.6 205.6 -	3 631 6 850 10 079 -	- 0.79 0.09 -
3	10 000 20 000 30 000 40 000	200 200 200 200	50 100 150 200	201.0 202.8 - 203.1	5 457 7 207 - 27 227	- 0.90 - 0.00

Table 5.3: Summary of the optimization tests performed

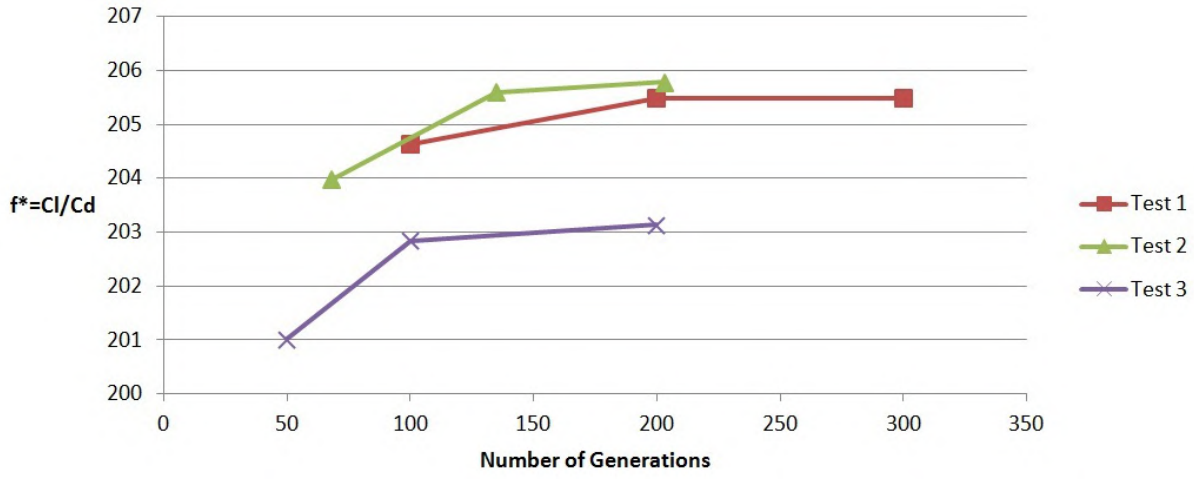

Figure 5.5: Chart illustrating how the optimizer converges to a solution, by changing the value of the stopping criteria (number of generations)

5.2.3 Optimization problems and issues

Some issues developed in the course of the several optimization procedures and though some were easily overcome, others may be a source of potential errors and are therefore relevant to point out. A very important issue regarding the Rfoil execution, would happen in the analysis of certain airfoils while the optimization *script* was running. That issue was in regard to the situations when Rfoil would not converge a solution and the files created with the BL computed values would not contain any information whatsoever, making SPL assessment impossible. For a completely automated procedure, it is required that the computer code discards these situations alone. Each time an airfoil geometry develops a situation like this, the values of both the aerodynamic coefficients and the total SPL, were then set at a reasonable penalizing value ($C_d = 1.0$;$C_l = 0.0001$;$SPL_{eq} = 100.0$).

The RFOIL software does not output a single file with only the values of the boundary layer parameters on the trailing edge nor the computed C_l and C_d for the airfoil. Instead, a distribution of all parameters over the airfoil surface against the x coordinate is given as well as the pressure coefficient

and friction coefficient distributions. It was necessary to create a specific routine that reads/extracts the BL parameters for the trailing edge coordinate in each file, and also integrates both the pressure and friction coefficients over the surface to obtain the final section values of C_l and C_d, as described next [de Brederode, 1997].

For a fixed axis to the chord of the airfoil, we have

$$\begin{cases} C_l = C_y \cos\alpha - C_x alpha \\ C_{d,airfoil} = C_x \cos\alpha + C_y \alpha \end{cases} \tag{5.3}$$

where C_y is computed as

$$C_y = \frac{Y}{1/2\rho U_\infty^2 c} = -\int_0^1 (\Delta Cp)_{x/c} d\left(\frac{x}{c}\right) \tag{5.4}$$

$(\Delta Cp)_{x/c}$ is the difference between Cp values of the upper and lower sides of the airfoil at the same x/c coordinate.

Following the same method, the C_x contribution is

$$C_x = \frac{X}{1/2\rho U_\infty^2 c} = \int_{y_l/c}^{y_u/c} ((\Delta Cp)_{y/c}) d\left(\frac{y}{c}\right) \tag{5.5}$$

As before, $(\Delta Cp)_{y/c}$ is the difference between Cp values of the up and downstream sides of the airfoil at the same y/c coordinate.

The C_d value of the above expression accounts only for the pressure term of drag but, since we know the skin friction coefficient distribution, we can obtain the drag value due to friction by integrating these values as one would do for the simple case of a flat plate (with the same width as the chord of the airfoil) and add the resulting value, that accounts for the friction effects ($C_{d,friction}$), to the previous value of $C_{d,airfoil}$

$$C_{d,friction} = \int_0^1 C_f d\left(\frac{x}{c}\right) \tag{5.6}$$

Finally, for the total C_d

$$C_d = C_{d,airfoil} + C_{d,friction} \tag{5.7}$$

Finally another issue was easily overcome regarding the situations when Rfoil would not converge a solution. When this happens Rfoil will not write any BL parameter information in the respective created files, so to identify this situations a specific routine was created to assess whether those files have the required information or not. In case they do not have any BL values, the total SPL is automatically fixed at 100dB(A) (this is used as a penalization criterion for optimization purposes) and an error message is presented to the user stating that no SPL prediction can be made.

Chapter 6

Optimization results and discussion

6.1 Introduction

This chapter presents a selection of the main results obtained from the several optimization tests along with a discussion of the same. This selection and summarized presentation of the results is required as the total number of optimizations performed during this work was too large (over 40 tests were conducted) and an individual analysis is also inefficient if one cannot make a comparison between the various geometries obtained. A simple nomenclature was set to identify the results using the name ”OptFoil” as in short for ”Optimized Airfoil”, followed by an integer that simply identifies the number of the optimization test performed that delivered the corresponding result.

The first section presented is a brief verification and validation of the code developed for this thesis, which can be perceived as a result of this work and because it is directly related with the final optimization results. The chapter continues with the description and overview of some reference airfoils usually integrated in a modern WT. The main results are presented in regard to the parameter being assessed and its effect on the geometry from the aerodynamic and aero-acoustic perspective, meaning that the sequence of discussion followed will be first the effect of the position of the airfoil relative to the blade, the effect of different flow speeds and the effect of variation in the relative position of the observer to the airfoil (or variation of the source-observer distance). All of these discussions are followed by the final corresponding geometries obtained. Finally, the most important results are detailed in the last section where the multi-objective optimization (MOO) is analyzed and a careful study of the Pareto front is performed.

6.2 Code verification and validation

As stated throughout this text, the several codes here developed are based on well established works about the several subjects handled. Most of these works, like the BP&M work, are semi-empiric in character and based themselves in several experimental results, from which the respective models were developed. This following section deals with the important task of verifying and confirming the correct

interpretation and use of all models considered throughout the work and that were applied in the form of computer code.

The most relevant points that require a good verification are the ones concerning the noise prediction schemes selected, which are more subject to interpretation and that allow for direct comparison to other codes developed. The original codes presented in the work of BP&M, that also present test cases to assess for the validity of the code, will be the reference to validate the reliability in predicting all noise mechanisms, except for the turbulent inflow, which in turn will be cross-referenced to the results presented in the works of Moriarty et al. [2005] and Zhu et al. [2005], two of the main base references for implementing the code here developed concerning this specific noise mechanism.

6.2.1 Comparison to the work of BP&M

In the work developed by Brooks et al. [1989], the original noise prediction scheme presented in Fortran by the authors, was tested using the parameters summarized in tab. 6.1. The tests were performed for all airfoil self-noise mechanisms except the TE bluntness and tip noise, as suggested in the original reference for simplicity. Figure 6.1 illustrates how close to the original code (blue line) are the results

Airfoil	NACA 0012
Chord [m]	0.3048
Airfoil span [m]	0.4572
Distance [m]	1.22
$\Theta_e[deg]$	90.0
$\Phi_e[deg]$	90.0
$\alpha[deg]$	1.516
Wind mean speed [m s^{-1}]	71.3

Table 6.1: Test parameters used for reference airfoil

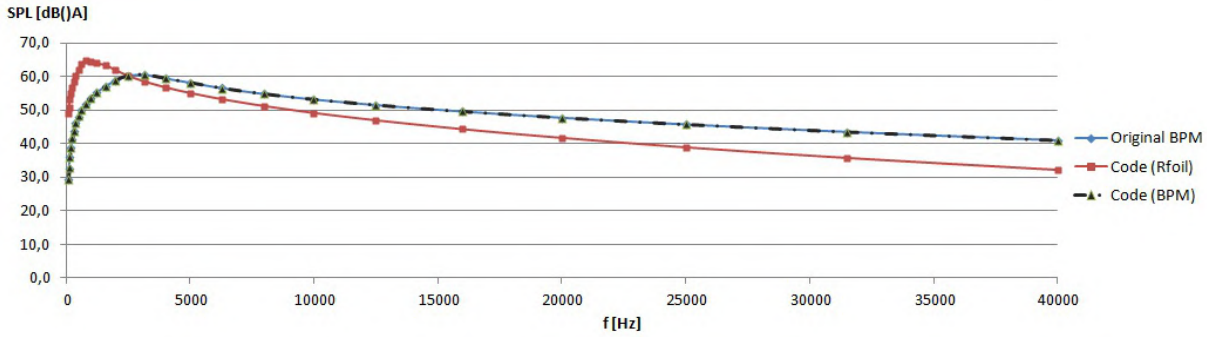

Figure 6.1: Results for the SPL computation of the NACA 0012 airfoil, for all airfoil self-noise mechanisms

here obtained (dashed black line), when using only the tools presented in that same work (BL parameters computed using the expressions from the original code - section 3.3). In the same graphic, it can be seen another set of total SPL values computed, when using the Rfoil software to compute the BL parameters (red line). The differences are obvious which is not surprising since the Rfoil software is expected to predict the BL parameter values following a different method than the more empirical expressions of the original work, shown in subsection 3.3.1. Those differences are notorious when comparing the resulting

BL parameter values from the BP&M expressions with the ones from Rfoil, for the same test parameters as seen in tab. 6.2. Basically, Rfoil seems to deliver higher values for the BL parameters which may result in a slight over-prediction of the final SPL values.

Computation tool	δ_s	δ_s^*	θ_s	δ_p	δ_p^*	θ_p
BP&M expressions	0.00755	0.00138	0.00088	0.00589	0.00094	0.00062
Rfoil results	0.01978	0.0045	0.00269	0.0116	0.00235	0.0015

Table 6.2: Comparison of BL parameters (BPM expressions vs. Rfoil)

6.2.2 Turbulent inflow prediction scheme

To ascertain if the code developed here is a reliable tool (or at least satisfactory in fulfilling the main objective) in regard to the computations of the turbulent inflow noise mechanism, two different strategies are possible: the direct comparison to the NAFNoise [Moriarty, 2005] code developed by the same authors of the work used as reference here for these computations [Moriarty and Migliore, 2003]; and the cross-reference to other works that successfully made use of this prediction model, when developing their own prediction codes. However both options present disadvantages. For one, the NAFNoise user's manual specifically states that the results obtained from that software should only be used in a qualitative way, meaning that they should not be interpreted as correct in absolute terms. On the other hand, though many works present results for this noise mechanism, it is difficult to compare them to others as most authors present the results only in a graphical manner.

Nevertheless, the most important idea here is to assess if the code has been correctly developed, or in other words, if the work of Moriarty and Migliore [2003], that presents the simplified Guidati method, has been correctly interpreted and can here deliver reliable results. Moreover, since this method makes use of the turbulent inflow prediction scheme of Amiet, corrected by Lowson (see chapter 4), this too will also be tested. Figure 6.2 presents the results obtained from both the code developed here as well as from the NAFNoise code, for the same test parameters as before and using a value for the turbulence intensity of 15.57% and a turbulent length scale of 69.8m (these total SPL values account for noise due to turbulent inflow only, and for frequencies up to 2500Hz, where $St \leq 75$). It is visible that for the

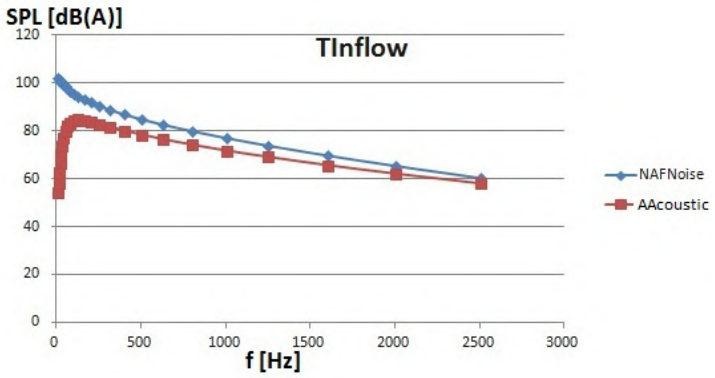

Figure 6.2: Results for the SPL computation for turbulent inflow noise, of the NACA 0012 airfoil

low frequency range, the NAFNoise code over predicts noise levels, with values as high as 100dB(A), which are not very realistic. Both curves follow the same trend for frequencies above 100Hz, though the NAFNoise code always delivers higher values. Both discrepancies are likely to be related with the computation methods used for the turbulence intensity and length scale, as both are of great relevance for the computation of this noise mechanism.

As a last remark it is worth to note that some ”fudge” factors can be found within the source code of the main reference used here for comparison (namely the NAFNoise software). Authors will often resort to additional factors to make the developed softwares to give better agreement with experimental values. Any existing discrepancies between these codes (like the ones referenced before), that are based on the same theoretical models, can be attributed to whether those factors are used or not. In this work, only the factors whose inclusion is clearly explained and detailed in the source codes, were used.

6.3 Reference airfoils

The aerodynamic and aero-acoustic evaluation of well known established geometries in the field of WT technology is presented here, which will be used for direct comparison when discussing in detail the main results. The selected airfoils for these tests are FFA-W3-211[Bertagnolio et al., 2001], S809 [Moriarty, 2005], NACA4421 and NACA63415 [Carmichael, 2010], [Dahl and Fuglsang, 1998] and were chosen as representatives of some of the most commonly used airfoil families in WT technologies. These reference airfoils were optimized to account only for the optimum angle of attack for both objective functions evaluated, which means that they will be analyzed as if integrated in a WT blade in the radial positions they are more likely to be found (as detailed in table 6.3). The major relevance of these benchmark tests is to have present the typical values for the C_l/C_d ratio of known airfoils and, most importantly, to make an estimate of the SPL values from these airfoils, while using the developed code. Both of these objective functions are evaluated for the same working conditions used for the main optimizations performed, as summarized in tab. 6.3 meaning that the optimum angle of attack of these airfoils for the maximum C_l/C_d ratio will be found for $U = 20[m.s^{-1}]$ and the SPL values will be assessed for the same flow speed and with $r_e = 250.0[m]$.

	FFA-W3-211	S809	N4412	N63415
U	20			
r_e	250.0			
r/R	0.10	0.10	0.65	0.90
c [m]	3.6	3.6	1.4	0.8
x	0.7	0.7	4.5	6.3
L [m]	7.2	7.2	2.8	1.6
t/c	0.21	0.21	0.12	0.15
$\Psi[deg]$	16.3	11.7	15.6	14.4
max $C_l/C_d(\alpha^*[deg])$	165.9 (6.4^o)	117.9 (3.4^o)	143.8 (9.1^o)	125.7 (2.2^o)
min $SPL_{Total}(\alpha^*[deg])$	33.8 (13.8^o)	35.8 (1.0^o)	62.0 (0.8^o)	64.2 (0.1^o)

Table 6.3: Constant parameters and best values for f_1 and f_2 for the reference airfoils

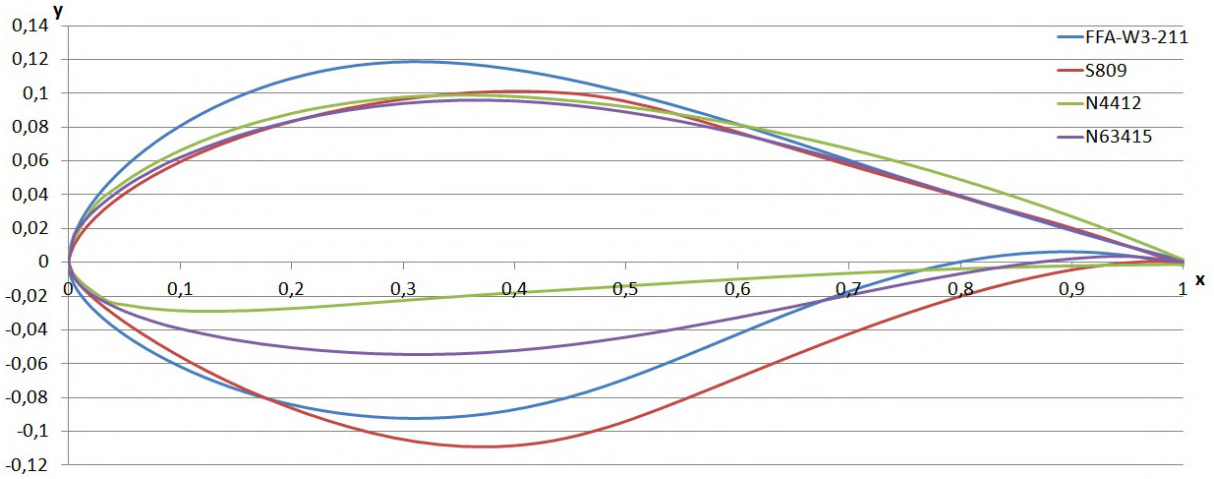

Figure 6.3: Geometries of the selected reference airfoils

Table 6.3 presents a set of airfoils that can be integrated (and are actually used worldwide) in the design of a real WT blade and, from the properties displayed by each airfoil, it is apparent that the C_l/C_d ratio can be generalized, for this set, to be in the range of values between 110.0 to 170.0. This leads to the conclusion that airfoils used in WTs present reasonable or even good aerodynamic performance characteristics, setting a useful set of reference values to compare the results from the optimized airfoils, that are being designed for the same radial positions considered for these. It will be interesting to see how much the aerodynamic performances of the optimized airfoils deviate from these references and, the evolution of the geometries in comparison to these reference airfoils.

What is also relevant to point out from this survey on some reference airfoils is that some geometries are introduced in the field of WT from the aeronautics industry, and its geometries were designed with different objectives in mind, where most likely aero-acoustic noise was never a major concern, being in some cases even overlooked. That is immediate from the total SPL values delivered by the NACA 4 and 6 series airfoils presented, which represent some of the most modern and commonly used airfoils in aeronautics. This higher values in regard to the ones delivered from the airfoils set at the near root section, are very likely affected by other parameters and not just radial position, but it is expected that overall, these representative airfoils are to always deliver higher SPL values.

6.4 Effect of the radial position

In this section, the resulting airfoil geometry is analyzed for the three radial positions considered ($r/R = 0.10, 0.65, 0.90$). From the aero-acoustic perspective, the highest SPL values are related to high flow speeds as well as close measuring distance considered. As such, the airfoil results were tested with $U = 20[m.s^{-1}]$ and $r_e = 250[m]$. Table 6.4 presents the specifics of the used airfoils in these optimized tests. Airfoils 3, 15 and 27 were optimized to deliver the maximum ratio of C_l/C_d whereas airfoils 7, 19 and 31 were optimized to deliver the minimum total SPL value.

$U = 20[m.s^{-1}]$ $r_e = 250.0[m]$						
Parameter/OptFoil	3	7	15	19	27	31
r/R	0.10		0.65		0.90	
c [m]	3.6		1.4		0.8	
x	0.7		4.5		6.3	
L [m]	7.2		2.8		1.6	

Table 6.4: Constant parameters used for obtaining OptFoils 3, 7, 15, 19, 27 and 31

Aerodynamic assessment: For the aerodynamic assessment, table 6.5 presents the respective optimization results for OptFoils 3, 15 and 27 whose geometries are illustrated in fig. 6.4.

	OptFoil3	OptFoil15	OptFoil27
t/c	0.19	0.13	0.13
$\Psi[deg]$	9.9	16.1	5.3
C_l	1.8399	1.134	1.1084
C_d	0.0072	0.0059	0.0057
$SPL_{Total}[dB(A)]$	33.4	61.7	64.3
$\alpha^*[deg]$	11.5	6.7	7.5
f_1^*	256.9	190.9	194.1

Table 6.5: Optimization results, to assess the effect of radial position on aerodynamic performance

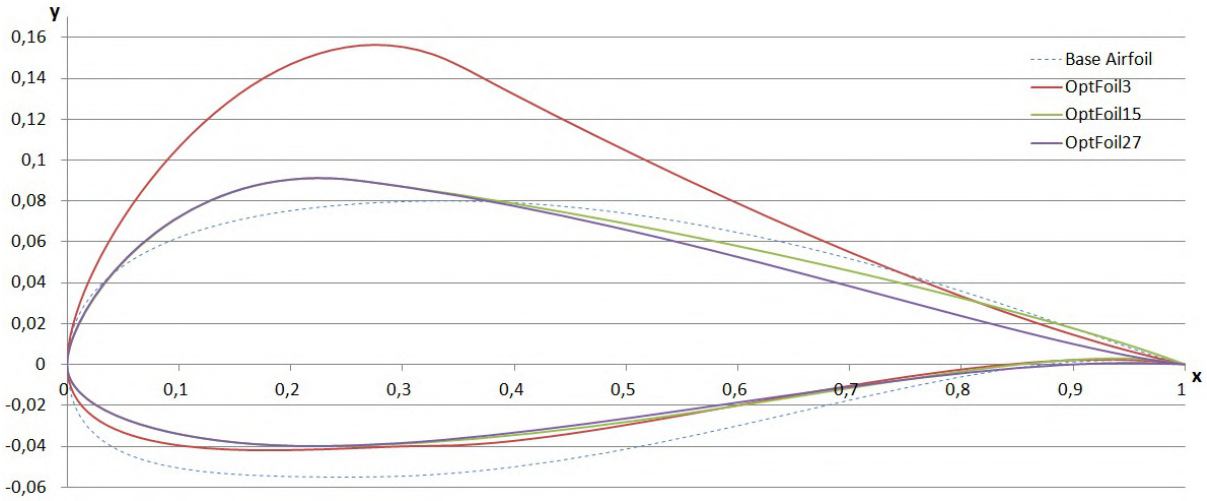

Figure 6.4: Optimized geometries, to assess the effect of radial position on aerodynamic performance

Let us begin by analyzing the three geometries displayed. First of all, it is obvious that none of the airfoils maintained its original (base) shape and the biggest difference between the three is the relative thickness. For OptFoil 3, the CPs responsible for defining the suction side worked together to force CP6 into developing a highly cambered LE (this is reinforced by the position that CP11 acquired). The same airfoil is also quite thick in its length, whereas the other two have a more traditional shape. In regard to OptFoils 15 and 27, it is worth to note how their overall shape is almost identical except for the slightly thicker half section of OptFoil 15 (from approximately x/c=0.40 to 1.0) and a small difference in the pressure side shape. During the optimization tests performed, no constraints were set for the relative x-coordinate for which y is maximum, so it is worth to note how this parameter evolved in these airfoils. It is immediate again, that OptFoil 3 makes the difference by setting the maximum thickness on

the suction side at $x/c \approx 0.28$ and both OptFoil 15 and 27 have this point at $x/c \approx 0.21$, slightly closer to the LE. A final remark to the TE shape is made, where it is possible to see that OptFoil 15 developed a much higher TE wedge angle than the other two airfoils and that OptFoil 3 makes a bigger difference in the slope, on the suction side. This slope is related with the slight depression of the geometry of that airfoil, which is most noticeable near the maximum thickness coordinates and that, theoretically should be responsible for a higher sensitivity to transition for the same airfoil. With this information about the geometries and combining it with table 6.5, we immediately realize how the bigger airfoils (OptFoils 1 to 12 and here represented by OptFoil 3) deliver the biggest C_l/C_d ratio in all of the tests. This is related with two subjects: the accepted maximum relative thickness value set for these near-root airfoils and the trend of the CPs that define the suction side to develop a big "bump" right after the LE, when the objective function is to maximize f_1. This is consistent with the theory of aerodynamics [de Brederode, 1997] which can also be used to explain that the resulting higher values of f_1 for the bigger airfoils, located in the radial position $r/R = 0.10$, are also related with the higher values of the optimum angle of attack found for these airfoils (OptFoils 15 and 27 actually use very similar values for α, below that of OptFoil 3). Overall, this aerodynamic assessment leads us to believe that the airfoils in the near root region, because they were optimized with more relaxed constraints namely a bigger maximum relative thickness, can deliver higher ratios of C_l/C_d, but this was only allowed to follow the trend in the WT field, where it is common practice to design the blades with bigger (thicker and lengthier) airfoil cross sections near the root for structural purposes and not for better aerodynamic performance. Resorting to table 6.3, we can see how radial position has this effect in typically used airfoils in WT blades as the reference airfoils set at the root are more likely to deliver high aerodynamic values because of the geometric freedom that is allowed in those positions. Furthermore, it is also worth to note the differences in the C_l/C_d ratio when comparing the reference airfoils with OptFoils 3, 15 and 27 and how the corresponding SPL values are very similar. If we analyze only the aerodynamically optimized airfoils placed in the mid-span or near-tip region of the blade (OptFoils 13 to 16 and 25 to 28), we will conclude that the optimum angle of attack is quite consistent in the range of 6 to 7 degrees and that the maximum values for f_1 are between 190.9 and 210.0 (this last value was obtained for OptFoil 25). Table 6.5 exemplifies this with OptFoils 15 and 27, meaning that a maximum relative thickness of 18% of the chord will allow the airfoil to obtain an acceptable maximum ratio of C_l/C_d.

Aero-acoustic evaluation: The same base airfoils were used in an optimization problem to minimize the SPL values, working under the same conditions.

Table 6.6 will immediately point out that the more exterior airfoils relative to the blade root will produce the highest SPL values, which was to be expected as the works of Oerlemans and Schepers [2009] concluded with detailed experimental tests. This was already apparent from the results in table 6.5, although the values now presented are the minimum SPL values obtained in the considered optimizations, with no consideration for aerodynamic performance. This direct relation between the increasing SPL value as radial position moves outward from the root of the blade is easily explained by the aerodynamics inherent to the working conditions of any WT, as stated in the beginning of chapter 3. The fact that

	OptFoil7	OptFoil19	OptFoil31
t/c	0.4	0.18	0.18
$\Psi[deg]$	6.2	7.4	4.6
C_l	0.3836	0.1587	0.1217
C_d	0.0093	0.0061	0.0062
$SPL_{Total}[dB(A)]$	22.7	59.0	61.6
$\alpha^*[deg]$	0.001	0.120	0.149
f_2^*	22.7	59.0	61.6

Table 6.6: Optimization results, to assess the effect of radial position on noise levels

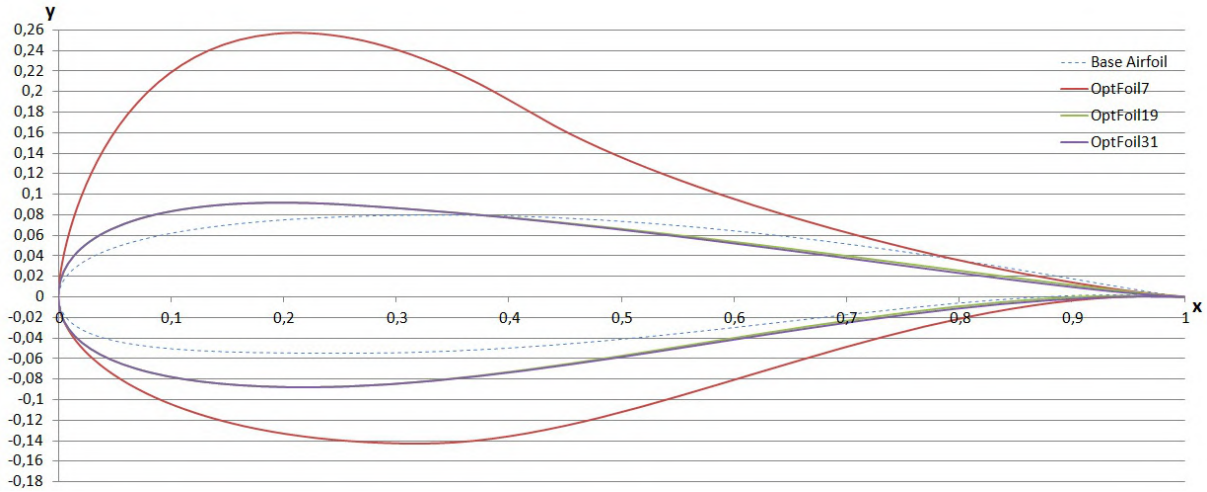

Figure 6.5: Optimized geometries, to assess the effect of radial position on noise levels

rotational effects are to be considered, makes the airfoils placed at the near tip region, develop quite elevated local relative flow speeds at the approach to the LE, which is the main responsible factor for developing more turbulent flows at those locations, contributing for an increase in the effect of TBL-TE noise mechanisms, thus resulting in noisier airfoils. Geometrically, this can be seen by the differences of OptFoil7 in regard to OptFoils 19 and 31, as the first, again with a bigger relative thickness, developed a cambered airfoil with very thick suction and pressure sides while the other two maintained a more similar shape, almost symmetrical and thinner. At first, this means that OptFoils 19 and 31 should be less sensitive to transition effects (hence generating less noise, namely due to TBL-TE or separation noise mechanisms) than OptFoil 3, that has a big depression in its geometry immediately after the maximum thickness point of the suction side. However, as the results show, this is not true and the main reason is precisely the bigger local flow speed at the more external radial positions. Another very important reason that may be responsible for making the thicker airfoils radiate the lower SPL values is the turbulent inflow noise mechanism, which is directly dependent of the LE geometry, especially its relative thickness (see section 4.2.2). The authors from Moriarty et al. [2005], in which the code developed here is based, concluded that the linear relation between the ΔSPL value and the *Strouhal* number was sensitive to both camber and thickness (though thickness was of greater relevance in this matter). In other words, the sense that airfoils with a ”blunt” LE produce less inflow turbulence noise becomes apparent, whereas airfoils with sharp (thinner) LE will not. As a final remark on the aero-acoustics of these airfoils, when comparing these to the SPL values delivered by the reference airfoils, it is notorious the difference of

noise levels as the reference airfoils commonly used in WT nowadays develop much more noise than the ones here optimized. Of course, this is not enough to state that these OptFoils are better than the reference airfoils.

6.5 Effect of the flow speed

Flow speed is a major parameter in any aerodynamic analysis and its influence on the optimization tests was already briefly commented in the previous section. The following results were obtained for the airfoils placed at the near tip region of the blade, which have demonstrated to be the most interesting to analyze on this matter. The other parameter that was fixed for these evaluations is the source-observer distance, set at $r_e = 250.0[m]$. Table 6.7 resumes this information.

$r/R = 0.90 \quad r_e = 250.0[m]$				
Parameter/OptFoil	25	29	27	31
U	15		20	
c [m]	0.8			
x	6.3			
L [m]	1.6			

Table 6.7: Constant parameters used for obtaining OptFoils 25, 29, 27 and 31

Aerodynamic assessment: For the evaluation of the aerodynamic performance, OptFoils 25 and 27 are selected to represent the optimized airfoils in this working conditions, where the main difference between the two is that OptFoil 25 accounts for the optimization with $U = 15[m.s^{-1}]$ and OptFoil 27 is the optimized geometry for $U = 20[m.s^{-1}]$. Table 6.8 presents the optimization results of these two airfoils and the respective geometries are shown in fig. 6.6. In the results presented in table 6.8,

	OptFoil25	OptFoil27
t/c	0.15	0.13
$\Psi[deg]$	8.6	5.3
C_l	1.2096	1.1084
C_d	0.0058	0.0057
$SPL_{Total}[dB(A)]$	59.5	64.3
$\alpha^*[deg]$	7.37	7.46
f_1^*	210.0	194.1

Table 6.8: Optimization results, to assess the effect of flow speed on aerodynamic performance

it is immediate that OptFoil 25, though optimized for the lower value of U, has developed the higher C_l/C_d ratio. It is notorious how by simply imposing an increase of 5 $m.s^{-1}$ in U lead the optimizer to develop such different geometries. Although the pressure side of both airfoils is almost identical, it is the bigger relative thickness, set at a higher x-coordinate for OptFoil 25, that indicate how it developed such C_l/C_d ratio. The shape of that airfoil indicates it may be slightly more cambered than OptFoil 27, which can explain the higher value of C_l. Even with such different suction sides and at a very similar angle of attack, both airfoils develop nearly the same drag coefficient, with a slight bigger value, again

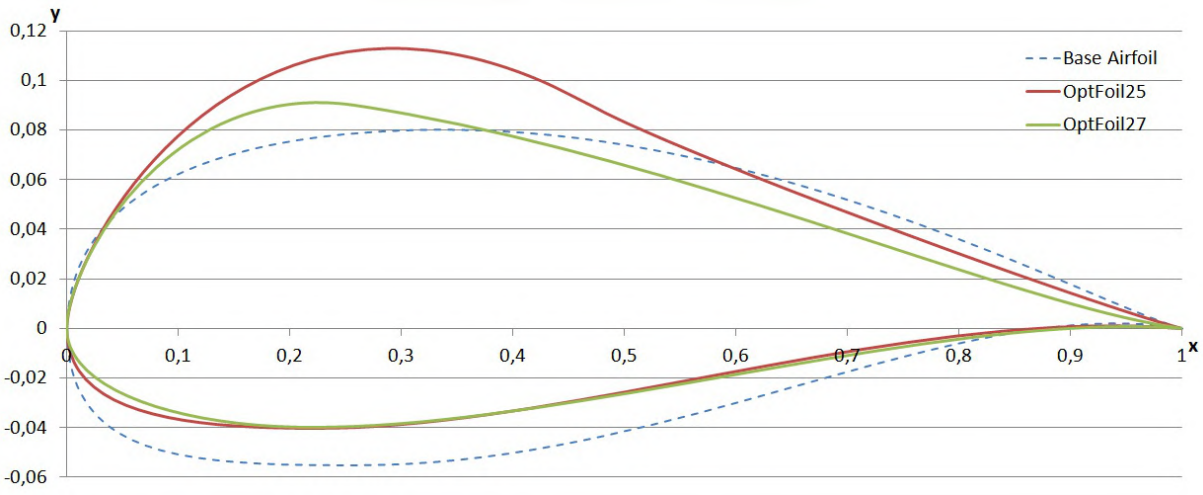

Figure 6.6: Optimized geometries, to assess the effect of flow speed on aerodynamic performance

for OptFoil 25 which can be explained for its higher sensitivity to transition effects due to the depression it presents after the maximum thickness point. Nevertheless, these results become very interesting when comparing the two airfoil geometries taking under consideration not just all of these aerodynamic parameters but also the respective total SPL values radiated. In this matter, it is obvious that the airfoil with the lower flow speed should deliver a smaller SPL value, as can be seen from the results for OptFoils 25 and 27, but a difference of 7.5% (or 4.8 dB(A)) can be acknowledged as a big difference, especially when considering the two airfoils under analysis in which the only difference is the flow speed. Put even more dramatically, it is impressive how the increase of 5 $m.s^1$ developed a thinner and less cambered airfoil that radiates nearly as many dB(A) as U was increased. This will be analyzed with care next.

Aero-acoustic evaluation: The optimization results for assessing the minimum SPL values for the same conditions described in table 6.7 delivered OptFoils 29 and 31, which results are presented in table 6.9 and the respective geometries are given in fig. 6.7.

	OptFoil29	OptFoil31
t/c	0.18	0.18
$\Psi[deg]$	6.7	4.6
C_l	0.1235	0.1217
C_d	0.0065	0.0062
$SPL_{Total}[dB(A)]$	57.1	61.6
$\alpha^*[deg]$	0.00	0.15
f_1^*	57.1	61.6

Table 6.9: Optimization results, to assess the effect of flow speed on noise levels

	25 $\rightarrow$ 29		Rel. diff [%]	27 $\rightarrow$ 31		Rel. diff [%]
C_l	1.2096	0.1235	-89.8	1.1084	0.1217	-89.0
C_d	0.0058	0.0065	+11.7	0.0058	0.0062	+7.2
$SPL_{Total}[dB(A)]$	59.5	57.1	-4.0	64.3	61.6	-4.3

Table 6.10: Direct comparison between OptFoils 25 and 29 and OptFoils 27 and 31

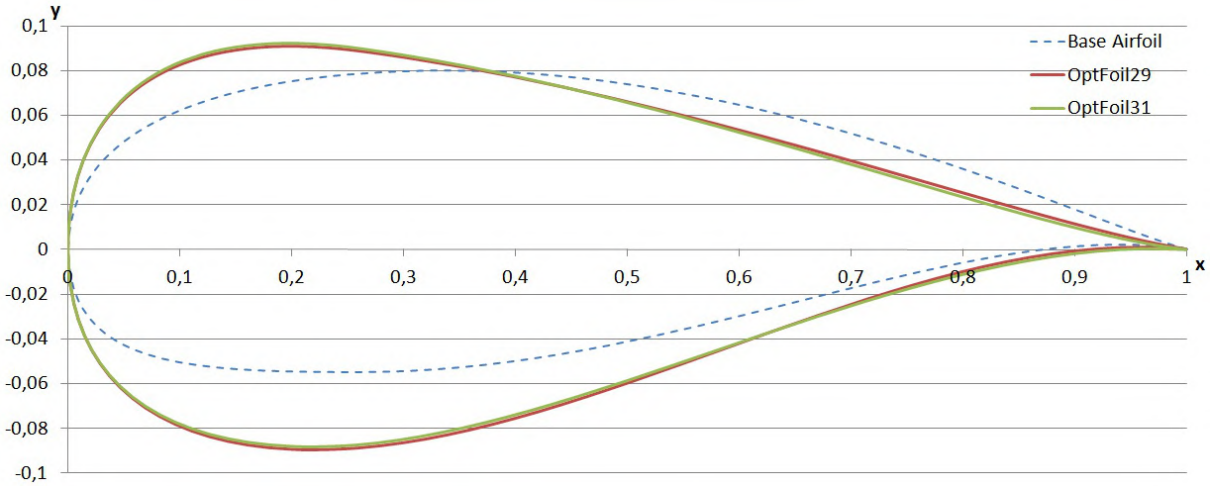

Figure 6.7: Optimized geometries, to assess the effect of flow speed on noise levels

The topic of aero-acoustic assessment for OptFoils 29 and 31 is very useful to assert the truth in the preliminary aero-acoustic analysis described at the end of the previous paragraph. Following what was acknowledged from the results for OptFoils 25 and 27, the same behavior is seen here with higher SPL values being radiated from the airfoil with increasing flow speed, meaning that OptFoil 29, which is under the lowest flow speed, delivers the least SPL value. What is relevant to point out is that the relative difference in the two lowest SPL values obtained in the considered optimizations retain a very similar value as that of the one found before for OptFoils 25 and 27. Put in numbers this means that OptFoil 29 radiates less 4.5 dB(A), roughly the same difference observed between OptFoils 25 and 27. This consistency reinforces the idea that an almost linear correlation may exist between the flow speed and the increase in the total SPL value. In addition to this, one must consider the geometries that delivered these minimum values. In comparison to OptFoils 25 and 27, the differences are obvious since OptFoils 29 and 31 evolved to a ”tear” like shape, with a relative maximum thickness of 18% set at, an abnormally close to the LE x-coordinate. And, unlike OptFoils 25 and 27, these evolved to a nearly identical shape. The thickness distribution observed for these airfoils seem to create a symmetrical shape, but it is visible that the TE at the pressure side bears a slight depression towards the inside of the airfoil. Again, the geometrical differences between OptFoils 29 and 31 are nearly negligible and that is sustained by the aerodynamics of these airfoils as both work at an angle of attack near 0^o and deliver very low values for C_l, for similar (and high) values of C_d. In fact, the increase in flow speed seems to have no effect here, regardless the increase in the SPL. This leads to the conclusion that flow speed has, as expected, a direct impact in the noise levels delivered by the optimized airfoil whether one wants to maximize aerodynamic performance or minimize aero-acoustic noise with a certain estimated consistency.

The geometries of OptFoils 25, 27, 29 and 31 allow for the direct comparison between each other as all are subjected to the same working conditions, being the only difference the objective function considered. This comparison allows for the conclusion that a minimization of the total SPL value is possible by varying the flow speed, but at great cost of the aerodynamic properties (see table 6.10) and a very slim reduction of the noise level. The gain in SPL values decrease are, at best, around 2.3 to

2.7 dB(A) but with a reduction in C_l of nearly 90% for both comparisons. From all this, it is obvious that OptFoils 25 and 27 are favourites as they radiate very similar SPL values to those of OptFoils 29 and 31, but with the advantage of much better aerodynamic performance. These, however, may not yet be the best aero-acoustic geometries.

6.6 Variation of the source-observer distance

Of all parameters considered in the optimization procedures, the source-observer distance (r_e) is the one more directly related with noise assessment, that was a subject of sensitivity analysis. Others were also considered and used in the several optimization tests, but none has as greater impact on all noise mechanisms considered as the distance factor and a sensitivity test of each noise mechanism and its main properties would create a too extensive work. For that reason, the conditions for the two distances considered in the tests, used to obtain the geometries that minimize SPL values, are as presented in table 6.11.

$r/R = 0.90\ U = 20.0[m.s^{-1}]$		
Parameter/OptFoil	31	32
r_e	250	1000
U	20	
c [m]	0.8	
x	6.3	
L [m]	1.6	

Table 6.11: Constant parameters for airfoils 31 and 32

Aero-acoustic evaluation: The representative airfoils selected for this assessment are OptFoils 31 and 32. The corresponding optimization results are described in table 6.12 and the geometries are illustrated in fig. 6.8.

	OptFoil31	OptFoil32
t/c	0.18	0.18
$\Psi[deg]$	4.6	4.6
C_l	0.1217	0.1809
C_d	0.0062	0.0063
$SPL_{Total}[dB(A)]$	61.6	49.6
$\alpha^*[deg]$	0.15	0.08
f_2^*	61.6	49.6

Table 6.12: Optimization results, to assess the effect of source-observer distance on noise levels

Stating the obvious, it is expected from the airfoil optimized with the greatest distance value under consideration, to deliver the lowest SPL value, which is consistent with the results for OptFoils 31 and 32, as shown in table 6.12, where OptFoil 32 presents 49.6 dB(A) for a distance 4 times greater than the distance considered for OptFoil 31. This is basically the effect that distance has on the final SPL values. In terms of geometry, OptFoil 31 has already been discussed in detail in the previous section (section 6.5) and both geometries do not add anything of relevance to the analysis of the effect of

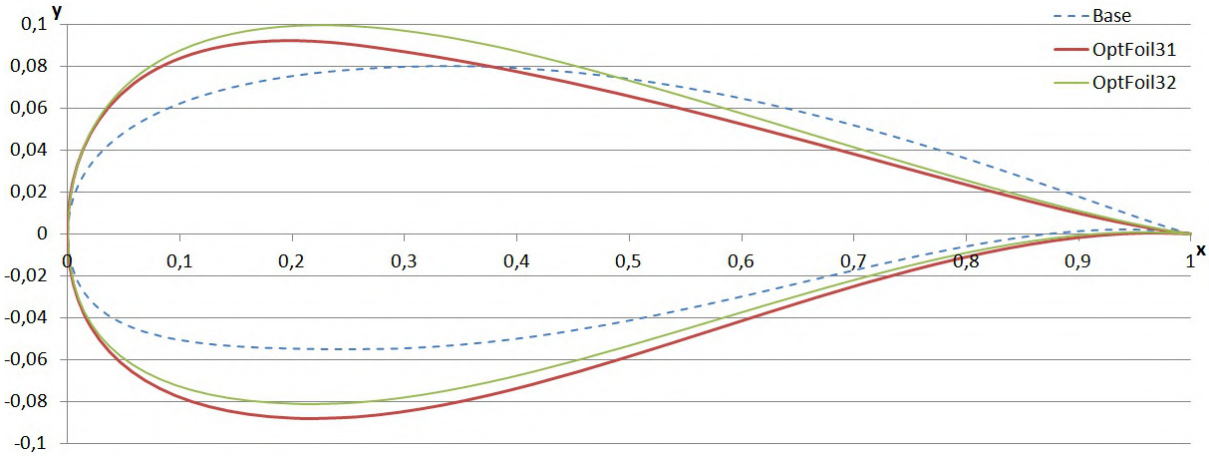

Figure 6.8: Optimized geometries, to assess the effect of source-observer distance on noise levels

distance. The major difference in shape is that OptFoil 32 has the maximum thickness point in the suction side slightly more above than OptFoil 31, with the opposing point (maximum thickness for the pressure side) accompanying that rise. Despite, this all other parameters are identical including the aerodynamic properties. If a similar comparison to the one performed in the previous section is made here between OptFoils 28 and 32, the same conclusion as before can be made as to which advantages are there for searching for the minimum SPL. Again, the gain in reducing the SPL value is very slim at a great cost of aerodynamic performance. It is interesting to see again that the airfoils optimized to deliver the less noise possible acquired a nearly identical shape for both distances considered and both developed a shape that is overall very symmetrical with a slight S-tail effect on the pressure side. This last feature may be related with TE bluntness noise, as it requires that the TE wedge angle to be as small as possible, which is most likely to blame for not allowing the optimizer to develop a completely symmetrical airfoil. This behavior had already been seen for OptFoils 19 and 31 (section 6.4) where both developed nearly symmetrical shapes and although being considered in different radial positions the optimizer followed the same trend. In any case, this detail in geometry evolution is good representation of the commitment of the optimizer in minimizing SPL values, since TE bluntness noise is not expected to be of major relevance in comparison to other noise mechanisms. This leads to the conclusion that this type of geometries are the one to more likely develop smaller amounts of SPL values in complete detriment of aerodynamic performance.

6.7 Multi-objective optimization and Pareto front analysis

In this section, the MOO performed for the airfoils considered at the near tip region of the blade, with the constant parameters as described in table 6.13, are analyzed. This evaluation is probably the most relevant of all analysis performed so far, as the compromise between aerodynamic performance and aero-acoustic properties is studied. For a better analysis of this compromise, the Pareto front of the MOO is very important and the same is illustrated in fig. 6.9.

The Pareto front consists on the relation between f_1 and f_2, delivered by the several geometries the

	OptFoil38	OptFoil39	OptFoil40	OptFoil41	OptFoil42
r/R	0.90				
U [m.s^{-1}]	20				
r$_e[m]$	250				
c [m]	0.8				
x	6.3				
L [m]	1.6				

Table 6.13: Fixed parameters for the selected MOO

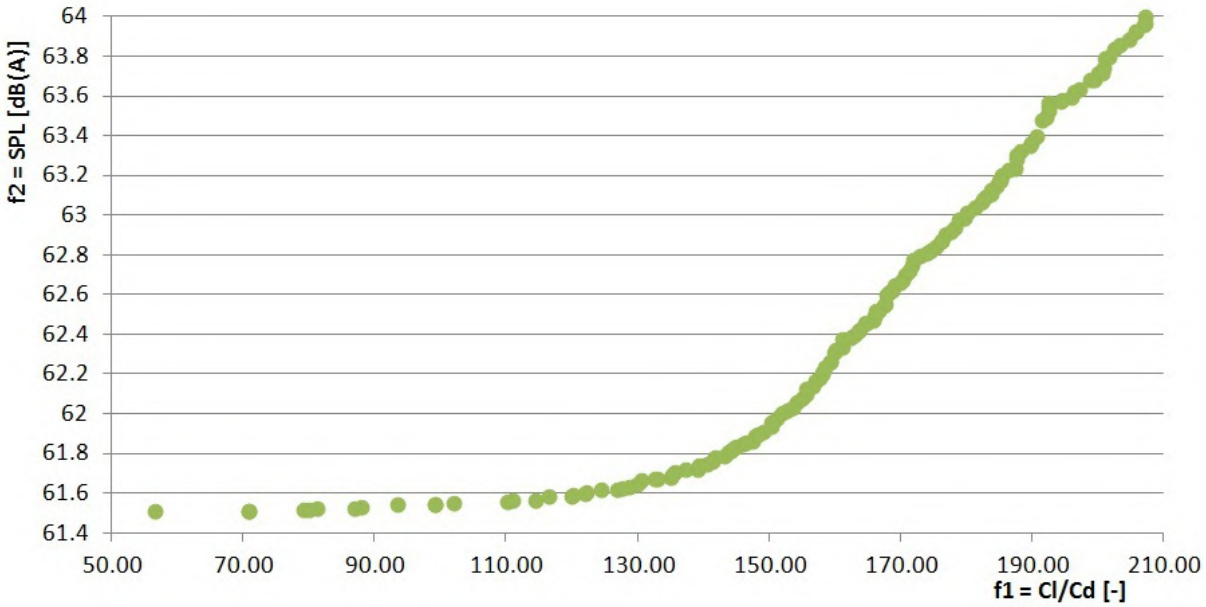

Figure 6.9: Pareto front for the MOO with $U = 20[m.s^{-1}]$, $r_e = 250.0[m]$ and $r/R = 0.90$

optimizer computes under these conditions. Each dot in fig. 6.9 represents a geometry (or rather a combination of CP values and optimum α -the design variables - that develop a specific geometry) and the respective values of both objective functions, that geometry delivers. Carefully analyzing the curve, the first and most relevant aspect to point out is the very small increase in SPL value of the geometries that deliver values of f_1 in the range of 56.6 to 151.0. These geometries have a minimum SPL value of $\approx$ 61.5 dB(A) up to 62.0 dB(A), but the difference in the value of the C_l/C_d ratio is staggering, with a gain in this value from 56.6 to 151.0 at the cost of only 0.5dB(A). In addition to this when thinking of the typical values for both the objective functions considered here, by the reference airfoils usually used in WTs, one may consider noisier geometry to attain better aerodynamic performance. Most modern WTs make use of the NACA63xxx airfoil series for the tip region [van Bussel, 2011], [A/S, 2009], which as seen in table 6.3, will deliver a ratio of C_l/C_d around 125 with minimum noise values of 64.2dB(A) for a worst aerodynamic performance. The noisiest geometries represented in the Pareto front, the ones with highest values for C_l/C_d, will not even attain such high SPL values meaning that a great gain in aerodynamic performance is possible. In fact, the noisiest geometry computed has a maximum of 64.0dB(A), a value still below that of the reference airfoils. Let us analyze now in detail a set of 5 geometries, two that favour the minimization of SPL values, an intermediate geometry that balances the relation between both objective functions and two more geometries that favour aerodynamic performance, as indicated in

fig. 6.10.

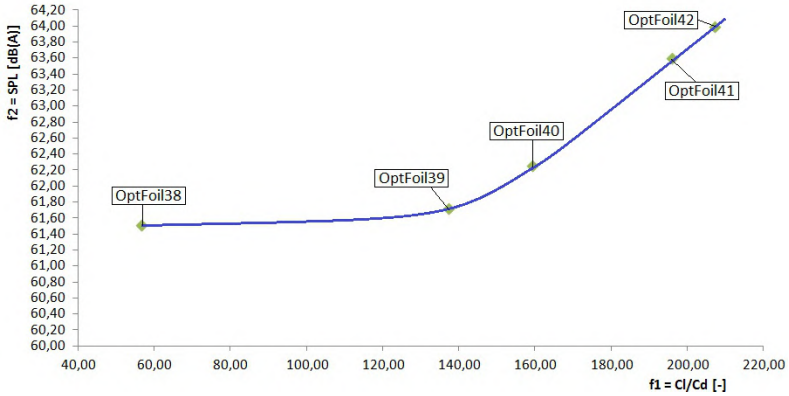

Figure 6.10: Selected optimized geometries taken from the Pareto front

As stated before, the selected geometries from the Pareto front were chosen to assess how the compromise between aerodynamic performance and aero-acoustic properties affect the final optimized geometries obtained. OptFoils 38 and 39 favour minimum SPL values, OptFoil 40 represents the more balanced geometries and OptFoils 41 and 42 deliver the best geometries from the aerodynamic point of view. The details of the optimization results of all airfoils are detailed in table 6.14.

	OptFoil38	OptFoil39	OptFoil40	OptFoil41	OptFoil42
t/c	0.18	0.18	0.18	0.16	0.16
$\Psi[deg]$	9.9	11.6	15.6	12.6	10.4
C_l	0.3837	0.9796	1.2546	1.2853	1.3696
C_d	0.0068	0.0071	0.0079	0.0066	0.0066
$SPL_{Total}[dB(A)]$	61.5	61.7	62.3	63.6	63.9
α^*	0.22	4.97	7.18	7.59	8.57
f_1^*	56.6	137.4	159.2	195.9	207.2
f_2^*	61.5	61.7	62.3	63.6	63.9

Table 6.14: Optimization results for OptFoils 38 to 42

Let us begin by the analysis of OptFoils 38, 39 and 40. Consider the geometries that correspond to the lower and fairly constant section of the Pareto front, in the SPL range that is comprised between 61 and 62 dB(A) and that make up a class of airfoils in which the geometries are responsible for a great evolution in the value of f_1 at a relatively small cost in the increase of f_2.

These geometries are all very similar and they follow the same evolution in terms of relative maximum thickness, as represented in fig. 6.11. The coordinate at which this point is set on all three geometries considered is identical and they all share the same shape for the LE. This reinforces the analysis advanced upon the discussion of the effects of radial position as the influence of thicker LE was found to be related with a smaller influence of the turbulence inflow noise mechanism, which is consistent with the final shape of these geometries. The influence of the TE bluntness noise mechanism can be described as very small as well, since all geometries developed well behaved TE shapes, with the exception of OptFoil 40, which has a TE wedge angle over 14^o and for that reason no noise related with TE bluntness was accounted for that airfoil. An interesting comparison can also be made between this class of airfoils,

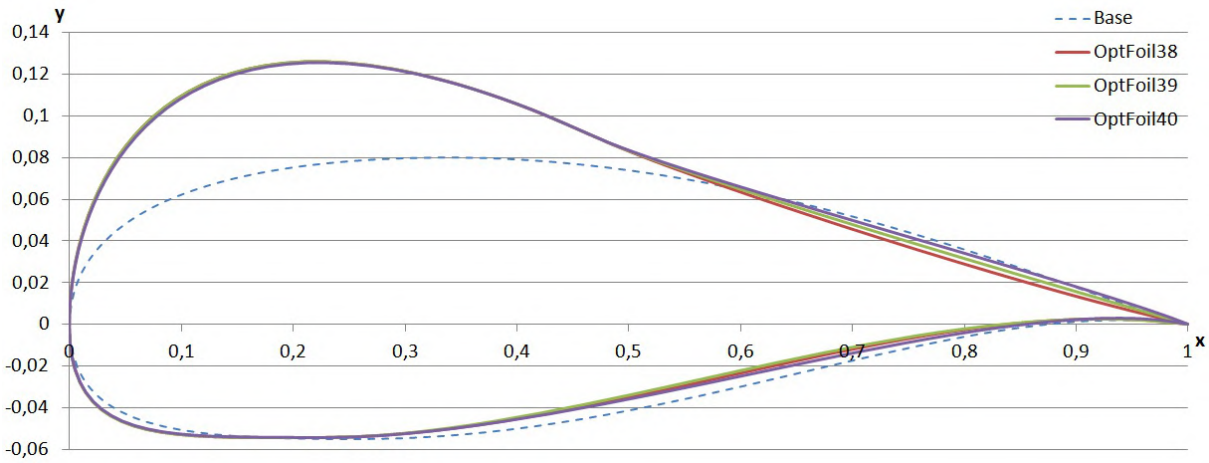

Figure 6.11: Geometries for OptFoils 38, 39 and 40, which minimize SPL values

that favour SPL minimization in detriment of aerodynamic performance and the geometry obtained from OptFoil 29. In section 6.5 this airfoil was described when analyzing the effect of flow speed and was concluded that the geometry obtained is not a very interesting one, as it delivers very low values of the aerodynamic coefficients. The geometry of that airfoil was described before as a "tear" like shape, nearly symmetrical apart from a small depression in the pressure side of the TE, and it was found that this shape was basically the same shape delivered in all the optimization tests in which the objective function is f_2 (OptFoils 17 to 20 and OptFoils 29 to 32). It is immediate that, if one was to generalize that shape to all airfoils that are to be optimized with the objective function as f_2, than none of those geometries could be included in the class of airfoils, detailed in the lower part of the Pareto front, since none deliver a similar relation between the respective values of C_l/C_d and SPL. On the other hand, the

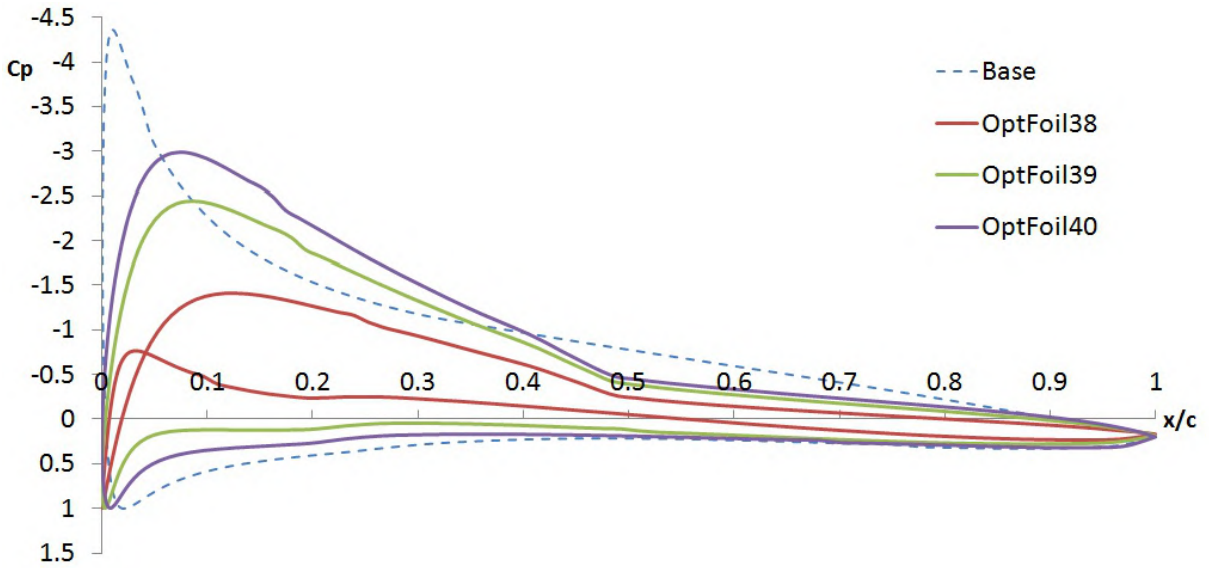

Figure 6.12: C_p distribution of the geometries that minimize SPL

TE shape is what seems to increase aerodynamic performance from OptFoil38 to 40, as it is notorious the evolution of the thickness distribution at the TE, from OptFoil 38 to 40 (fig. 6.11). Although, the C_p

distribution shown in fig. 6.12, presents a major difference in the LE region and makes us believe that it is the LE which may have a more significant effect. In any case, if that increase is geometrically related it must be because of the changes visible at the TE. OptFoil 38, which delivers the least amount of noise,

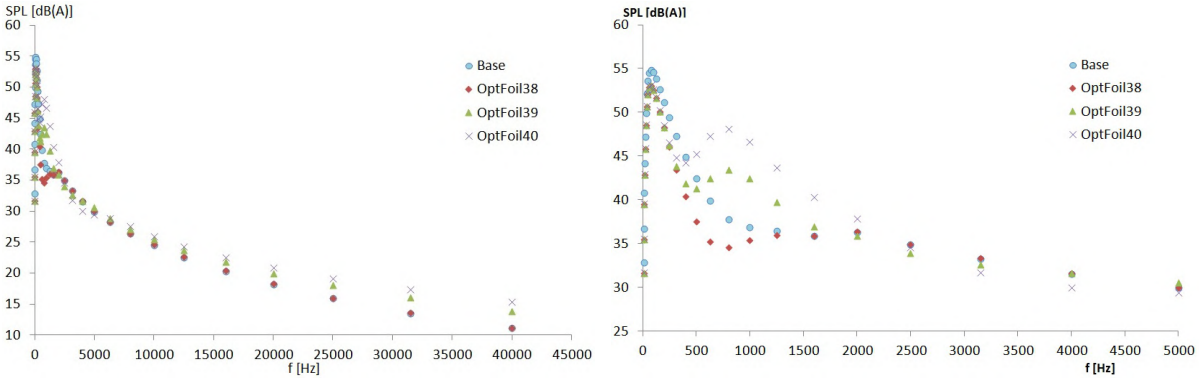

(a) Complete $1/3$ octave spectra

(b) Detail of the low to mid frequency range

Figure 6.13: $1/3$ octave spectra of the geometries that minimize SPL, with detailed view of the low to mid frequency range

is slightly thinner on the rear half section of the airfoil, and this seems to be the main cause for the major increase in the value of f_1 at a very low cost in SPL increase. This means that these geometries represent a class of airfoils that deliver noise levels within a gap of 1.5dB(A). Figure 6.13 helps understanding how the total $1/3$ octave spectra delivered by each airfoil is related with the geometric differences. The general spectra data follows a similar trend for all airfoils, but in the range of 200 to 3000 Hz, as detailed in fig. 6.13, a major increase of the SPL values, for the corresponding frequencies occurs, where it is obvious that the slight increase in the TE thickness distribution may have caused this. One reason for this increase, in the low to middle frequency range, could be related with the interaction of the separated flow over the TE, in the form of TBL-TE noise. For the rest of the frequency range, it is notorious as the thinner OptFoil at the TE, always delivers less noise, showing an obvious increase in the SPL values for the corresponding frequencies, as we consider the airfoils from the one with a thinner TE to the airfoil with the thicker TE.

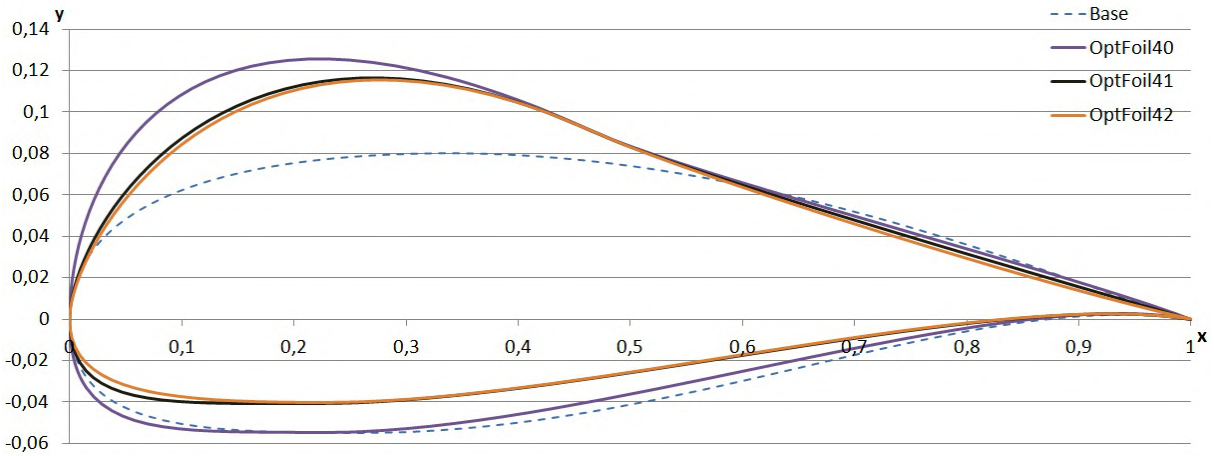

Figure 6.14: Geometries for OptFoils 40, 41 and 42 which maximize aerodynamic performance

Using as representation of the class of the most silent airfoils the geometry of OptFoil40, which is the one that sits more or less at the apex of the Pareto front and that delivers a reasonably much better relation between the values of both objective functions in regard to the NACA 63415 reference airfoil, we can evaluate the evolution of the geometries that develop better C_l/C_d ratios. Figure 6.14 illustrates that evolution with the geometries for OptFoils 40, 41 and 42 and immediately we find that more has happened on these optimizations than expected. To begin with, it is apparent that the class of airfoils that contains these selected OptFoils, has a more negative relation in the compromise between f_1 and f_2, as the increasing gain in the C_l/C_d ratio leads to a much bigger increase in the SPL values, than the evolution that is observed for the class of airfoils previously analyzed. Nevertheless, the stipper slope of the Pareto front for these geometries never deliver prohibitive SPL values, as none of the referred geometries (including the one corresponding to OptFoil 42) exceed the typical SPL value of the reference airfoils usually used in WTs at this radial position, such as the NACA 63415 airfoil already mentioned before.

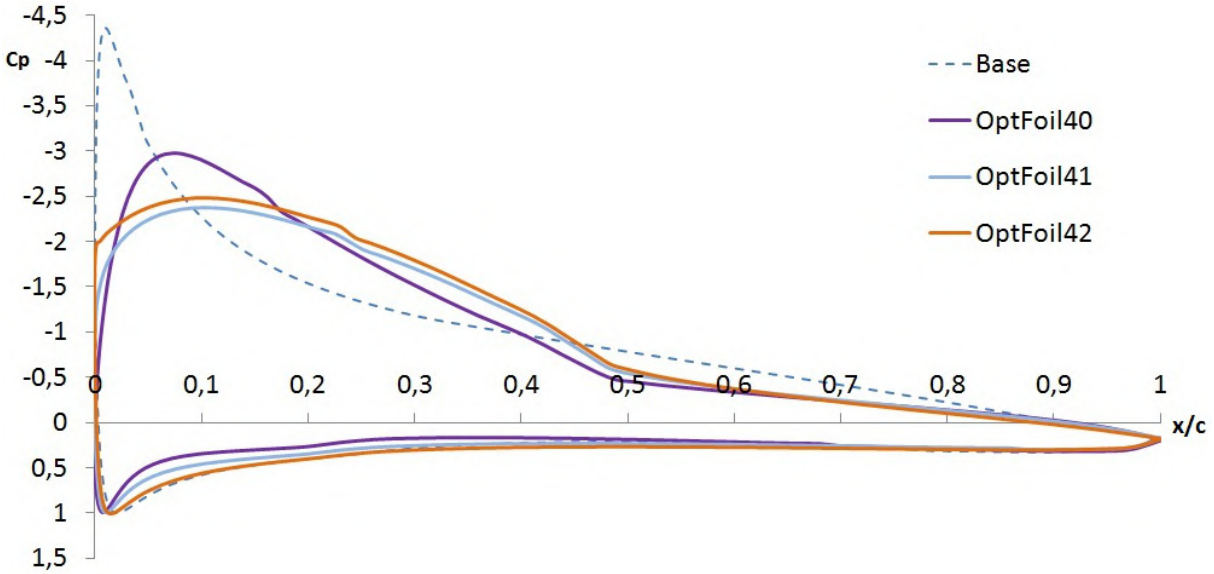

Figure 6.15: C_p distribution of OptFoils which maximize aerodynamic performance

Following what was said in the previous paragraph, it is noticeable in the TE shape that it did not follow the same trend as before where the noisiest airfoil in the previous assessment was the one with the thicker TE. In fact the geometries evolved in the reverse manner, but much bigger differences on the shape of the LE can be seen. OptFoils 41 and 42 evolved very little their TE geometries when in comparison to OptFoil 40, but the LE was dramatically reduced and the point of maximum thickness was transported away from the LE. In the pressure side the geometry maintained a similar shape, but followed the trend observed in the suction side. In terms of aerodynamic performance, the gains are even more considerable, meaning that these changes in the overall surface were advantageous and at a relatively small cost in the amount of noise radiated. Figure 6.15 shows the C_p distribution of OptFoils 40, 41 and 42 and, immediately the different areas contained within each set of C_p distributions show how the increase in C_l has been possible. The evolution of the LE shape from OptFoil 40 to 42 can be seen as the gain in area that the OptFoils 41 and 42 show in comparison to OptFoil 40. That gain completely

compensates the small increment that OptFoil 40 develops in the airfoil section from $x/c \approx 0.05$ to 0.17. The geometry and shape change of the pressure side, though quite different from OptFoil 40 to OptFoils 41 and 42, seem to introduce small effect in aerodynamic performance as all three lines seem to follow the same trend, but the fact that for the rear half section of the airfoil, the C_p distribution lines seem to almost coincide, helps understand how little effect on aerodynamic performance the changes in the TE shape had. The geometries that represent the lower and upper limits of the Pareto front (OptFoils 38 and 42 respectively) stand for an increase of around 2.5 dB(A) and a relative gain in the value of C_l/C_d in the order of 72.7%. In a last remark about the aerodynamic performance of these airfoils, it is relevant to note that the value of C_d stabilized at a value around 0.0066.

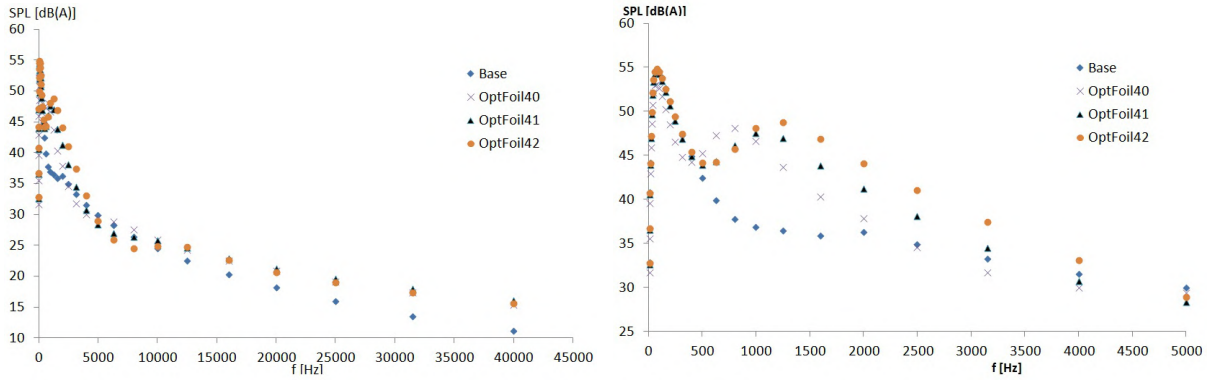

(a) Complete $1/3$ octave spectra

(b) Detail of the low to mid frequency range

Figure 6.16: $1/3$ octave spectra results of the geometries that maximize the C_l/C_d ratio

The noise $1/3$ octave spectra radiated, illustrated in fig. 6.16, by these geometries are fairly different from those displayed by the geometries that minimize SPL values. All airfoils favouring aerodynamics, will show a very similar trend in the complete frequency range considered but, again a low to mid-frequency set of values seem to present the major difference form one geometry to the next. The noise levels radiated from these geometries are higher than the geometries previously analyzed, from as low as 50 Hz in frequency and the overall increase in the noise spectra explains the observed higher SPL values in the results. It is in the range from 1000 to 10 000 Hz, as shown in fig. 6.16, that significant changes in the spectra are observed for the geometries that favour higher C_l/C_d ratios, which is not surprising as the most important noise mechanisms considered (namely TBL-TE and turbulent inflow noise) will likely be very influent in this range of values.

All in all, the MOO described in detail here is a major source of information as to which sections of the optimized airfoils are responsible for the evolution of the objective functions. If one wants to minimize noise levels as much as possible, a geometry closer to that of OptFoil 38 could be used as base and a consequent study of the effects of changing the TE shape would suffice to optimize aerodynamic performance. If instead, the gain in C_l/C_d was to be favoured at all costs, then a geometry similar to that of OptFoil 42 could be considered as base and the study of the LE thickness would be required to minimize SPL value radiated. In conclusion to the results presented, the illustrated examples of airfoil geometries are proof that classes of airfoils with high aerodynamic performance and low noise emission can be obtained with promising results and, a direct comparison to known airfoil geometries dedicated to

WT technology allows for the conclusion that the optimized airfoils here developed present the possibility for viable practical application, in this context.

Chapter 7

Conclusions

7.1 Achievements

This chapter concludes the presentation of the work developed in the thesis. The main achievements and outputs of the work developed fit very well within the WT aero-acoustic subject, adding some new aspects to the topics involved. An easy integration in the universe of all authors and entities who develop, or have developed, works in this field can be done. The main topics that make this work stand out are the developed computational tools to obtain the main set of results and the synergy accomplished between the various components that make up the final optimization framework. The theoretical background and bibliographic research performed about the subject of airfoil and WT aero-acoustics can be said to have been very thorough and ultimately very useful.

In a more technical perspective, all airfoil geometry related research and reference material was properly interpreted and implemented, even if not ultimately used, from the base airfoil geometries builder to the parameterization techniques interpreter. The Bezier curves method has proved to have been an excellent choice for the task at hand, just as the many authors who published their experience when working with it in similar works have reported.

One major achievement of this work was the successful use and integration of the Rfoil software as the BL parameters computational tool. Moreover, apart from the software creators and a few others, not many studies on airfoils for WT aero-acoustics seem to have use it, either because the respective authors relied on available computational tools at the time of development of their works (namely Xfoil) or because they chose to use numerically more detailed and computationally demanding tools, in most cases presenting fairly identical results at greater costs. Nevertheless, it is known that Rfoil can be a very useful and reliable tool for making flow analysis on generic airfoil geometries, especially because its reliability as been extensively compared to WT experimental tests. In conclusion, the use of Rfoil can be described as an excellent choice for the use in the WT context and very relevant for achieving the main objective, leaving here a positive feedback.

The noise prediction scheme considered in this work is based on well established works and very important reference studies on the subject being discussed here, specifically the works of Brooks et al.

[1989]. No major new developments were achieved on better understanding the five airfoil self-noise mechanisms as it was never intended, but the integration of the fairly recent studies of Moriarty et al. [2005] on the interaction between the turbulent characteristics of the approaching flows and the shape of the LE of the airfoils can be seen as a major improvement to the original model of BP&M. However, it is the conjugation between these models and the Rfoil software in the form of a single computer code that present a major achievement of this work, especially when accounting for the turbulent inflow noise, which is known to have only been used with Xfoil [Moriarty et al., 2005], [Zhu et al., 2005] for BL modeling and being here introduced in this context.

The optimization framework developed has made use of the Python module *pyOpt* [Ruben E. Perez, 2011] which provided for a valuable help in integrating and building the final optimization scheme, through its simplicity and object-oriented environment. It also provided for a very robust link between the several components of the optimization performed. Overall, *pyOpt* has shown great usefulness and relevance in the work here developed and proved to be a very reliable software for future works.

In overview of the work developed, the first goal was to assess the relevance and identify key features that play a role in the compromise between aerodynamic performance and noise levels delivered by several airfoil geometries. Careful analysis and study of the effect in those parameters by changing either locally or globally the overall geometry of the airfoil, was to be performed. This lead ultimately to the development of several unique airfoil geometries, all with their own specific aerodynamic and aero-acoustic characteristics that allow the following statement: it is indeed possible to perform such an analysis and relate airfoil shape with noise levels produced. And in addition to that conclusion, one can conclude as to which geometric properties are responsible for improving aerodynamic performance in detriment of noise levels radiated, or vice-versa or to find the most ”balanced” geometries between the two objectives. In other words, the work has evolved favorably, complied with all guidelines and indications set from the beginning and fulfilled all suggested objectives formulated at the beginning.

7.2 Future work

There are interesting ideas that emerged during the development of this work and might be considered for follow up of this thesis. These possible improvements of the work developed can be quite technical in nature or simply intended to strengthen the work as a working tool.

To begin with the most relevant, which are the parameters that could have an effect on the results, some parameters related with specifics of flow and/or noise assessment were neglected purposefully to maintain the work focused on the most important and not to deviate too much from what is intended. The effects of BL tripping were never considered in any optimization tests and, this parameter could exert some influence in the noise levels, specifically for the TBL-TE noise mechanism. This was left untouched (set over the TE at all times) because no general agreement exists amongst the several referenced authors on the subject, as to which criteria to follow when choosing the x-coordinate over which the trip is to be set. The major effect expected is a slight increase in the total SPL value, as turbulence levels over the airfoil are likely to increase.

A sensitivity analysis on the effects of considering different relative positions of the observer towards the airfoil was not performed, as the method used here fixed those parameters in the combination that delivered the biggest SPL values (observer directly upwards and perpendicular to the TE of the airfoil). This analysis can be easily introduced and accounted in the optimization framework developed, by simply changing the relative angles of the coordinate systems, meaning that future studies on this subject be made for more realistic situations in this matter.

The definition of the parameters responsible for the height above ground and ground roughness, required in the definition of the turbulent inflow noise mechanism, were kept constant, because the considered situation is enough to assess the influence of these parameters. Remember that any change in these parameters would affect turbulence intensities and length scale values which could probably affect the LE shape of the optimized airfoils, but when considering a very adverse condition, like the one specified for the tests performed, that influence was also acknowledged to a certain extent.

As a final suggestion, an upgrade idea of the main code developed is left here as exercise for potential interested parties. Since no specific nomenclature was used to define the airfoil geometries here optimized, it would be interesting to enable the code to communicate with an airfoil data-base, that contained several known airfoil geometries, currently used in the WT industry. The objective is to ascertain which optimized geometries obtained from the framework correspond to existing airfoils and account for direct comparison between the optimized airfoil and a selected reference airfoil taken from the data-base.

The resulting geometries in the several optimization tests, when possible compared with each other whenever such is possible, presented in many cases very slight geometric differences in specific sections of the airfoil, such as the example of the case where TE changes in the identified airfoil family contained in the lower region of the Pareto front. This opens space for future optimization evaluations that are more suitable for local refinement of the solutions, namely for the movement of the CPs that define the corresponding section. In addition to that assessment, local and small refinements in specific sections of the geometry may be improved with simpler usage of other parameterization techniques, such as the Hicks & Henne functions. Following this, it is immediate that the use of gradient-based algorithms is more suitable for performing those local refinements.

A direct follow up of this work is the continuation of this multidisciplinary analysis and multi-objective optimization, to the 3D domain, or in other words the analysis should now proceed to the entire blade geometry. Having a sufficiently reliable tool for optimizing the several cross sections that can be integrated in the blades of the WT, it makes sense the evolution of this analysis and progress to the assessment of the all blade geometry or even the entire WT.

It would also be of great interest, the inclusion of other disciplines in this work. Structural concerns in the airfoil geometry or effects observed on estimated electrical power output, are some examples of future considerations, since none of the previous examples mentioned were accounted for in the optimization framework developed, in the form of constraints or decision variables.

7.3 Final remarks

The codes developed and the optimization framework presented in this work, can be acknowledged as very useful tools for providing a reasonable estimate in total SPL prediction. The developed codes will provide for a simple to use geometric tool capable of introducing changes in available airfoils, either locally or in global sense, as well as a semi-empiric model to assess for the aero-acoustic behaviour of any airfoil geometry to be considered. When considering this aero-acoustic evaluation code, supported by the major reference for WT dedicated computations, the Rfoil software, it is immediate the valuable amount of information and help it can provide to those working in the design stages of blade sections (and ultimately blade geometries) in the WT context. The immediate test results give good estimates as to which geometries are achieving good results in terms of both objective functions.

In addition to this, the optimization framework developed presents itself as a very complete tool, where several key features directly intervening in the working conditions of any WT, can be changed and worked upon to deliver more optimized airfoil geometries, being the objective a very detailed assessment or a general aero-acoustic evaluation. Moreover, the integration into one single shell of the all optimization process, provides a user friendly environment, at relatively low costs in time consumption and computational requirements.

Appendix A

AAcoustic: User's Manual

A.1 Code structure and usage

At the main screen of the code, the user may choose one of two menus: "Airfoil Geometric analysis" and "Aero-Acoustic analysis". The options available throughout the program are always very direct and simple, just like in this main screen and the interface with the user is kept simple and user friendly throughout the program, presenting available choices on screen and when suitable, gives examples for the operation at hands.

Choosing the"Airfoil Geometric analysis" option enters the menu that allows for airfoil geometry build and parameterization. A key aspect to bear in mind when using the following options, is that the code will always have one set of coordinates (two vectors) that define the geometry, stored in the virtual memory, which at the beginning are NULL (not present) but when present in the memory, any modification then performed on the airfoil will be stored on that memory, meaning that if one wants to restart an operation after performing alterations, the original geometry must be rebuilt or reloaded:

- **NACA** –the option is responsible for creating a reference airfoil geometry resorting to either the 4 or 5 digit series of the NACA airfoil specifications. The set of coordinates is set in virtual memory.
- **HIHE** –in this option the Hicks & Henne parameterization method is used. This option will only become available after a reference geometry is in the virtual memory.
- **BEZR** –The Bezier lines related operations are available in this option. Here both operations of building and parameterization of an airfoil can be performed by selecting one of them at the first input. As before in the HIHE option, parameterization will only be available if a set of coordinates is stored in the virtual memory.
- **LDFL** –This option allows for loading a set of coordinates, written in a generic *.txt* file, to the virtual memory. The load format should be as the one used in XFOIL/RFOIL software.
- **SVFL** –Any set of coordinates in the virtual memory, at the moment, may be stored in a *.dat* file using this option. The name of the file is automatically given and displayed instantly on screen and the save format will be as the one used in XFOIL/RFOIL software.
- **QUIT** –Returns to the main screen

The "Aero-Acoustic analysis" menu has a small requirement the user must bear in mind. Here, in order to perform an aero-acoustic analysis, the virtual memory must first have stored an airfoil geometry (set of coordinates) meaning this menu though available at the beginning, will always warn the user if no set of coordinates are in memory. The menu presents the following options:

- **BLPR** –The method for computing the BL parameters used in the original work of BP&M are available through this option, for the set of coordinates presently in memory. If none are available an error message is displayed.
- **RFOL** –This option is responsible for calling the Rfoil software and using this for computing BL parameters in regard to the set of coordinates presently in memory (the action is completely automatic and accounts for rotational effects always). If none are available an error message is displayed.

- **SPLC** –Here the aero-acoustic assessment is performed for the airfoil geometry in memory. This option will only be available if a set of coordinates and the BL parameters are presently in memory. If none is available an error message is displayed.
- **LDFL** –As before this option loads a generic file *.dat* file, only this time around it is prepared to read a file with BL parameters and aerodynamic coefficients, in the usual XFOIL/RFOIL format.
- **SVFL** –The option can be used in two ways: if the user just finished computing the BL parameters using the BLPR or RFOL options, the code saves the BL parameters to a generic file. On the other hand if the SPLC option was last used the code saves a generic file containing the computed SPL values for all centered frequencies
- **QUIT** –Returns to the main screen.

Each option presents always a small text box with relevant information for the task at hands or a small sentence for each required input from the user, which means that, in principle, the code is quite simple and straightforward to use.

A.2 Contents, functions and tools used in the code

As stated before the code splits its purpose in two main tasks at the beginning. A description of the main operations for each type of analysis possible in the code follows.

Saving and loading a set of coordinates: In the "Airfoil Geometric analysis" screen the LDFL option reads a generic *.dat* file containing a set of x and y-coordinates (required input is the name of the file). The SVFL saves whatever set of coordinates currently in the virtual memory of the code, to a similar *.dat* file (name of saved file is automatically written as follows: NACAxxxx_p000_d0_.dat" where xxxx accounts for the series number, p000 is the number of points and d0 is the point distribution used).

In the "Aero-Acoustic analysis" screen the SVFL option has a dual function depending on what information is currently in memory: if a BL computation has just been made than *.dat* file is written with that information; if an SPL computation was made instead the code writes the $1/3$ octave spectra results to the file. The LDFL option can only be used here to load a file containing BL related information, written in the typical Xfoil/Rfoil format.

Airfoil Geometric analysis

- **Building an airfoil geometry**: the options NACA and BEZR both allow for the build of an airfoil geometry, the first using the NACA series guidelines and the later using a set of four connected Bezier lines. When choosing one of these, the main difference is that the NACA option requires the input of which series the user wants (4 or 5 digits) and the digit code. The BEZR option will ask for the coordinates of the CPs to be used. This last method, though apparently more complex, is quite easy to use as some of the coordinates are preset in order to comply with the Bezier lines connectivity rules (see 3) and to always create a shape similar to that of an airfoil. Both options will require the number of points that set the airfoil geometry, and with this a major difference occurs: the NACA airfoils created here are supposed to be used merely as a starting point, from which the geometry is later reshaped using the Hicks & Henne method, and when inputting the number of points the user is also presented with the option to choose the distribution of points over the airfoil surface. Different distributions over the surface allow for a more realistic shape of either the LE, TE or both or if no detail is required a simple uniform distribution may be used. This is important for the more accurate evaluation of SPL values, which are directly related with the precision with which the airfoil surface is set. On the other hand, when using the BEZR option the user is asked for how many points should each Bezier line contain, meaning that an airfoil shaped with Bezier lines can always be more accurate if the user inputs a large amount of points. Furthermore, the BEZR option is very efficient for an optimization procedure as it allows the user to input a small set of CP coordinates, that may serve as optimization variables, thus allowing the code to continuously reshape the airfoil, by making small changes to the same set of CP coordinates.
- **Reshaping an airfoil surface**: Having created an airfoil surface, the user may now use one of the two parameterization methods available, where basically both methods create one or more lines and then either add or replace the coordinates of the points that make up those lines. As stated before, the HIHE option allows for the more traditional method of Hicks & Henne, where the code requires from the user the number of bumps to add to the surface, the type of disrupting function to use, which side of the airfoil to change and all the parameters required for the disrupting function. For the BEZR option, a

similar procedure may be taken. The code first requires the number of lines to be created and if it is supposed to be a 2^{nd} or 3^{rd} order line. Than the section of the airfoil to be replaced must be set by giving the first and last $\frac{x}{c}$ coordinate. Note that the order in which these values are given are important as the code will read the airfoil set of coordinates counter-clockwise (starting from the TE at $x/c = 1.0$ and $y/c = 0.0$) finding the closest values for the xx coordinates that were input and using those coordinates (and its yy correspondents) for setting the first and last CP coordinates of the Bezier line (e.g. if the values 0.3 and 0.7 are given the code will replace the lower section of the airfoil between 30% and 70% of the chord). Finally the coordinates of the inner CP(s) of the line(s) are requested.

Aero-Acoustic analysis

- **Computing BL parameters**: The code can evaluate the required BL parameters for the aero-acoustic SPL computations, making use of the original expressions in the work of BP&M or resorting to the RFOIL software. The first is possible through the BLPR option and the second with RFOL option. Both options have four inputs in common: the (effective) angle of attack (α), the freestream velocity (U), the airfoil chord (c) and the airfoil span (L), these last two are only required for SPL value prediction. From this point on, the BLPR option requires one additional input which is the BL tripping method to be assumed. On the other hand, the Rfoil software will request all parameters used while accounting for rotational effects: blade radius (R) and velocity ratio (x). Both methods deliver on screen the resulting values for all relevant BL parameters, with one major difference: the original work of BP&M does not compute the aerodynamic coefficients, whereas the Rfoil software will deliver all the required information. This means that the BP&M expressions are here only present for later validations of specific results, not for actual optimization use. In fact one of the original ideas of this work was to make use of the Rfoil software on this matter. Therefore, it is important to note that, because the main code developed, as well as the Rfoil software, are both being continuously used in the automatic optimization procedure, a specific routine has been created to facilitate this procedure and is responsible for operating the Rfoil software resorting to *batch* like files, to do so. The routine first creates the *batch* and *.txt* files containing the required commands and inputs, respectively, for running Rfoil (which are all at some point, input for the main code) and then calls the software and the *batch* file from the system directory, thus integrating the external program in the main code, and never presenting the actual Rfoil software to the user.
- **Computing SPL values**: After setting the airfoil geometry and computed the BL parameters for the desired flow conditions, the user may now proceed to the noise assessment stage. Following the selected models for computing SPL values described in the 4, the SPLC option allows for the aero-acoustic noise emission from the airfoil. The most important inputs in the SPLC screen are the angles which set the observerâs position relative to the airfoil: the absolute observer angles (Θ_e from the x axis and Φ_e from the y axis - 4.2.3); the distance to the airfoil; and the selection of which noise mechanisms the user wants to account for in the noise assessment being performed. In this last input some noise mechanisms require additional specific inputs: for the bluntness related mechanism the user may either use the TE bluntness height and solid angle computed for the geometry in memory or set a different fixed value. For the tip noise mechanism (which will not be used in this work) the tip angle and tip shape are also required. Finally for the turbulent inflow mechanism, one of the most relevant for this work, more information is needed: first which turbulent inflow model is to be used, secondly the height above ground and finally the surface roughness. As always all numerical values requested are followed by its respective units.

Appendix B

Example script files

B.1 Python script example of a MOO

```
#!/usr/bin/env python

'''
OPTIMIZATION procedure:

    Bezier curves

    Objective function  f1  max Cl/Cd;
                        f2  min SPLeq;
                s.t.        max thickness (0.18c for airfoils #2 and #3)
                            Restrictions for CP relative locations

- Optimization routines: NSGA2
'''

# ----------------------------------------------------------------------
#      Python Modules
# ----------------------------------------------------------------------
import subprocess as sp
import string, os, sys, time, pdb
from numpy import *

# ----------------------------------------------------------------------
#      PyOpt Extension Modules
# ----------------------------------------------------------------------
from pyOpt import Optimization

from pyOpt import NSGA2

# ----------------------------------------------------------------------
#      Set objective function and constraints
# ----------------------------------------------------------------------
```

```
33 def objfunc(x):
34
35 # 1 - Delete any RFOIL outputs from previous sessions
36 # ------------------------------------------------------------------
37     runDEL = sp.Popen('C:\\Tese_res\\del_RFOIL_output_files.bat')
38
39 # 2 - Disturb airfoil shape
40 # ------------------------------------------------------------------
41     outFile = open('outputFile.dat','w')  # Output file from where the
42                                           #Cd, Cl and the thickness
43                                           #values are collected
44     errFile = open('errFile.dat','w')     # Error output file
45     # 2.1. Variable runAA responsible for calling AAcoustic
46     runAA = sp.Popen('C:\\Tese_res\\AAcoustic.exe', stdin=sp.PIPE,
47                      stdout=outFile, stderr=errFile)
48
49     # 2.2. Type of command to be used by the interpreter
50     print "*** Running program ***"
51     def inCmd(cmd,echo=True):
52         runAA.stdin.write(cmd+'\n')
53         if echo:
54             print cmd
55
56 # 3 - Formalize optimization input (variables setting)
57 # ------------------------------------------------------------------
58     print "*** Issuing commands ***"
59     U = 20.0          # Wind speed:                15, 20 [ms-1]
60     c = 0.8           # Chord length:              3.6,  1.4, 0.8 [m]
61     R = 44            # HAWT radius (fixed)
62     xVel = 6.30       # Velocity ratio:            0.7, 4.55, 6.3
63     LL = 1.6          # airfoil span:              7.2,  2.8, 1.6 [m]
64     r_e = 250.0       # Distance source-observer: 250, 1000 [m]
65     z = 80            # Height to the ground (fixed)
66     z_0 = 0.3         # Ground roughness (fixed)
67
68     res = runAA.communicate( string.join([
69                              '1','BEZR','B',
70                              '80',                    # number of points
71                              '2',
72                              # 3.1. Variables 0-14 are the CP coords
73                              #for the Bezier curves
74                              '%f ' %x[0],'%f ' %x[1],   # CPxx2, CPyy2
75                              '%f ' %x[2],'%f ' %x[3],   # CPxx3, CPyy3
76                              '%f ' %x[4],'%f ' %x[5],   # CPxx4, CPyy4
77                              '%f ' %x[6],               # CPxx6
78                              '0.0','%f ' %x[7],         # CPxx7, CPyy7
79                              '0.0',                     # CPxx10
80                              '%f ' %x[8], '%f ' %x[9],  # CPxx11, CPyy11
81                              '%f ' %x[10],'%f ' %x[11], # CPxx12, CPyy12
```

```
                                '%f' %x[12],              # CPxx14
                                '%f' %x[13],'%f' %x[14], # CPxx15, CPyy15
                                'SVFL','QUIT','2','RFOL',
                                # 3.2. Flow conditions and airfoil specs
                                '%.3f' %x[15],            # alpha
                                '%f' %U,                  # Wind speed (U)
                                '2',
                                '%f' %c,                  # chord length (C)
                                '%f' %R,                  # HAWT radius
                                '%f' %xVel,               # velocity ratio (x)
                                'SVFL', 'SPLC',
                                # 3.3. Aero-acoustic inputs
                                '%f' %LL,                 # airfoil span (LL)
                                '90.0',                   # Theta_e
                                '90.0',                   # Phi_e
                                '%f' %r_e,                # Distance
                                '1',                      # TBL-TE
                                '2',                      # Separation
                                '3',                      # LBL-VS
                                '4',                      # Bluntness
                                '0',                      # Tip
                                '6',                      # Turbulent Inflow
                                'N','1',
                                '%f' %z,                  # Height above ground
                                '%f' %z_0,                # Ground roughness
                                'SVFL','QUIT','3'],'\n'
                                        )
                                 )
    print res
    outFile.close()
    errFile.close()

# 4 - Collect aerodynamic values from output files
# ------------------------------------------------------------------
    # 4.1. Cd, Cl and thickness values are acquired
    print "*** Retrieving Cd value ***"
    inFile1 = open('outputFile.dat','r')
    for line in inFile1:
        if 'CD =  0.' in line:
            results = line.split()
            Cd = float(results[5])   # Collect Cd
        elif 'CL =' in line:
            results = line.split()
            Cl = float(results[5])   # Collect Cl
        elif ' VISCAL:  Convergence failed' in line:
            Cl = 0.00001
            Cd = 1.0 # If warning message appears on-screen than
                     #Rfoil did not converge a solution
        elif 'Relative thickness:' in line:
```

```
131             results = line.split()
132             thk = float(results[2])  # Collect thickness
133     inFile1.close()
134 
135 # 5 - File 'BL_Param_RFOIL.dat'
136 # ------------------------------------------------------------------------
137     print "*** Retrieving Cl and alpha values ***"
138     inFile2 = open('BL_Param_RFOIL.dat','r')
139     inFile2.readline()
140     inFile2.readline()
141     line = inFile2.readline()
142     values = line.split()
143     inFile2.close()
144     alpha  = float(values[0]) # Obtain alpha
145 
146 # 6 - File 'SPLTOTAL_xxxxxx_x_x.dat' contains the total SPL results
147 # ------------------------------------------------------------------------
148     inFile3 = open('SPLTOTAL_{0:d}.dat'.format(123406), 'r')
149     print "*** Opening file with total SPL values ***"
150     for line in inFile3:
151         total = line.split()
152     SPLeq = float(total[3])  # Acquire total SPL value
153     inFile3.close()
154 
155     # 6.1. Session summary displayed on-screen
156     print ('{0:8s}|{1:8s}|{2:8s}|{3:8s}|{4:8s}'.format('Cd','Cl',
157                                                 'alpha','t/c','SPLeq'))
158     print ('{0:2.3f}   |{1:2.3f}   |{2:2.3f}   |{3:2.3f}   |{4:2.3f}'.format(Cd,
159                                                       Cl,alpha,thk,SPLeq))
160 
161 # 7 - Set objective function and constraints
162 # ------------------------------------------------------------------------
163     f = [0.0]*2       # Number of objective functions
164     f[0] = -Cl/Cd     # maximize Cl/Cd (written here as a minimization problem)
165     f[1] = SPLeq      # minimize SPLeq
166 
167     g = [0.0]*16      # Number of constraints
168     # g[0] to g[7] are the constraints that limit the CPs relatively
169     #to the x-coordinatexx coords of the CPs
170     g[0] = x[2] - x[0]
171     g[1] = x[0] - 1.0
172     g[2] = x[4] - x[2]
173     g[3] = x[6] - x[4]
174     g[4] = x[8] - x[10]
175     g[5] = x[10] - x[12]
176     g[6] = x[12] - x[13]
177     g[7] = x[13] - 1.0
178     # g[8] to g[17] restrain CPs relative to the y-coordinate
179     g[8] = x[1] - x[3]
```

```
    g[9] = x[3] - x[5]
    g[10] = x[7] - x[5]
    g[11] = x[11] - x[9]
    g[12] = x[11] - x[14]
    # Additional geometric constraints
    g[13] = x[13] - x[0]
    g[14] = x[14] - x[1]
    # Maximum thickness
    g[15] = thk - 0.18

    fail = 0

    return f, g, fail

# ------------------------------------------------------------
#     Instantiate Optimization Problem
# ------------------------------------------------------------

# 8 - Set variables and constraint initial values
# ------------------------------------------------------------
opt_prob = Optimization('Aero-Acoustic Optimization: Bezier disrupt',objfunc)

opt_prob.addObj('f0')
opt_prob.addObj('f1')

opt_prob.addVar('CPxx2','c',lower=0.850,upper=0.945,value=0.92201102 )     # x[0]
opt_prob.addVar('CPyy2','c',lower=0.006,upper=0.04,value=0.01122900 )      # x[1]

opt_prob.addVar('CPxx3','c',lower=0.550,upper=0.740,value=0.63376403 )     # x[2]
opt_prob.addVar('CPyy3','c',lower=0.070,upper=0.095,value=0.07786300 )     # x[3]

opt_prob.addVar('CPxx4','c',lower=0.260,upper=0.470,value=0.35144600 )     # x[4]
opt_prob.addVar('CPyy4','c',lower=0.070,upper=0.090,value=0.08755900 )     # x[5]

opt_prob.addVar('CPxx6','c',lower=0.070,upper=0.180,value=0.13917001 )     # x[6]

opt_prob.addVar('CPyy7','c',lower=0.016,upper=0.058,value=0.04868000 )     # x[7]

opt_prob.addVar('CPxx11','c',lower=0.100,upper=0.250,value=0.11575100 )    # x[8]
opt_prob.addVar('CPyy11','c',lower=-0.095,upper=-0.040,value=-0.05218800 ) # x[9]

opt_prob.addVar('CPxx12','c',lower=0.350,upper=0.500,value=0.24485300 )    # x[10]
opt_prob.addVar('CPyy12','c',lower=-0.090,upper=-0.040,value=-0.05496800 ) # x[11]

opt_prob.addVar('CPxx14','c',lower=0.550,upper=0.650,value=0.53448099 )    # x[12]

opt_prob.addVar('CPxx15','c',lower=0.750,upper=0.860,value=0.80914801 )    # x[13]
opt_prob.addVar('CPyy15','c',lower=0.005,upper=0.018,value=0.01334700 )    # x[14]

```

```
229 opt_prob.addVar('alpha','c',lower=0.0,upper=24.0,value=6.0 )                # x[15]
230
231 opt_prob.addCon('g0','i')
232 opt_prob.addCon('g1','i')
233 opt_prob.addCon('g2','i')
234 opt_prob.addCon('g3','i')
235 opt_prob.addCon('g4','i')
236 opt_prob.addCon('g5','i')
237 opt_prob.addCon('g6','i')
238 opt_prob.addCon('g7','i')
239 opt_prob.addCon('g8','i')
240 opt_prob.addCon('g9','i')
241 opt_prob.addCon('g10','i')
242 opt_prob.addCon('g11','i')
243 opt_prob.addCon('g12','i')
244 opt_prob.addCon('g13','i')
245 opt_prob.addCon('g14','i')
246 opt_prob.addCon('g15','i')
247
248 print opt_prob
249
250 # ----------------------------------------------------------------------
251 #      Execute the solution for the Optimization Problem
252 # ----------------------------------------------------------------------
253
254 # 9 - Compute solution
255 # ----------------------------------------------------------------------
256
257 # Instantiate Optimizer (NSGA2) & Solve Problem
258 #Reference values for: popSize -> | 148 |, 100
259 #                      maxGen  -> | 135 |, 200
260 nsga2 = NSGA2()
261 nsga2.setOption('PopSize',148) # Only multiples of 4
262 nsga2.setOption('maxGen',135)
263 nsga2(opt_prob,store_hst=True) # Optimization history
264 print opt_prob.solution(0)
```

MOO_example_script.py

Bibliography

Jeanne Adams, Walter S. Brainerd, Richard A. Hendrickson, Jeanne T. Martin Richard E. Maine, and Brian T. Smith. *The Fortran 2003 Handbook The Complete Syntax, Features and Procedures*. Number ISBN: 978-1-84628-378-9. Springer, 2003.

Yalçin Aksu. http://www.turbinesinfo.com/wind-turbine-aerodynamics/ (Accessed September 2011), 2011.

Marcelo Alonso and Edward J. Finn. *Physics*. Number ISBN 84-7829-027-3. Addison Wesley Longman, 2^{nd} edition, 1999.

R.K. Amiet. Acoustic radiation from an airfoil in a turbulent stream. *Journal of Sound and Vibration*, 41 (4):407–420, 1975. doi: DOI:10.1016/S0022-460X(75)80105-2.

Eleftherios I. Amoiralis and Ioannis K. Nikolos. Freeform deformation versus b-spline representation in inverse airfoil design. *Journal of Computing and Information Science in Engineering*, February 2008. Department of Production Engineering and Management, Technical University of Crete, Greece.

Siemens Wind Power A/S. *Outstanding efficiency: Siemens Wind Turbine SWT-2.3-93*. Siemens AG, Denmark, 2009. Product manual.

AWEA. Wind energy: The difference wind makes. http://www.awea.org/pubs/factsheets.html (Accessed February 2012).

J. Bosschers R. P. J. O. M. van Rooij B. O. G. Montgomerie, A. J. Brand. *Three Dimensional Effects in Stall*. ECN, June 1997. Project funded by the Netherlands Agency for Energy and the Environment NOVEM.

Taylor Walton B. Woodcroft. Pneumatics. In *Translation from the Greek of The Pneumatics of Hero of Alexandria*. Maberly, 1851. London.

Matt Bair, Greg Adamczyk, and Rob Miller. Evolution of wind turbines, September 2007. Western Michigan University.

Franck Bertagnolio. Trailing edge noise model applied to wind turbine airfoils. Technical report, Technical University of Denmark, Wind Energy Department, Roskilde, Denmark, January 2008.

Franck Bertagnolio, Niels Sorensen, Jeppe Johansen, and Peter Fuglsang. wind turbine airfoil catalogue. Technical Report ISBN: 87 550 2910, Riso National Laboratory, August 2001.

John J. Bloomer. *Practical Fluid Mechanics for Engineering Applications*. Number ISBN 0-8247-9575-X. Marcel Dekker, Inc., New York, 2000.

J. Frédéric Bonnans, Charles Gillbert J, Claude Lemaréchal, and Claudia A. Sagastizábal. *Numerical Optimization: Theoretical and Practical Aspects*. Number ISBN 3-540-35445. Springer, 2^{nd} edition, 2006.

Koen Boorsma. *SILANT Software*. ECN, The Netherlands, 2011. Commercial Brochure.

T. F. Brooks, D. S. Pope, and M. A. Marcolini. Airfoil self-noise and prediction. Reference Publication 1218, National Aeronautics and Space Administration, USA, July 1989.

Thomas F. Brooks and Casey L. Burley. Rotor broadband noise prediction with comparison to model data. In *Proceedings of the* 7^{th} *AIAA/CEAS Aeroacoustics Conference*, number AIAA2001-2210, Maastricht, The Netherlands, May 2001.

Thomas F. Brooks and Robert H. Schlinker. Progress in rotor broadband noise research. *Vertica*, 7(4): 287–307, 1983.

Ralph Carmichael, 2010. http://www.pdas.com/sections6.html, (Accessed February 2012).

R. Carson. *Silent Spring*. Houghton Mifflin, 1962. New York.

Ozlem Ceyhan. *Training Aerodynamic Blade Design Tools*. ECN, The Netherlands, 2011. Commercial Brochure.

W. David Colby, Robert Dobie, Geoff Leventhall, D. M. Lipscomb, R. J. McCunney, Michael T. Seilo, and Bo Sondergaard. Wind turbine sound and health effects an expert panel review. Technical report, American Wind Energy Association and Canadian Wind Energy Association, December 2009.

J. Cummings. Acoustic ecology institute fact sheet: Wind energy noise impacts. *AEI Special Report: Wind Energy Noise Impacts*, 2010. www.AcousticEcology.org/srwind.html.

João Miguel da Costa Sousa. Introdução à Programação. Apontamentos das aulas, 2006. Instituto Superior Técnico, Dep. de Engenharia Mecânica.

Kristian S. Dahl and Peter Fuglsang. Design of the wind turbine airfoil family riso-a-xx. Technical report, December 1998.

Brynhild Davidsen and Per Trojgaard Andersen. Low frequency noise emission from wind farms, potential health effects. Technical report, Lloyd's Register ODS, Copenhagen, Denmark, 2009.

Vasco de Brederode. Fundamentos de aerodinâmica incompressível. Edição de autor, Instituto de Engenharia Mecânica, Instituto Superior Técnico, Lisboa, Portugal, 1997. ISBN 972-97402-0-8.

R. W. Derksen and Tim Rogalsky. Bezier-parsec: An optimized aerofoil parameterization for design. *Advances in engineering software*, (41):923–930, April 2010.

Jean-Antoine Désidéri and Ales Janka. Multi-level shape parameterization for aerodynamic optimization - application to drag and noise reduction of transonic/supersonic business jet. July 2004. European Congress on Computational Methods in Applied Sciences and Engineering, ECCOMAS 2004.

Jean-Antoine Désidéri and Jean-Paul Zolésio. Inverse shape optimization problems and application to airfoils. *Control and Cybernetics*, 34(1), 2005. OPALE Project.

Urmila Diweakar. *Introduction to applied optimization*. Number ISSN: 1931-6828 in ISBN: 978-0-387-76634-8. Springer, New York, USA, 2^{nd} edition, 2008.

Mark Drela. *Frontiers of Computational Fluid Dynamics*, chapter Pros and Cons of Airfoil Optimization. Number ISBN 981-02-3707-3. World Scientific, Department of Aeronautics and Astronautics, M.I.T., Cambridge, MA, 1998.

Mark Drela and Harold Youngren. Xfoil 6.94 user primer. Software Documentation, December 2001. Latest update.

Allan L. Drewitt and Rowena H. W. Langston. Assessing the impacts of wind farms on birds. *Ibis*, (148): 29–42, 2006. The Royal Society for the Protection of Birds, Sandy, UK.

S. A. Dunn. Modified genetic algorithm for the identification of aircraft structures. *Journal of Aircraft*, 34 (251), 1997.

Luís Eça. Aerodinâmica. Apontamentos das aulas, 2010. Departamento de Engenharia Mecânica, Instituto Superior Técnico.

Enercon. *Aerogeradores Enercon: Gama de produtos*. Enercon GmbH, Aurich, Alemanha, 2010. Manual comercial.

António F. O. Falcão. Energia eólica. Apontamentos de Energias Renováveis, 2007. Instituto Superior Técnico, Departamento de Engenharia Mecânica.

Rita Ferreira. Tecnologia: Energias renováveis. *Revista Quero Saber*, (7):50–51, April 2011.

J. E. Ffowcs-Williams. Aerodynamic sound generation by turbulent flow in the vicinity of a scattering half-plane. *Journal of Fluid Mechanics*, 40(4):657–670, 1970.

Roger Fletcher. *Practical methods of Optimization*. Number ISBN 0-471-4963-1. Wiley & Sons Ltd., 2^{nd} edition, May 2000.

Nuno Fonseca. *Introdução à Engenharia de Som*. Number ISBN 978-972-722606-1. Lidel, 2^{nd} edition, January 2007.

Christian Bak Franck Bertagnolio, Helge A. Madsen. Experimental validation of TNO trailing edge noise model and application to airfoil optimization. Technical report, National Laboratory for Sustainable Energy, Wind Energy Division, Roskilde, Denmark, 2008. Riso DTU Technical University of Denmark.

Peter Fuglsang and Helge Aagaard Madsen. Implementation and verification of noise prediction model for wind turbines. (ISBN 87-550-2149-2), March 1996. Riso National Laboratory, Roskilde, Denmark.

Peter Fuglsang, Kristian S. Dahl, and Ioannis Antoniou. Wind tunnel tests of the Riso-a1-18, Riso-a1-21 and Riso-a1-24 airfoils. Technical report, Riso National Laboratory, Roskilde, Denmark, June 1999.

B. Allen Gardner and Michael S. Selig. Airfoil design using a genetic algorithm and an inverse method. Number AIAA 2003-0043, Department of Aeronautical and Astronautical Engineering, University of Illinois, Urbana, Illinois, January 2003. 41^{st} Aerospace Sciences Meeting and Exhibit.

Luís Gato. Energias renováveis parte I. Apontamentos das aulas, 2010. Dep. Engenharia Mecânica, Instituto Superior Técnico.

Ilia Gherman and Volker Schulz. Efficient methods for aerodynamic optimization. University of Trier, MEGADESIGN-Project, September 2006.

P. Gliebe, R. Mani. H. Shin, B. Mitchell, G. Ashford, S. Salamah, and S. Connell. Aeroacoustic prediction codes. Technical Report NASA/CR-2000-210244, NASA, August 2000.

M. E. Goldstein. *Aeroacoustics*. McGraw-Hill, 1976.

F. Grasso. Usage of numerical optimization in wind turbine airfoil design. In *Aerodynamic design: analysis, methodologies & optimization techniques*, 1755 LE, Petten, 28 June - 1 July 2010. Energy Research Center of the Netherlands, The Netherlands. 28^{th} AIAA Applied Aerodynamics Conference Chicago Illinois USA.

Francesco Grasso. *Multi-Objective Numerical Optimization applied to Aircraft Design*. Doctoral thesis, Universitá degli Studi di Napoli "Fedrico II", Facoltá Ingegneria, Dipartimento Ingegneria Aerospaziale, December 2008.

F. W. Grosveld and H. H. Hubbard K. P. Shepherd and. Measurement and prediction of broadband noise from large horizontal axis wind turbine generators. Technical Report N95-27990, NASA, 1985.

Ferdinand W. Grosveld. Prediction of broadband noise from horizontal axis wind turbines. *Journal of Propulsion and Power*, 1985,.

Avinash G.S. and S. Anil Lal. Inverse design of airfoil using vortex element method. 2011. Department of Mechanical Engineering, College of Engineering, Thiruvananthapuram, Kerala, India.

Raymmond M. Hicks and Preston A. Henne. Wing design by numerical optimization. In *Journal of Aircraft*, volume 15. American Institute of Aeronautics and Astronautics, July 1978.

Soren Hjort. *Noise optimization of a Siemens Multi-MegaWatt turbine*. Siemens, Siemens Wind Power A/S, Brande, Denmark, 2005.

E.L. Houghton and P.W. Carpenter. *Aerodynamics for engineering students*. Number ISBN 0-7506-5111-3. Butterworth-Heineman, Oxford, Burlington, MA, 5^{th} edition, 2003.

Harvey H. Hubbard and Kevin P. Shepherd. Wind turbine accoustics. Technical Paper 3057 DOE/NASA/20320-77, National Aeronautics and Space Administration, USA, 1990. Work performed for the U.S. Dep. of Energy and Solar Energy Research Institute.

INEGI. Parques Éolicos em Portugal. Final report, Instituto Nacional de Engenharia Mecânica e Gestão Industrial, December 2009.

Eastman N. Jacobs and Robert M. Pinkerton. Tests in the variable-density wind tunnel of related airfoils having the maximum camber unusually far forward. Technical Report 537, Langley Memorial Aeronautical Laboratory, Langley Field, VA, May 7^{th} 1935.

Kyo K. Jin, Mustafa Ghulam, Jin H. Kim, and Sung K. Ha. Life prediction of wind turbines. In *Wind Turbine Applications*, volume A7:4, 2009.

Nuno Maia Júlio M. Silva. Vibrações e ruído: Teoria. Associação dos Estudantes do Instituto Superior Técnico, 2008. Instituto Superior Técnico.

Helmut Klug. Noise from wind turbines standards and noise reduction procedures. Technical report, German Windenergy Institute, 1998.

Fernando Lau. Elementos de aeroacústica. Apontamentos das aulas, 2010/11, Fevereiro 2011.

Giorgios Leloudas, W. J. Zhu, J. N. Sorensen, W. Z. Shen, and S. Hjort. Prediction and reduction of noise from a 2.3mw wind turbine. *Journal of Physics: Conference Series 75*, (doi:10.1088/1742-6596/75/1/012083), 2007. IOP Publishing.

Geoff Leventhall. A review of published research on low frequency noise and its effects. Technical report, Department for Environment, Food and Rural Affairs, London, UK, 2003.

M. V. Lowson. A new prediction model for wind turbine noise. *Renewable Energy: Conference Publication*, (385):17–19, November 1993a. University of Bristol, UK.

M. V. Lowson. Assessment and prediction of wind turbine noise. (ETSU W/13/00284/REP), 1993b.

T. Lutz, A. Herrig, W. Wurz, K. Braun, and E. Kramer. Constrained aerodynamic & aeroacoustic design of wind rotor airfoils. volume First International Meeting on Wind Turbine Noise, Stuttgart, October 2005. Institute of Aerodynamics and Gas Dynamics & University of Stuttgart.

T. Lutz, A. Herrig, W. Warz, K. Braun, and E. Kramer. Design and wind tunnel verification of low-noise airfoils for wind turbines. *AIAA Journal*, 45(4):779 – 785, April 2007.

J. F. Manwella, J. G. McGowan, and A. L. Rogers. *Wind Energy Explained: theory, design and application*. Wiley, 2^{nd} edition, 2009.

B.G. Marinus. Influence of parameterization and optimization method on the optimum airfoil. 2010. 27^{th} International Congress of the Aeronautical Sciences.

R.T. Marler and J.S. Arora. Survey of multi-objective optimization methods for engineering. 26:369–395, 1997. Optimal Design Laboratory, College of Engineering, The University of Iowa, U.S.A.

W. H. Mason. *Applied Computational Aerodynamics*, volume I. Virginia Polytechnic Institute and State University, 1995.

D. H. Meadows, D. L. Meadows, J. Randers, and W. W. Behrens III. *Limits to Growth*. Universe Books, 1972. New York.

Juan Méndez and David Greiner. Wind blade chord and twist angle optimization by using genetic algorithms. Technical report, Institute of Intelligent Systems and Numerical Applications in Engineering, Univ. Las Palmas de Gran Canaria, Las Palmas, Spain, 2003.

Michael Metcalf and John Reid. *Fortran 90/95 Explained*. University of Oxford, 2^{nd} edition, 2000. ISBN 0-19-850558-2.

Paul Migliore and Stefan Oerlemans. Wind tunnel aeroacoustic tests of six airfoils for use on small wind turbines. Technical report DE-AC36-99GO10337, National Renewable Energy Laboratory, Golden, Colorado, U.S.A., November 2004.

Melanie Mitchell. *An Introduction to Genetic Algorithms*. Number ISBN 0-262-13316-4. The MIT press, 5^{th} edition, 1999.

Patrick Moriarty. Modelling of aeroacoustic noise from wind turbines. In AAM Sayigh, editor, *World Renewable Energy Congress VIII*. National Renewable Energy Laboratory, Elsevier, 2004a.

Patrick Moriarty. Development and validation of a semi-empirical wind turbine aeroacoustic code. In *2004 ASME Wind Energy Symposium*, number AIAA2004-1189, 2004b. 42^{nd} AIAA Aero. Sci.Mtg.

Patrick Moriarty. *NAFNoise User's Guide*. National Wind Technology Center, National Renewable Energy Laboratory, USA, Golden, Colorado, July 2005.

Patrick Moriarty and P. Migliore. Semi-empirical aeroacoustic noise prediction code for wind turbines. Technical report DE-AC36-99-GO10337, National Renewable Energy Laboratory, Golden, Colorado, U.S.A., December 2003.

Patrick J. Moriarty, Gianfranco Guidati, and Paul Migliore. Recent improvement of a semi-empirical aeroacoustic prediction code for wind turbines. In 10^{th} *AIAA/CEAS Aeroacoustics Conference*, number AIAA 2004-3041, 2004. Manchester, UK.

Patrick J. Moriarty, Gianfranco Guidati, and Paul Migliore. Prediction of turbulent inflow and trailing edge noise for wind turbines. Technical report, American Institute of Aeronautics and Astronautics, 2005.

H. Muller-Steinhagen and J. Nitsch. The constribution of renewable energies to a sustainable energy economy. In *Process Safety and Environmental Protection*, volume 83, pages 285–297. Institution of Chemical Engineers, July 2005. 7^{th} World Congress of Chemical Engineers, Glasgow 2005.

NLR, 2010. http://www.nlr.nl/, (Accessed May 2011).

NWCC. Permitting of wind energy facilities: A handbook. Technical report, National Wind Coordinating Committee, 1998. Washington.

NWCC. Wind turbine interactions with birds, bats and their habitats. Summary of research results, National Wind Coordinating Collaborative, 2010.

S. Oerlemans and J. G. Schepers. Prediction of wind turbine noise and validation against experiment. In *International Journal of Aeroacoustics*, volume 8, pages 555–584. Multi-Science Publishing Co. Ltd., National Aerospace Laboratory NLR, Emmeloord, The Netherlands, April 2009.

S. Oerlemans, M. Fisher, T. Maeder, and K. Kogler. Reduction of wind turbine noise using optimized airfoils and trailing-edge serrations. Executive Summary NLR-TP-2009-401, National Aerospace Laboratory, August 2009. Unclassified report.

Sharon Padula and Wu Li. Options for robust airfoil optimization under uncertainty. In *9th AIAA Multidisciplinary Analysis and Optimization Symposium*. NASA Langley Research Center, September 2002. http://mdob.larc.nasa.gov/.

R. Parchen. Progress report draw: A prediction scheme for trailing-edge noise based on detailed boundary-layer characteristics. TNO Report HAG-RPT-980023, TNO Institute of Applied Physics, 1998. The Netherlands.

Pablo Pedregal. *Introduction to applied Optimization*. Number ISBN 0-387-40398-1. Springer, 1^{st} edition, 2004.

Ruben E. Perez, Peter W. Jansen, and Joaquim R. R. A. Martins. pyOpt: A Python-based object-oriented framework for nonlinear constrained optimization. *Structures and Multidisciplinary Optimization*, 2011. doi: 10.1007/s00158-011-0666-3.

Heitor Pina. *Métodos Numéricos*. Number ISBN 972-9298-04-8. 1^{st} edition, 1995. Dep. Engenharia Mecânica, Instituto Superior Técnico.

V. Prasanth and S. Anil Lal. Bezier parameterization of an airfoil using genetic algorithm. 2010. Department of Mechanical Engineering, College of Engineering, Thiruvananthapuram, Kerala, India.

Peter W. Jansen Ruben E. Perez. *pyOpt Reference*. Python Software Foundation, release 1.0.1 edition, June 2011.

Sara Sá and Alexandra Rosa. Especial VISãO: A revolução energética em portugal. *VISÃO*, pages 131 – 144, Setembro 2008.

Jamshid A. Samareh. A survey of shape parameterization techniques. In *CEAS/AIAA/ICASE/NASA Langley International Forum on Aeroelasticity and Structural Dynamics*, pages 333–343, NASA Langley Research Center, Hampton, VA 23681, June 1999. NASA.

William T. Scarbrough. Naca four digit airfoil section generation using cubic parametric curve segments and the golden section. Master of science of mechanical engineering, Department of Mechanical Engineering, Rochester Institute of Technology, Rochester, New York, April 1992.

Sociedad Espanola de Acústica. http://www.sea-acustica.es/ (Accessed June 2011), 2005.

Wenbin Song and Andrew J. Keane. A study of shape parameterization methods for airfoil optimisation. *American Institute of Aeronautics and Astronautics*, 2004. University of Southampton, Southampton, United Kingdom.

R. H. Spencer. Noise generation of upwind rotor wind turbine generators. Technical report, The Boeing Vertol Company, 1981. Philadelphia, U.S.A.

David A. Spera. Collected papers on wind turbine technology. Technical Report DOE/NASA/5776-2, National Aeronautics and Space Administration, U.S.A., May 1995.

David S.Stephens, Kevin P. Shepherd, Harvey H. Hubbard, and Ferdinand W. Grosveld. Guide to the evaluation of human exposure to noise from large wind turbines. Technical Report 83288, National Aeronautics and Space Administration, May 1982.

Zhi Li Tang and Jean-Antoine Désidéri. Towards self-adaptive parameterization of bézier curves for airfoil aerodynamic design. Research report 4572, Institut National de Recherche en Informatique et en Automatique, September 2002.

James L. Tangler and Cyrus Ostowari. Horizontal axis wind turbine post stallairfoil characteristics synthesization. Technical Report DE-AC04-76DP03533, U.S. Department of Energy, U.S.A., 1984.

C. E. Tickell, J. T. Ellis, and M. Bastasch. Wind turbine generator noise prediction - comparison of computer models. In *Proceedings of Acoustics*, November 2004.

W. A. Timmer and R. M. van Rooij. Summary of the delft university wind turbine dedicated airfoils. Technical Report AIAA-2003-0352, Delft University Wind Energy Research Institute, Stevinweg 1, 2628 CN Delft, The Netherlands, 2003.

Gerard van Bussel. Rotor aerodynamics. TUDELFT, Section Wind Energy, Faculty of Aerospace Engineering, February 2011. Lecture notes.

Frits van den Berg, E. Pederson, J. Bouma, and R. Bakker. Project windfarm perception: Visual and accoustic impact of wind turbine farms on residents. Final Report Project no. 044628, University of Groningen and University of Gothenberg, June 2008.

Guido van Rossum. *Python Tutorial Release 3.2.1*, volume 1. Python Software Foundation, September 2011. http://docs.python.org/.

L. F. C. Vargas, J. M. G. S. Oliveira, and F. J. P. Lau. Developpent of a wind turbine noise prediction model. In 7^{th} *EUROMECH Solid Mechanics Conference*, September 2009.

Luís F. C. Vargas. Wind turbine noise prediction. Masters thesis, Universidade Técnica de Lisboa, Instituto Superior Técnico, November 2008.

Vestas. *V90 3.0MW*. Vestas Wind Systems A/S, Denmark, 2011a. Product Manual.

Vestas. *V80 2.0MW, V90 1.8/2.0MW, V100 1.8MW*. Vestas Wind Systems A/S, Denmark, 2011b. Product Manual.

Larry A. Viterna and David C. Janetzke. Theoretical and experimental power from large horizontal-axis wind turbines. (DOE/NASA/20320-41), September 1982. NASA.

H. P. Vowles. *An inquiry into the origins of the windmill*, chapter 11, pages 1–14. Journal of the Newcomen Society, 1930.

H. P. Vowles. *Early evolution of power engineering*, volume 17. Isis, 1932. 412-420.

Damir Vucina, Zeljan Lozina, and Igor Pehnec. A compact parameterization for shape optimization of aerofoils. I(ISBN:978-988-98671-9-5), July 2008. World Congress on Engineering 2008, London.

S. Wagner, R. Bareib, and G. Guidati. *Wind Turbine Noise*. Springer, 1996. Berlin.

Linda Bevard Patricia Weis-Taylor and Alex Taylor. Annual report. Technical report, IEA Wind, July 2007a.

Linda Bevard Patricia Weis-Taylor and Amber Taylor. Annual report 2006. Technical report, IEA Wind, July 2007b.

Zhou Wenming, Qin Ming, Dai Haitao, Ding Yonggang, and Chang Hui Ying. Wind turbine blade design and optimization based on free modeling with bezier curve. Technical report, Guodian United Power Technology Company Ltd., 2008. Beijing, P.R.C.

WWEA. World wind energy report. Technical report, World Wind Energy Association, WWWEA Head Office, Charles-de-Gaulle-St. 5, 53113 Bonn, Germany, April 2011. 10^{th} World Wind Energy Conference Exhibition, Cairo, Egipt.

Wei Jun Zhu. Modelling of noise from wind turbines. Masters thesis, Technical University of Denmark, February 2004.

Wei Jun Zhu, Nicolai Heilskov, Wen Zhong Shen, and Jens N. Sorensen. Modelling of aerodynamically generated noise from wind turbines. Technical report, Technical University of Denmark, Denmark, June 2005. Contributed by the Solar energy division of the ASME.

Lex Zwang. Boundary layer suction on a horizontal axis wind turbine: An aerodynamic design of a thick airfoil for application. Masters thesis, Delft University of Technology, November 2009.